2011-01-01

Evaluation Methods for Health Monitoring of Aerospace Structure Rotary Joints

Sergio Armando Navarro
University of Texas at El Paso, sanavarro2@miners.utep.edu

EVALUATION METHODS FOR HEALTH MONITORING OF AEROSPACE STRUCTURES

ROTARY JOINTS

SERGIO A. NAVARRO

Department of Civil Engineering

APPROVED:

_____
Cesar Carrasco, Ph.D., Chair

_____
Carlos Ferregut, Ph.D.

_____
Noe Vargas Hernandez, Ph.D.

_____
Benjamin Flores, Ph.D.
Interim Dean of the Graduate School

EVALUATION MEHODS FOR HEALTH MONITORING OF AEROSPACE STRUCTRURES ROTARY JOINTS

by

SERGIO A. NAVARRO

THESIS

Presented to the Faculty of the Graduate School of

The University of Texas at El Paso

in Partial Fulfillment

of the Requirements

for the Degree of

MASTER OF SCIENCE

Department of Civil Engineering

THE UNIVERSITY OF TEXAS AT EL PASO

December 2011

ACKNOWLEDEMENTS

I would like to acknowledge with appreciation to my advisor, Dr. Cesar Carrasco of the Department of Civil Engineering at The University of Texas at El Paso, for his numerous and valuable comments, advise, suggestions, patience, and support. His helped was important during the research and writing of this thesis. He always gave me clear explanations in order to clarify concepts.

I also would like to thank, besides my advisor, the thesis committee, Dr. Carlos Ferregut of the Department of Civil Engineering and Dr. Noe Vargas Hernandez of the Department of Mechanical Engineering, both from the University of Texas at El Paso. Their involvement in the thesis was important due to their comments, suggestions, and questions.

This study was conducted under Boeing contract No. 420188. My sincere appreciation to Michael R. Liable, for his guidance and for providing the information used in this thesis.

My sincere thanks to all the professors of the college of engineering for their class dedication and providing me a lot of knowledge.

Finally, I would like to thank my whole family, especially my parents, Ruben Navarro and Araceli Navarro, and big brother, Ruben Rene Navarro, for support me, taught me, and love me throughout my life

ABSTRACT

In September 2007, the excessive vibrations played a significant role in the station operation since one of the rotary joints, which provides the station electrical energy, presented an anomaly. The replacement of its bearing components and re-lubrication were necessary to reduce the problem. To avoid a new anomaly, the inspection of the rotary joints performance continues by using the accelerometers data. This thesis presents three new approaches to monitor the vibrations at the International Space Station based on Root-Mean-Square, kurtosis, and Approximate Entropy (ApEn). MATLAB functions and codes were necessary to implement the three monitoring techniques results from the provided accelerometer datasets. The analyses consist in detecting the datasets with considerable vibrations and perform plots of the three techniques versus time for those datasets. In the end, the plot results are compared with Power Spectral Densities (PSD) plots. The plots results had shown that the RMS method was able to detect most vibrations, kurtosis was able to detect the two most excessive ones, and ApEn only detected the most excessive one.

TABLE OF CONTENTS

LIST OF FIGURES

Page

Chapter 1

INTRODUCTION

The rotary joints are important devices that connect the A3 and A4 truss segments of the International Space Station, on one side, and B3 and B4 truss segments, on the other side (see Figure 1.1. They can rotate 360 degrees clockwise and counterclockwise by using bearing assemblies and a control system. They have a diameter of 10 feet and an approximate weight of 2560 pounds. The rotary joints main purpose is to enable the solar arrays to always point to the sun in order to convert solar energy into electrical energy. Its is composed of twelve bearing assemblies per joint, two race rings per joint, a utility transfer assembly, two drive/lock assemblies per joint, and two rotary joint motor controllers per joint. There is a gold plating on the bearing assembly rollers, which is used to transfer a lubricating film from the race ring to the roller so the friction can be reduced. In September 2007 there was a notable increase in vibration and electric currents on the Rotary Joint A indicative of sever damage on the race ring surface. In order to avoid the race ring surface damage to propagate, excessive vibrations, accelerated fatigue, and other problems, the Rotary Joint A movement was limited. Inadequate lubrication was initially believed to be the main cause of the problem due to the excessive friction between the rollers and race ring. However the problem was investigated more in depth to determine the actual cause. Some of the tests performed included metallurgical inspection, traction kinematics tests, detailed bearing measurements, thermal and structural analyses, and lubrication interval tests. Also, on-board instrumentation systems were used and continue to be used to monitor the evolution of the damage. The aerospace structure instrumentation systems consist of internal instrumentation and the most recently installed, external instrumentation. Some of theses instruments consist of accelerometers units, remote sensor units, and strain gages [5]. Using the

data acquired through these units, specially the external instrumentation data, a series of analysis were conducted to monitor the state of several components of the space structure including the rotary joints. The monitoring of the rotary joints using these data was limited to the visual comparison of Power Spectral Density (PSD) and Spectrogram plots of the accelerometer data.

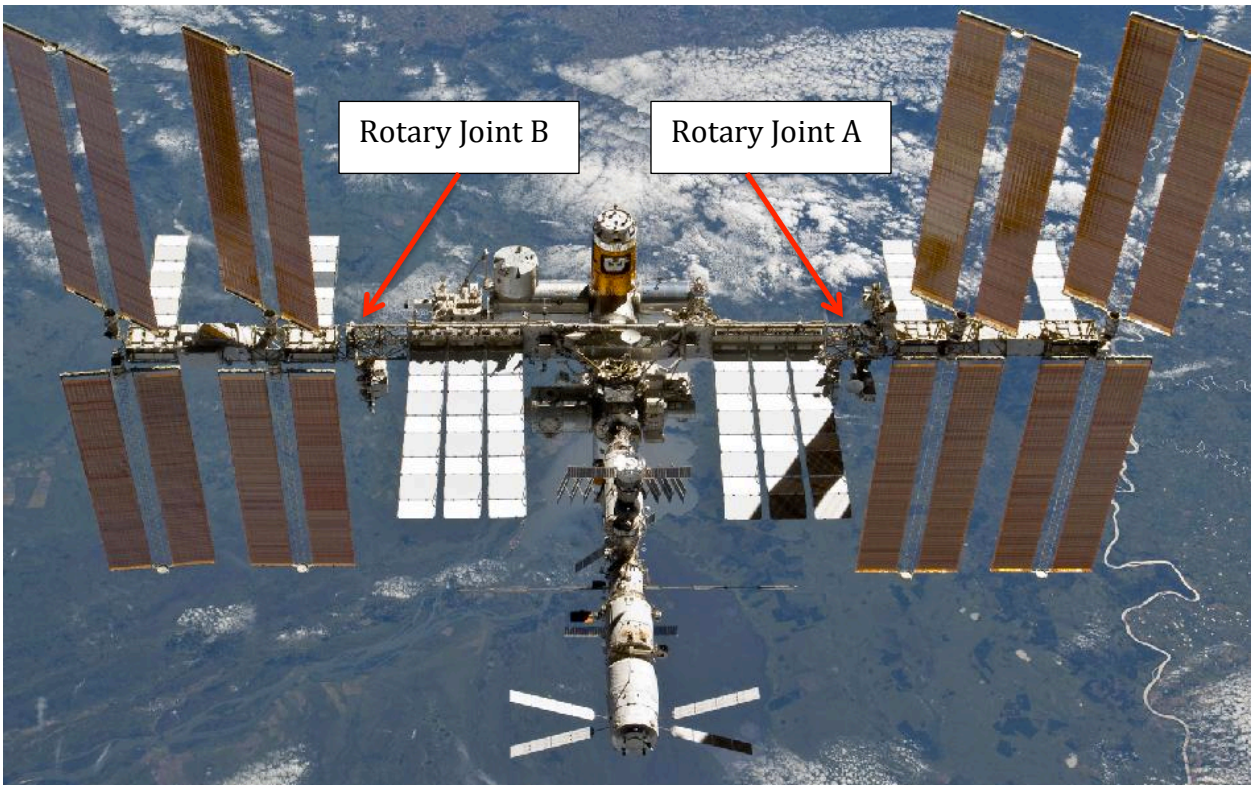

Figure 1.1 – Aerospace Structure Rotary Joints Location (NASA Website)

1.1 Objective

The objective of the project discussed in this thesis was to study different stochastic techniques for the monitoring of the health of the rotary joints. These techniques still used the accelerometer data but were no longer based on visual comparison of plots but on the measurement of performance metrics and their change over time. The techniques selected were

the Root Mean Square (RMS), kurtosis, and approximate entropy (ApEn).

1.2 Content

The thesis is divided into a total of five chapters where the research, analyses, results, and conclusions of the project are explained in detail. Chapter 2 discusses the anomalies identified in the structure rotary joints. Problems in the bearing assemblies such as lack of lubrication and excessive vibrations are mentioned. Chapter 3 provides information related to several bearing health monitoring techniques and failure analyses techniques published in the literature. Chapter 4 contains the results obtained using the RMS, kurtosis, ApEn techniques after their application to the accelerometer data. This chapter also shows the analysis and interpretation of the results. Chapter 5 includes the conclusions and some recommendations resulting from the work conducted for this thesis.

Chapter 2

Rotary Joint A ANOMALY

In September of 2007 the aerospace structure Rotary Joint A began to respond outside of its normal envelop. Severe vibrations and electric current fluctuations in the control systems were detected that prompted the suspension of rotary joints operation and triggered a detailed investigation to identify the source of the problem. This caused a reduction of the station power generation and a shift of mission priorities. The anomaly was investigated by performing different inspections. Harik *et al.* thought that the problem could be the controller software, as had previously occurred in the Rotary Joint B, which was fixed by resetting the software [6]. However resetting the Rotary Joint A did not improve its performance. The logical command strings, which control the velocity control loop and motor power source, were also switched but there was not an appreciable change in the response of the rotary joint. The controller parameters were also modified to determine if the controller was over-correcting changes in the mechanism performance; however, the controller logic review did not show any evidence. After these initial correction attempts, the conclusion was that the possible cause could be mechanical and an extravehicular activity task was scheduled to find the possible cause. The crew noticed metallic debris on the surface of the race ring and debris samples as well as a rotary joints bearing assemblies were taken to Earth for further investigation of the source of the anomaly.

2.1 Bearing Assemblies and Race Rings Evaluation

The bearing assemblies consist of two upper rollers and a lower one, which is wider than the upper ones. The rollers are made of 440C stainless steel and they are lubricated. The rollers assemblies include pivot cambers and fixed arms. The race rings are made of nitrided 15-5 PH.

They have a triangular cross-section and three of their surfaces are in contact with the bearing rollers. The surface that are in contact with the upper rollers are called outer 45 and inner 45 and the surface that is in contact with the lower roller is called datum A. One race ring is called the inboard race, which is not allowed to move, and the other one is called the outboard race, which passes through the lubricated rollers to move without friction.

Stereomicroscopy, Scanning Electron Microscopy (SEM), Energy Dispersive Spectroscopy (EDS), and laser confocal microscopy were used to determine the metallic debris origin [15]. The initial findings, from the debris spectrum, showed that the majority of the debris was nitrided 15-5 PH steel and some gold, fluorinated grease, and trace contaminants. A martensitic core was not observed as in typical nitrided stainless steel. The two types of large particles size found were agglomerations and solid chips/flakes. Crack propagation was observed in larger flakes where the path did not have a preferential path. Also, it was discovered that what appeared to be initially as a cracks on the nitride layer were Discontinuous Inter-granular Separations (DIGs) [2]. Their presence is not desired since they diminish the original engineering requirements. Figure 2.1 illustrates the degraded race ring.

Further tests showed that the structure deterioration was caused by high stresses on the race ring surface due to a bearing assembly rollers misalignment. It was found that the surface friction increased as the mistracking angle increases, which cause the load to be distributed unevenly. The rollers being misaligned less than 0.5 degrees with respect to the race ring caused mistracking and lead to nitrite spallation.

To correct the problem, all the debris on the race ring surface was removed, all the bearing assemblies were replaced and a new roller lubricant was applied (see following section). However, the race rings remain with the deteriorated surface.

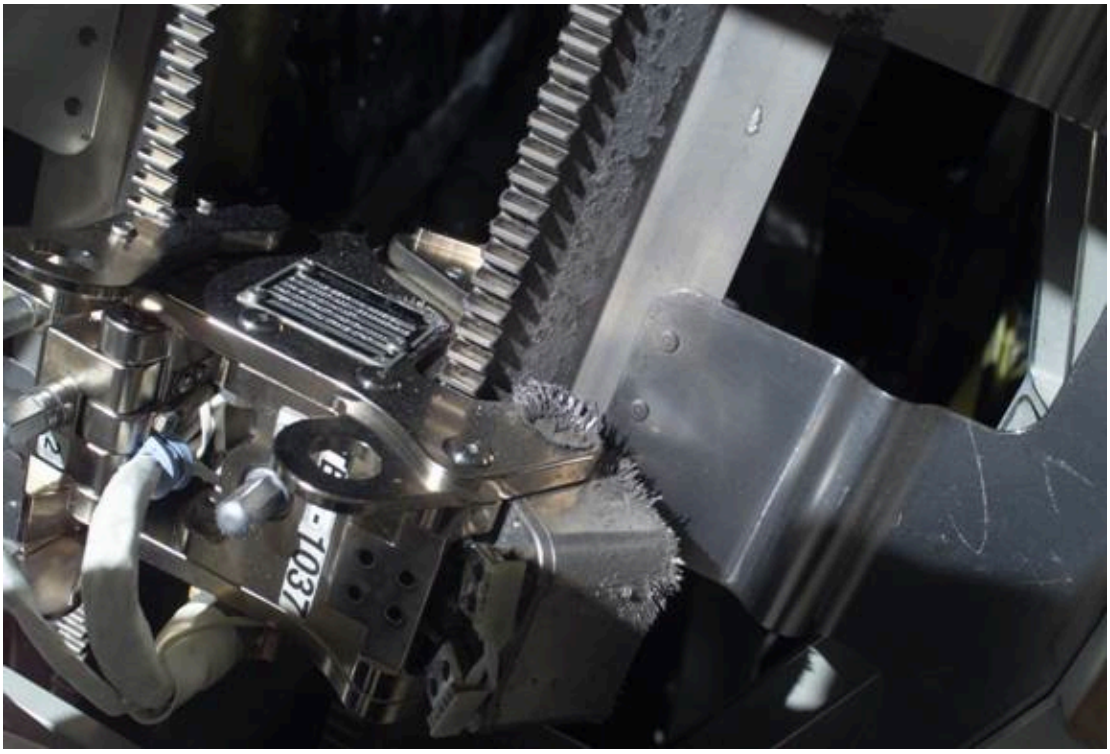

Figure 2.1 – Degradation of the Rotary Joint Outer 45 Canted Race Ring (NASA Website)

2.2 Lubrication Evaluation

The bearing rollers were lubricated with 1250-2250 Angstroms of ion-plated gold coating in order to reduce the contact friction between the bearing assembly rollers and the race ring. However, the lubricant did not last as expected which caused an increase in the coefficient of friction. One of the bearing assemblies was taken to Earth for investigation of the possible cause of failure and it was discovered that the roller coating had degradated significantly.

Several tests were conducted to determine the performance of the ion-plated gold lubricant aged using different temperature and humidity [2]. The tests showed that gold

adhesion loss occurred at high temperature and humidity. The adhesion loss was more widespread by the end of 21 days of testing. The conclusion was that the gold plating was not the appropriate lubricant for the rollers and a replacement grease lubricant was identified and a re-lubrication schedule was developed. Tests with the new grease showed significant coefficient of friction reduction and longer life.

2.3 Post-Remediation Performance

The rotary joint anomaly manifested it self as high drive motor current and excessive vibrations. Under normal conditions, the drive motor current required to overcome the joint drag and applied load during rotary joint rotation was calculated to be 0.25 amperes, which corresponds to a torque of about 590 ft-lb. After the anomaly occurred, the current increased to over 1.2 amperes with a corresponding torque of 2810 ft-lb. Also the accelerometers detected acceleration as high as 0.0172 g, when the initial acceleration, prior to the anomaly, was 0.0003 g. This increase in electric current brought the requirements closer to the 1.4 amperes limit of the rotary joint.

After the corrective measures were implemented the electric current and accelerations were reduced to as low as 0.172 amperes and 0.0013 g respectively. However, continuous monitoring is still required to assess the progression of the anomaly.

Chapter 3

HEALTH MONITORING TECHNIQUES

For electro-mechanical systems that rely on bearings for their proper operation, monitoring of their performance over time can be of great importance; especially if their failure can lead to a catastrophic failure of the entire system. To determine what methods to use in the monitoring of the aerospace structure rotary joints, a literature review was conducted.

Ericsson *et al*. studied several techniques that can detect local bearing defects in rotary machines [4]. Their studies were based on vibration based experimental results on bearing with artificially induced surface faults post-processed using wavelet, envelope and periodization techniques. Although these techniques showed good results, the authors indicate that their performance on "real" situations might not be as good due to the complexity of possible faults and great variety bearing systems. Because of the results they obtained, they propose further refinement of the techniques.

Harvey *et al*. proposed an electrostatic monitoring system for an accelerated taper-roller bearing test rig [8]. Electrostatic monitoring consisted of detecting the electrostatic charge generation on the deteriorating surface. The rig consisted of four bearings, two were located in the end housing and the other two were located in the center housing. For their study, an intentional defect was introduced into one inner race of a bearing. Thermocouples, electrostatic sensing, vibration sensing, debris production measurement devices were added to the test. The results indicated that wear started at or near the intentional defect, after a time, the debris production as well as the temperature increased, at 6.5 hours before failure there was a steady state temperature.

Zhen *et al.* proposed two techniques, the Shock Pulse Method (SPM) and Improved Redundant Lifting Scheme (IRLS), to be combined for bearing condition monitoring [22]. The redundant lifting scheme was improved by adding normalized factors due to the deficiencies. In the SPM, the maximum normalized shock value (dB) indicates the bearing condition. The proposed method, SPM and IRLS combined, was analyzed by performing an experimental simulation. The simulated signals and bearing vibration signals were used to verify the proposed method simulation. The results show that this combination was more efficient in bearing condition monitoring.

Singh and Al Kazzaz used the Wavelet Transform (WT) method to analyze measured signals from an experimental set-up [16]. The signals were three line-to-line voltage, three currents, two vibration signals, four temperatures, and one speed signal. The dry bearing faults were correlated with the wavelet transform. The test was performed on healthy bearings as well as fault bearings. On-line analysis of the acquired signals was performed using C^{++} code and the off-line analysis was performed on MATLAB. The results concluded that WT could be used to specify one fault but not multiple faults simultaneously.

Cao and Xiao talked about a comprehensive dynamic model of double-row spherical roller bearing. It consisted of a contact-damping model that was created in order to determine the spherical roller bearing (SRB) defects [3]. This model is useful for a broad range of operation conditions and geometry, transient and steady state operations, different load scales and fix inner race and fixed outer race configurations. Lagrange equations were used to derive the model. In order to understand the impact of operating condition, several cases were studies. Geometry features such as radial clearance and system defects, including surface waviness and point defects on all the major contact surfaces were some of the defects/damages considered. The

simulation results lead to the conclusion that the model is helpful for machine design, optimization, and health monitoring.

The most mentioned technique by many articles is the Acoustic Emission (AE) [10, 11, 12, 18, and 19]. The AE signal articles talked about experimental setups consisting of a spindle, variable speed motor, and a stand-by bearing test rig. A different amount of bearings were used for the test rigs, which were a healthy bearing and other with various size defects. An AE traducer was placed to collect the AE signals in different directions. The results indicated that AE is better than sound or vibration condition monitoring techniques and it allows the diagnosis of locations of localized defects on bearings.

The problem with the techniques mentioned above is that they required special devices or equipment to perform them. However, the only aerospace structure data available is from the external instrumentation accelerometers in the Space Station; thus, the techniques mentioned above cannot be applied in the problem with the rotary joints.

Some articles discussed statistical methods that are able to detect bearing defects by using vibrations signal data. These methods are Root Mean Square (RMS), kurtosis, Approximate Entropy (ApEn) and were selected for this study because they can use accelerometer data which is available in the case of the rotary joints.

3.1 Root Mean Square

Root Mean Square, a time-domain approach, is a method used to detect localized defects.[13, 17]. This technique measures the magnitude of a varying quantity, and it is useful when random variables vary from positive to negative like in sinusoidal signals. Deviations

from the un-damaged or baseline response signal generally indicates the presence of damage. For continuous signals, the RMS can be calculated as follows,

$$rms = \sqrt{\frac{1}{t_2 - t_1}\int_{t_1}^{t_2} x(t)^2\, dt} \tag{3.1}$$

where *x(t)* is the time-domain signal, and t_1 and t_2 define the domain of interest. For discrete signals, the RMS is defined as follows,

$$rms = \sqrt{\frac{1}{N}\sum_{i=1}^{N} x_i^2} \tag{3.2}$$

where again x_i are time-domain discrete values and N is the number of discrete samples.

3.2 Kurtosis

Kurtosis, also a time-domain approach, is another method proposed in the detection of bearing defects [9, 13, 17, 20]. The authors in these references discuss several experimental tests using new undamaged and damaged ball bearings. These tests were conducted under different load conditions and rotational speeds. Vibration data were analyzed to localized defect formation and propagation.

Kurtosis is a measure of weather the probability distribution of the data is peaked or flat when compared to the standard-normal distribution. A high Kurtosis indicates that the data has a sharp peak near the mean and then declines rapidly, while a low Kurtosis indicates that the data probability distribution has a flat top near the mean. The kurtosis is defined as the fourth order moment about the mean divided by standard deviation to the fourth power, and is defines a follows for discrete data,

$$Kurtosis = \frac{M_4}{\sigma^4} = \frac{\frac{1}{N}\sum_{i=1}^{N}(x_i - \bar{x})^4}{\left(\frac{1}{N}\sum_{i=1}^{N}(x_i - \bar{x})^2\right)^2} \tag{3.3}$$

where $\bar{x}$ is the mean, x_i is the discrete data, N is the number of data points, and σ is the standard deviation. A bearing in good condition would produce a response signal (i.e. vibrations measured with accelerometers) with a Gaussian distribution and a Kurtosis equal to 3.0, while a damaged bearing would produce a non-Gaussian response with a Kurtosis significantly larger than 3.0. The disadvantage of the Kurtosis is that sometimes it cannot indicate when failure occurs since the value can be close to three (3.0) when the damage is very advanced.

3.3 Approximate Entropy

Approximate entropy is a statistical measure that quantifies the regularity of a time series. The time series can be measurements of vibrations from rolling bearings and electrical motors like in the case of the rotary joints. When defects or damage is present, the approximate entropy would increase with respect to the baseline undamaged case. Yan and Gao proposed a test signal formulation and an experiment to apply this technique [21]. The test signal formulation, obtained from measured vibration signals of a rolling bearing, concluded that the ApEn value can measure the degradation of a dynamic signal as the noise increases. The experiment, performed to four bearings with different damage conditions, revealed that the ApEn value increases as the defect size and its rotational speed increases.

The theory background consists of a time series S having N data points, {x (1), x (2), …, x (N)}, a series of vectors as:

$X(1)= \{x(1),x(2),\ldots,x(m)\}$
$X(2)=\{x(2),x(3),\ldots,x(m+1)\}$
to
$X(N-m+1)=\{x(N-m+1),x(N-m+2),\ldots,x(N)\}$ (3.4)

In Equation (3.4), each vector has a size equal to m, known as pattern length or window size, and the series of vector are composed of the discrete data points of the time series. The total number of them is equal to N-m+1. The distance between two vectors, from the series, is the difference of their maximum corresponding elements. Each of the vectors in the series are subtracted with this equation as illustrated in Equation (3.5):

$$d(X(i),X(j)) = \max_{k=1,2\ldots,m}([x(i+k-1)-x(j+k-1)]) \tag{3.5}$$

where i, j= 1, 2, …, N-m+1 and N is the number of data points. The distance is then used to calculate another constructed vector, which is a measure that describes the similarity between a vector X(i) and all other vectors in the series as:

$$C_i^m(r) = \frac{1}{N-(m-1)}\sum_{j\neq i}\Theta\{r-d[X(i),X(j)]\} \tag{3.6}$$

where,

$$\Theta\{x\} = \begin{cases} 1, & x \geq 0, \\ 0, & x < 0. \end{cases} \tag{3.7}$$

where i, j= 1, 2, …, N-m+1 and r is the tolerance value, defined as:

$r=k\bullet std(S)$ (3.8)

where k is the tolerance constant, which must be greater than zero, and std is the standard deviation of the time series. Equation (3.6) shows the difference between the tolerance and distance, if their difference is greater than or equal to zero the value is changed to a one otherwise it is changed to a zero and the summation is then calculated. The summation result is divided by total number of vectors in the series. Then, a phi variable is calculated by using the

summation of the constructed vector natural logarithm divided by total number of vectors in the series, as expressed in Equation (3.9)

$$\phi^m(r) = \frac{1}{N-m+1}\sum_i \ln[C_i^m(r)] \tag{3.9}$$

where i=1,2,..,N-m+1, r is the tolerance, and C_i^m is the constructed vector. In order to calculate the approximate entropy, the difference between a phi variable with a series of vector with size m and another phi variable with a series of vectors with size m+1 needs to be calculated. An entropy with a fixed range for m and r of a time series is expressed as:

$$ApEn = (m,r) = \lim_{N\to\infty}\left[\phi^m(r) - \phi^{m+1}(r)\right] \tag{3.10}$$

For a finite time series consisting of given N data points, the estimated ApEn value of the times series is calculated as:

$$ApEn(m,r,N) = \phi^m(r) - \phi^{m+1}(r) \tag{3.11}$$

Equation (3.11) is used for practical purposes; it shows the similarity between the m to m+1 vectors in a time series. This estimated approximate entropy can determine a value based on the type of data such as periodic or complex time series. In order to implement this equation, the time series m to m+1 must be rearranged into dimensional vectors. Then, the distance between the data point vectors are calculated. The constructed vector is calculated by using a selected tolerance value for each dimension, Equation (3.6). Finally the ApEn value is obtained but the data length, N, an appropriate pattern length, m, and tolerance, r, must be determined.

3.4 Implementation of Techniques

In order to implement the three methods mentioned above, a series of MATLAB functions were developed for the calculation of RMS, kurtosis, and ApEn for the rotary joints data. The code developed made used of already available function in MATLAB for the calculation of the RMS and Kurtosis. However, the calculation of the Approximate Entropy is not already available in MATLAB and the algorithm described above was implemented.

Chapter 4

RESULTS

The rotary joints (A and B) were instrumented during fabrication with accelerometers to measure vibrations in the x, y and z (longitudinal) directions during their operation. For the study presented in this thesis, 27 datasets corresponding to different dates of operation were used. The RMS, Kurtosis and Approximate Entropy were calculated for all datasets for both the A and B rotary joints using the x and y acceleration data.

4.1 Rotary Joint A Datasets

The first procedure was to determine the datasets that show significant vibrations by using the accelerometer data in the form of subsets. The reason of using subsets was that the ApEn data results could not be calculated for the whole data set due to the technique code execution time. It was divided to a subset with 1000 elements since this gave the analysis the most efficient time. In order to make a better comparison between the three methods, subsets with 1000 elements were chosen for the three techniques.

The RMS mean, for the Rotary Joint A in the x and y directions, were calculated to determine the datasets with the more considerable values. These are illustrated in Figure 4.1 where the x-axis shows all the provided datasets. The results show that September 9, 2010 at 13 hr. and 25 min. and October 13, 2010 at zero hr. have the highest values of all the datasets. The RMS mean highest values are 61.71 μg and 54.06 μg for x and y respectively. Those results occurred on October 13, 2010. The other higher values are 54.46 μg for x and 46.10 μg for y on September 9, 2010. The rest of the datasets shown do not have mean values greater than 30 μg. Also, most of the mean values have higher values for the x than the y direction.

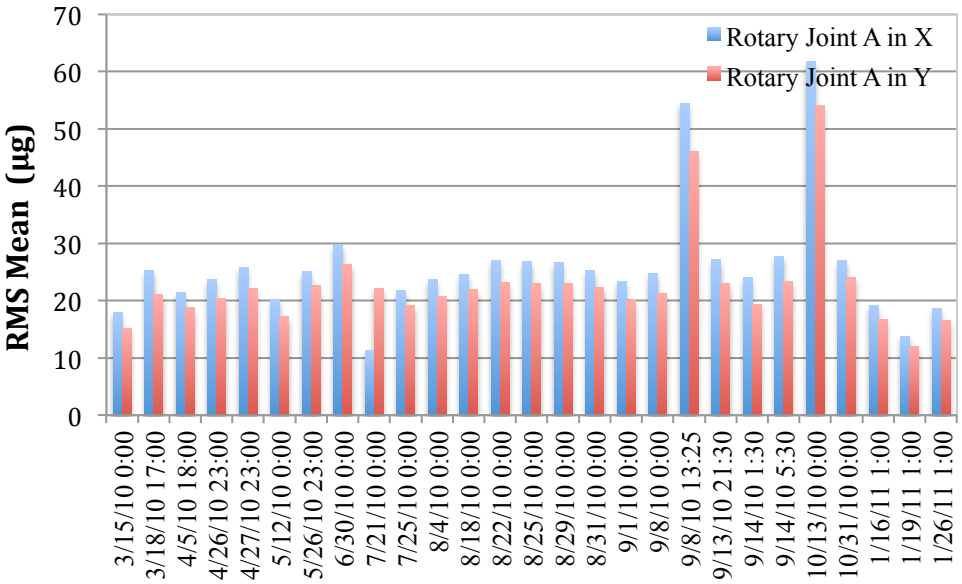

Figure 4.1 –Rotary Joint A Datasets RMS Mean

Kurtosis mean values were also calculated for all the given datasets. Figure 4.2 shows the x and y directions Rotary Joint A data. This technique has two datasets that show high mean values, which are September 8, 2010 at 13 hr. and 25 min. and October 13, 2010 at 0 hr. The

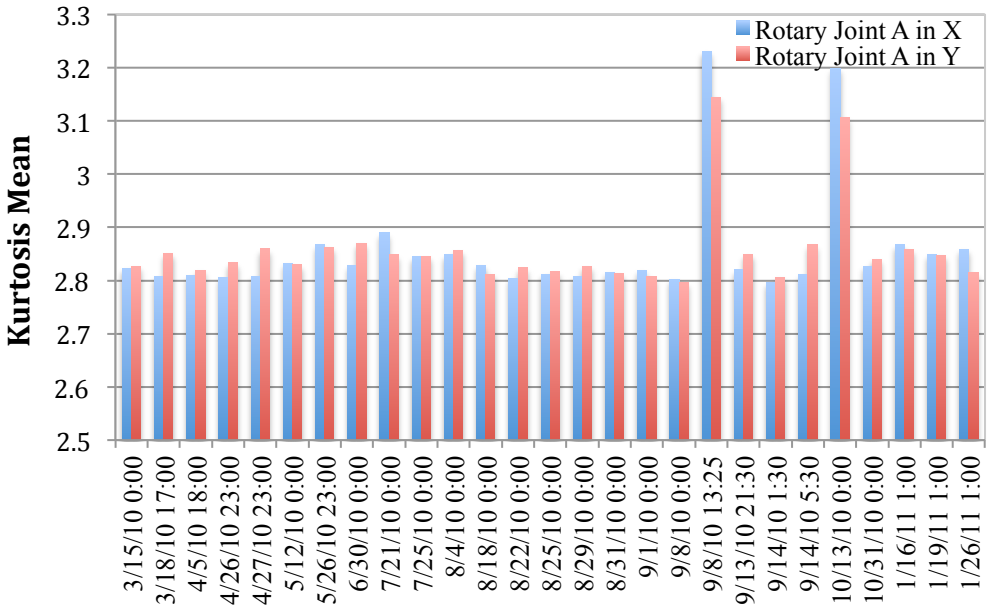

Figure 4.2 –Rotary Joint A Datasets Kurtosis Mean

results show that September 8 mean values have higher values, in both directions, than October 13 mean values. These are results greater than three which might indicate a possible defect. All the other data sets have similar values, which are less than 2.9.

Rotary Joint B Approximate Entropy mean values had similar results to the previous techniques mentioned. The highest mean values are on October 13, 2010 data set, which are above 1.40×10^{-5} as shown in Figure 4.3. The second most highest are on September 8, 2011 at 13:25, which are above 6.00×10^{-6}. The other dates show mean values below 6.00×10^{-6}. The x direction shows higher values than the y direction in most cases.

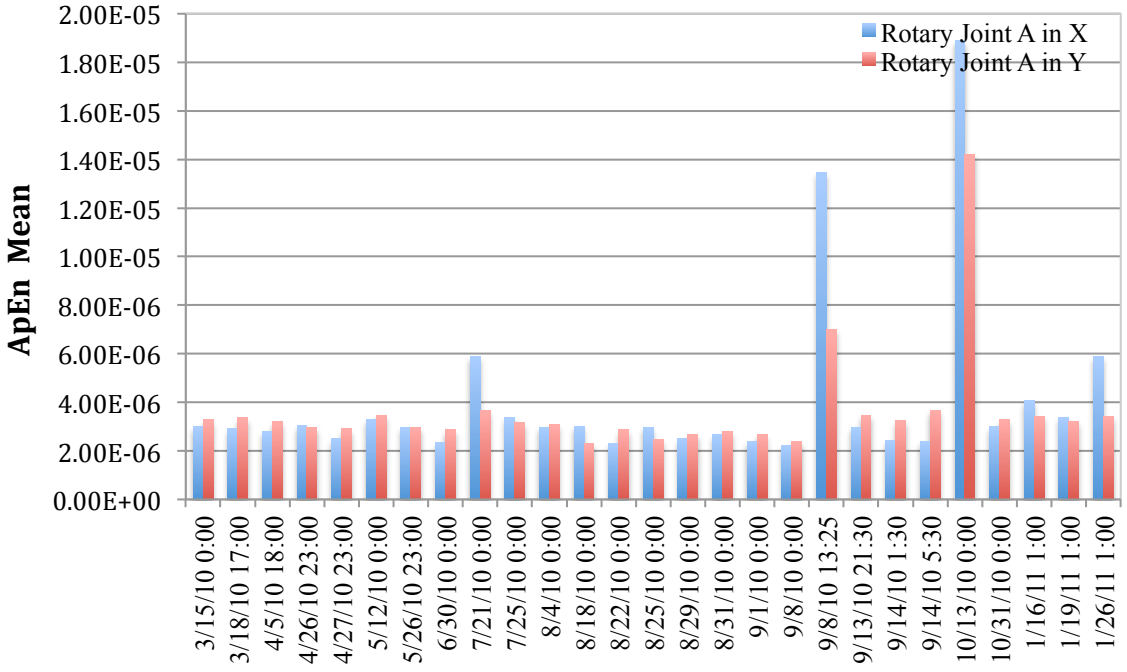

Figure 4.3 –Rotary Joint A Datasets ApEn Mean

4.2 Rotary Joint B Datasets

The Rotary Joint B datasets were also analyzed similarly to Rotary Joint A. The data was divided into subsets of 1000 elements to compare the RMS, kurtosis, and ApEn. Then, the three techniques mean values were calculated for all the dataset to determine significant values.

The RMS mean was the first method analyzed for Rotary Joint B. The results indicated that there are other datasets with significant mean values than the ones obtained in Rotary Joint A. These were May 26 at 23 hr., July 7 at 0 hr., August 22 and 25 at zero hr., and October 13, 2010 at zero hr. One difference is that the high mean values were only for the x direction. Also, September 8, 2010 at 13 hr. 25 min. did not show significant mean value as it did in Rotary Joint A. There was also more variability in the mean values since some had very high values while some have very low ones. These results are shown in Figure 4.4.

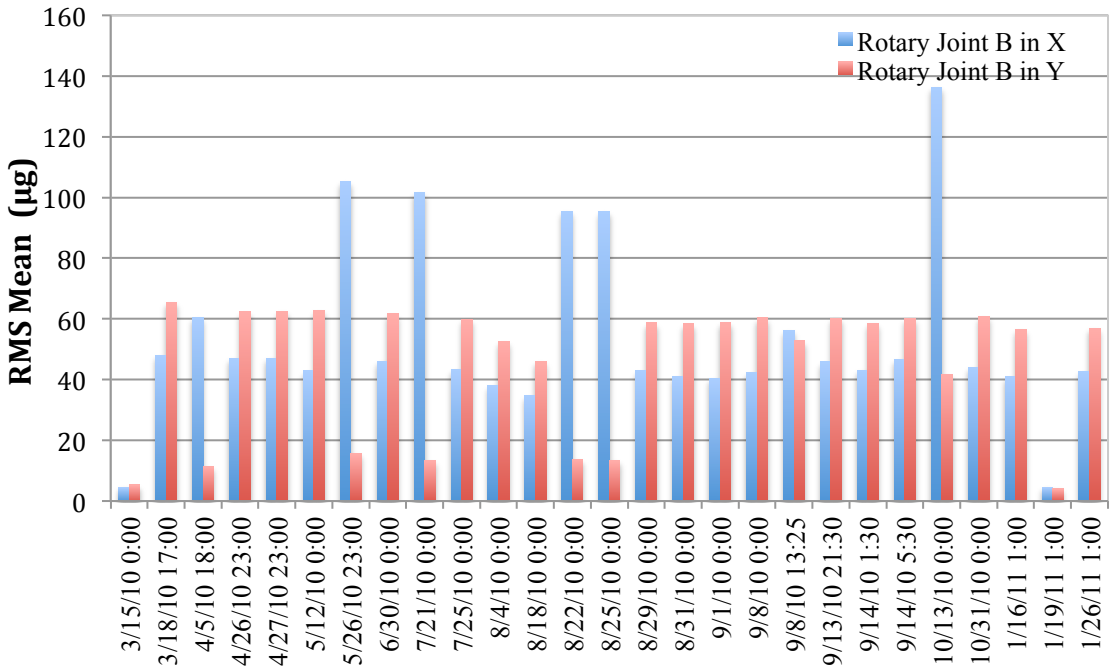

Figure 4.4 - Rotary Joint B Dataset RMS Mean

Rotary Joint B kurtosis means values showed different results than the technique previously mentioned. There was low variability with the results compared to other ones above. There were only two datasets that have mean values greater than 3, which were September 8,

2010 at 13 hr. 25 min. and October 13, 2010 at 0 hr. The data results do not show a prefer direction with high men values. This is illustrated in Figure 4.5.

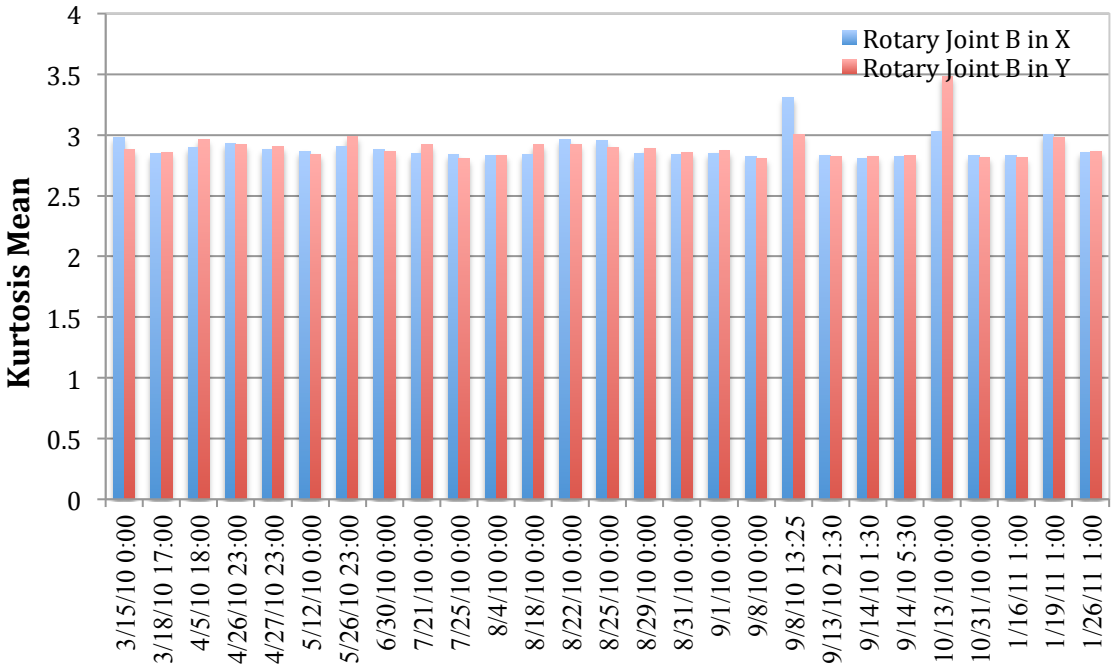

Figure 4.5 - Rotary Joint B Dataset Kurtosis Mean

Approximate Entropy mean values results were also different since it was only able to detect high variability in the dataset for October 13, 2010. The highest value for this was 4.49×10^{-5}, which is in the y direction. All the other datasets including October 13 data for the x direction did not show values greater than 1.50×10^{-5}. There were also higher mean values in the y direction than the x direction. Figure 4.6 has the ApEn results.

4.3 Spectrograms

Another analysis performed were the spectrograms, created by Boeing, for both rotary joints in the x and y directions. In order to create the Power Spectral Density (PSD) plots, a

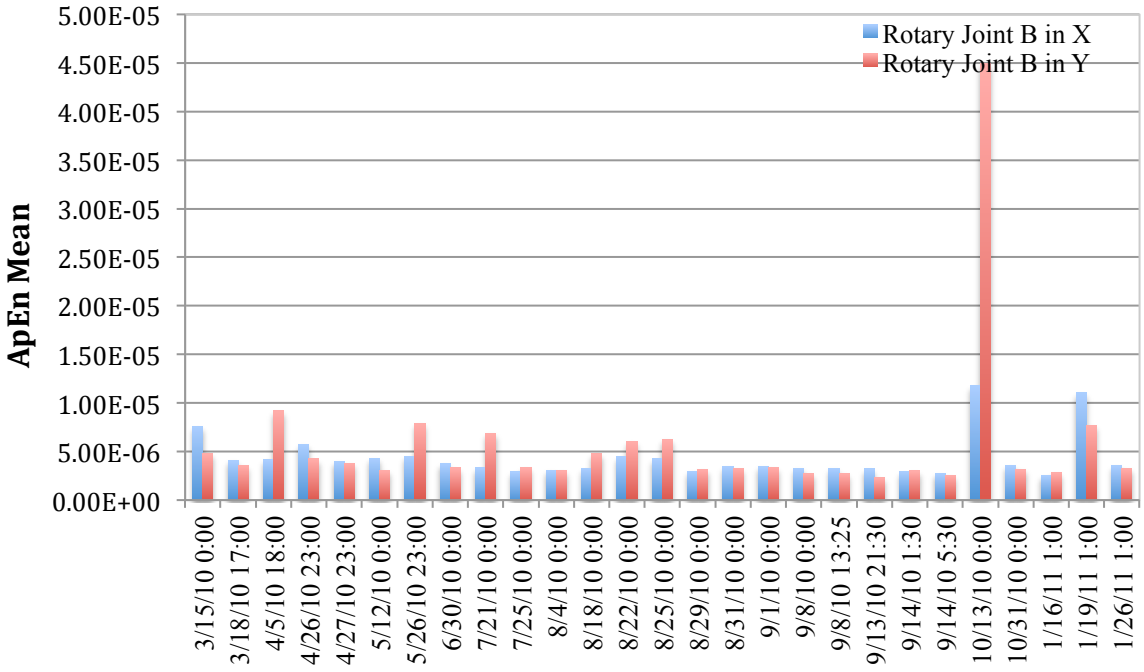

Figure 4.6 - Rotary Joint B Dataset ApEn Mean

MATLAB function called spectrogram was used. This function requires information such as the data to be analyzed, a windows function, the number of samples that each segment overlaps, the window function length, and the sampling frequency. The windows function used was a hamming window, the number of samples that overlap were 1024 with a 0.25 overlap fraction, and the sampling frequency used was 80 Hz. A total of four plots were created to compare them later with the three vibration signal techniques results. This includes two plots for the Rotary Joint A in the x and y directions and two for the Rotary Joint B as well. The datasets chosen were September 8 and October 13 for the Rotary Joint A and May 26, July 21, August 22, August 25, September 8, and October 13 for the Rotary Joint B. These datasets showed significant mean values than other datasets. The first plot created was for Rotary Joint A data in the x direction. Figure 4.7 illustrates the PSD plot and the results indicate that October 13 has a higher intensity than September 9 initially. The highest value is at frequency of approximately 0.5 Hz with a

value of 4.5 to 5 μg^2/Hz. September shows that the amplitude is not changing much at 1 and 2 Hz, after 0.3 sec., with a value approximate to 3.5 μg^2/Hz.

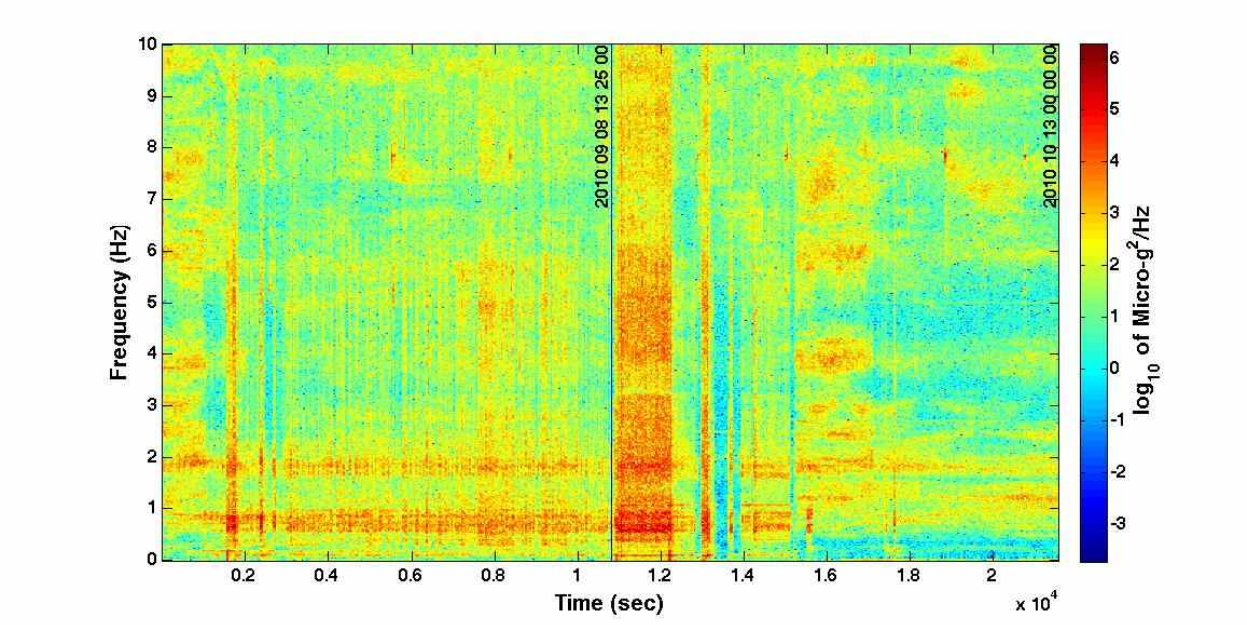

Figure 4.7 – Rotary Joint A Spectrogram in the X Direction

Another plot created was for the Rotary Joint A data in the y direction. Figure 4.8 illustrates the PSD plot and the results indicate that October 13 has significant intensity than September 9 initially. The highest value is at frequency of approximately 0.5 Hz with a value of 4.5 to 5 μg^2/Hz too. This figure looks very similar to Figure 4.7 since the datasets showed approximately the same amplitudes.

The Rotary Joint B results, in the x direction, were considered as well, which shows other datasets with significant peaks. Figure 4.9 shows the PSD plot and the results indicate that October 13 dataset has a higher intensity and longer time than the Rotary Joint A results. These high amplitudes are located at 0.5 to 1 Hz and close to 2 Hz with values of 4.5 to 5 μg^2/Hz too. The other dates from May to August seemed to show uniformity with amplitude of 3.5 to 4.5 μg^2/Hz.

The last PSD plot created was for the y direction. The results look similar to the Rotary Joint A in the y direction since the dates of May through August did not show the significant peaks and similar amplitudes. Figure 4.10 illustrates the PSD plot and the results indicate that

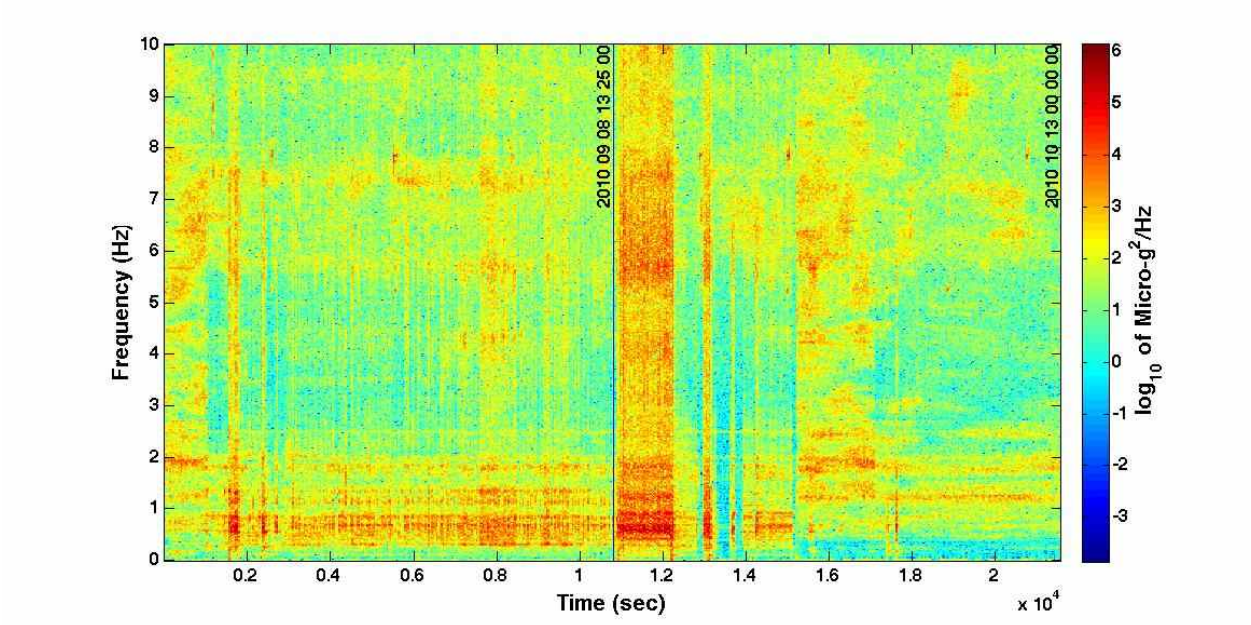

Figure 4.8 – Rotary Joint A Spectrogram in the Y Direction

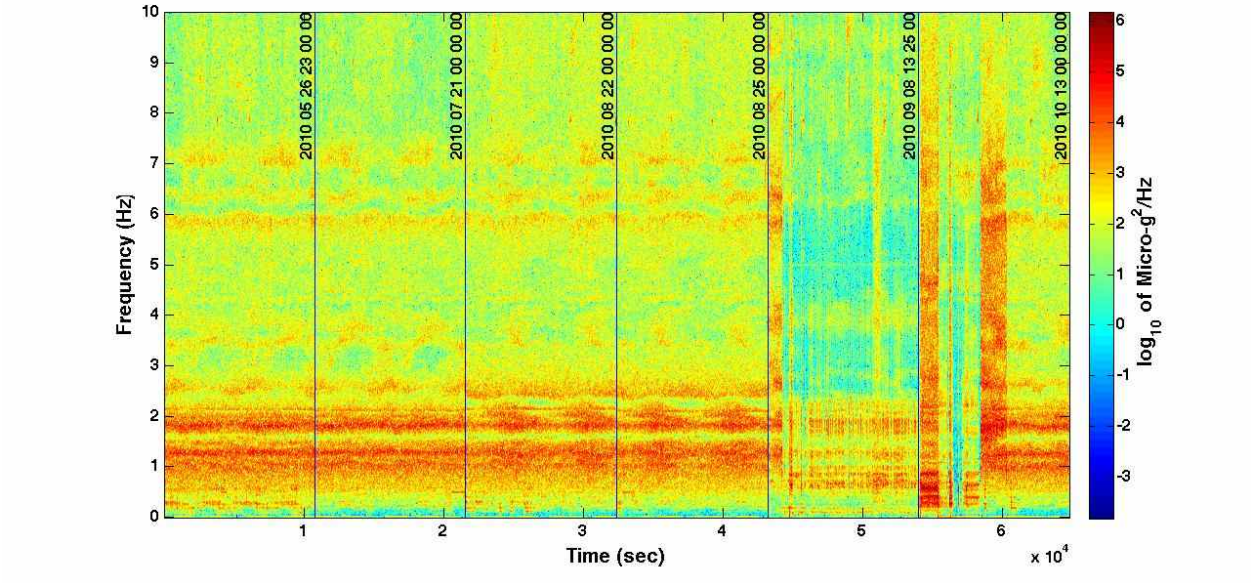

Figure 4.9 – Rotary Joint B Spectrogram in the X Direction

October 13 has significant intensity than September 9 initially. This figure does not look similar to Figure 4.9 since it does not show the same October amplitude intensity as the Rotary Joint B in x direction.

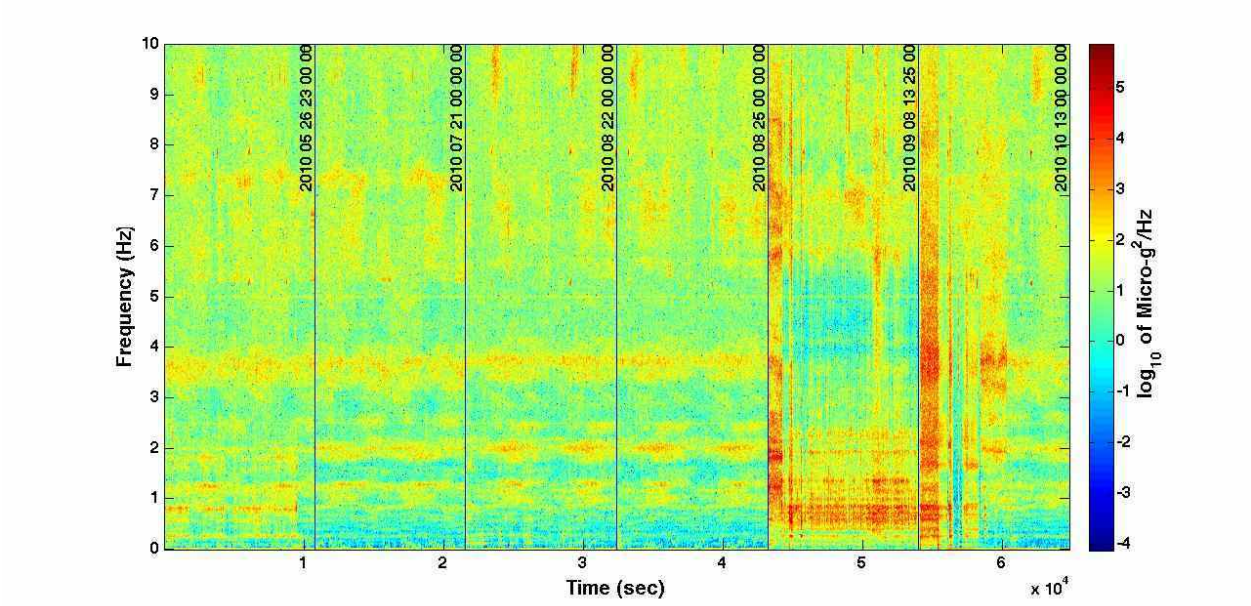

Figure 4.10 – Rotary Joint B Spectrogram in the Y Direction

4.4 Rotary Joint A Results in the X Direction

The techniques selected, to identify Rotary Joint A problems, were RMS, kurtosis, and ApEn. The datasets selected for the analyses are the ones studied in the previous section that had considerable amplitudes. In order to perform this investigation for the three methods, their data sets were divided into subsets as well.

The RMS, for Rotary Joint A data, had two particular datasets that shown high values compare to other ones. These were September 8 and October 13 as mentioned in Section 4.3. Three different analyses were performed to show the results for these two datasets, two analyses have low-pass filters of 5 Hz and 15 Hz respectively. However, the results with a low-pass filter

of 15 Hz and the analyses with no filter are only shown in the appendix. Figure 4.11 illustrates the RMS plot with 5 Hz low-pass filter, which shows a high initial RMS value, above 600 µg for October 13, then decreases rapidly. Then it starts to increase gradually between times 20 to 115 of 1000 sec., which approaches a RMS value of 630.1 µg. There is another significant RMS value at time 185 of 1000 sec. with a 396.7 µg magnitude. The plot has a high reduction after time 300 of 1000 sec. September dataset does not have values as high as October 13 but they are significant too. The more notorious are at time 127 and 191 of 1000 sec. with magnitudes of 320.9 and 297.2 µg respectively. The data starts to become more stable afterwards similarly to the PSD plot.

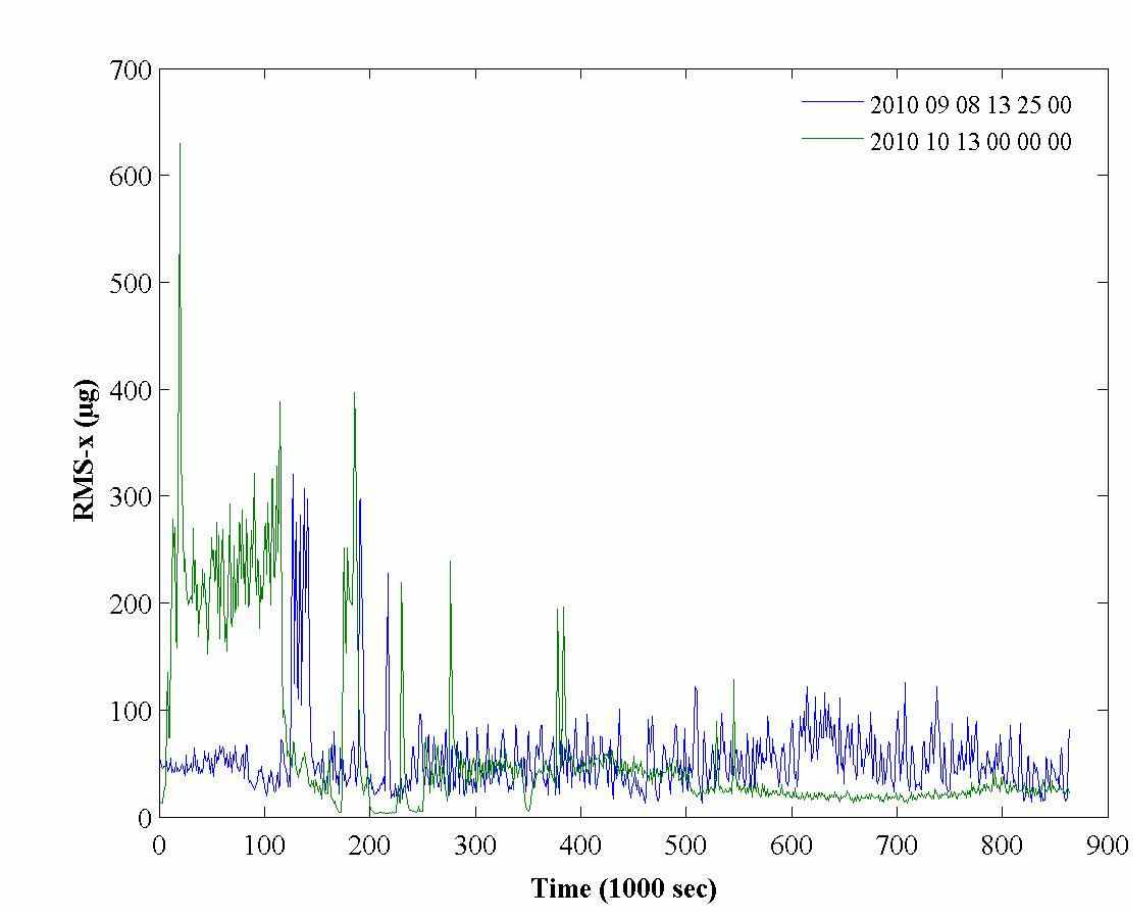

Figure 4.11– Rotary Joint A RMS in X with Low Pass Filter 5 Hz

Kurtosis, which is the other method, was also plotted. The dates that showed a significant kurtosis value, in the x direction, were September 8 and October 13. Similar to the RMS, the plot has a low-pass filter of 5 Hz as illustrated in Figure 4.12. For September 8, the more significant kurtosis values are located at time 291 of 1000 sec., which shows the highest value for the whole plot. The kurtosis doesn't have the stability at the final time as the RMS plots since the there is a kurtosis of 13.66 at time 845 of 1000 sec. October 13 data does not have the highest value as the previous plot. This might imply that one of the two methods is giving a spurious result. The only three peaks that are notorious are at time 226, 251, and 528 of 1000 sec. where time 226 of 1000 sec. has the highest magnitude of 18.44. It is able to detect the excessive vibrations but not at the same time as the PSD plot.

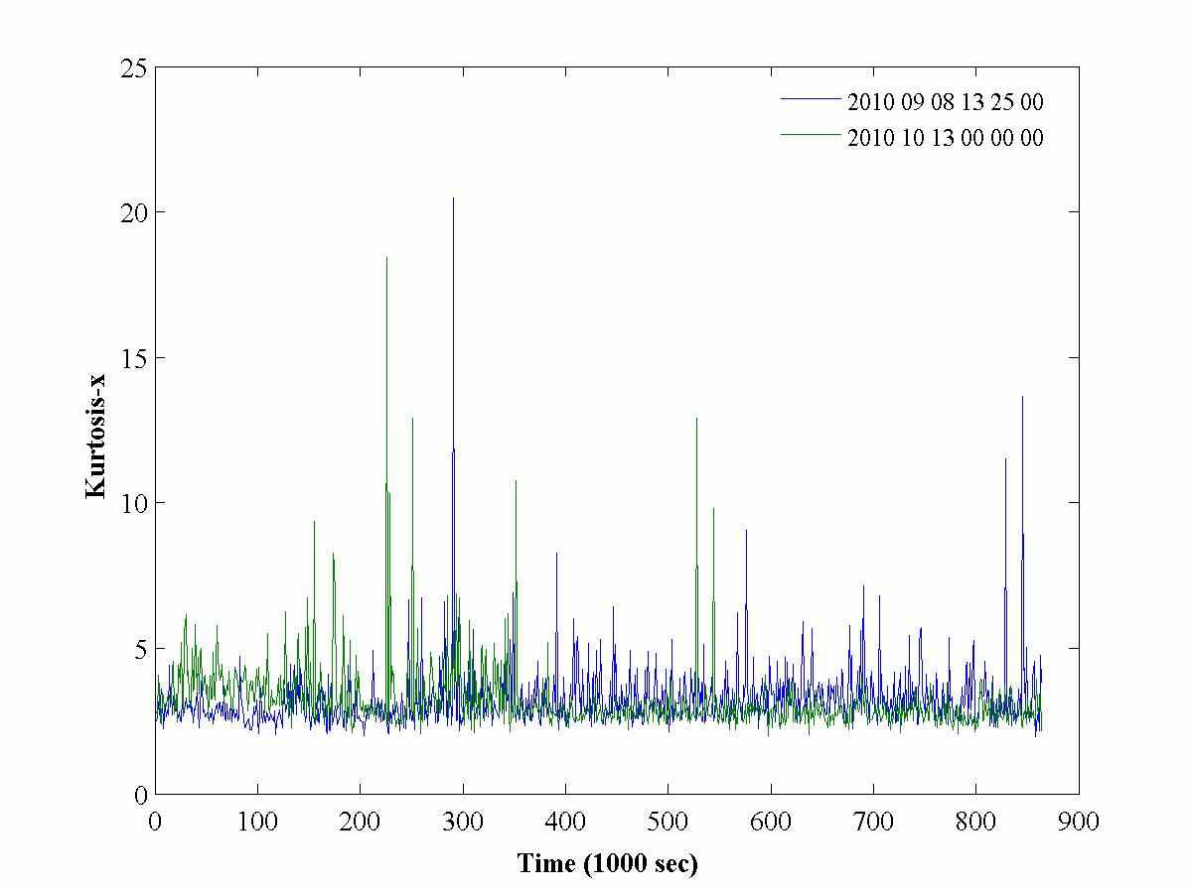

Figure 4.12 – Rotary Joint A Kurtosis in X with Low Pass Filter 5 Hz

The final technique used was the Approximate Entropy (ApEn) where two parameters were selected to perform the ApEn analyses. Those are the pattern length, m, and the tolerance constant, r as explained in chapter 3. The m is a parameter that changes the dimensional vectors size created from the time series data. The m chosen for this analysis was two since the higher the pattern length implies a higher computational cost. Yan and Gao explained that an increase in m from two to ten leads to three times the computation time [21]. The tolerance constant, k, which is needed to get the tolerance, r, and the similarity calculation vector, C_i^m, was selected as six. Yan and Gao explained that a k greater than 0.4 reduces the variation of ApEn with different m values, therefore a high k value implies a reduction in the variability. This is not desired since a small variability indicates small ApEn values causing the data to show that there are not rotary joint possible damage. In order to get the tolerance constant, different numbers were considered from 0.4 to 8 where a k of 6 was chosen. Lower values than 6 gave an approximate entropy with no real solution and higher values than 6 reduced the variability significantly. Figure 4.13 shows the Approximate Entropy with 5 Hz low-pass filter. The highest value is located at time 226 of 1000 sec with a value of 0.0039 for October 13 data. Unlike the RMS plot, the October data tends to be higher initially while the September data do not show any significant peak. It is only able to detect one of the excessive vibrations, October 13, as the PSD plot does.

4.4 Rotary Joint A Results in the Y Direction

The RMS plots in the y direction were first created for the Rotary Joint A data that showed high values compare to other datasets. These were September 8 and October 13 as mentioned in Section 4.1. One plot was created to show the results for these datasets, which have a low-pass filters of 5 Hz. Figure 4.14 illustrates the RMS plot, which shows a high initial RMS

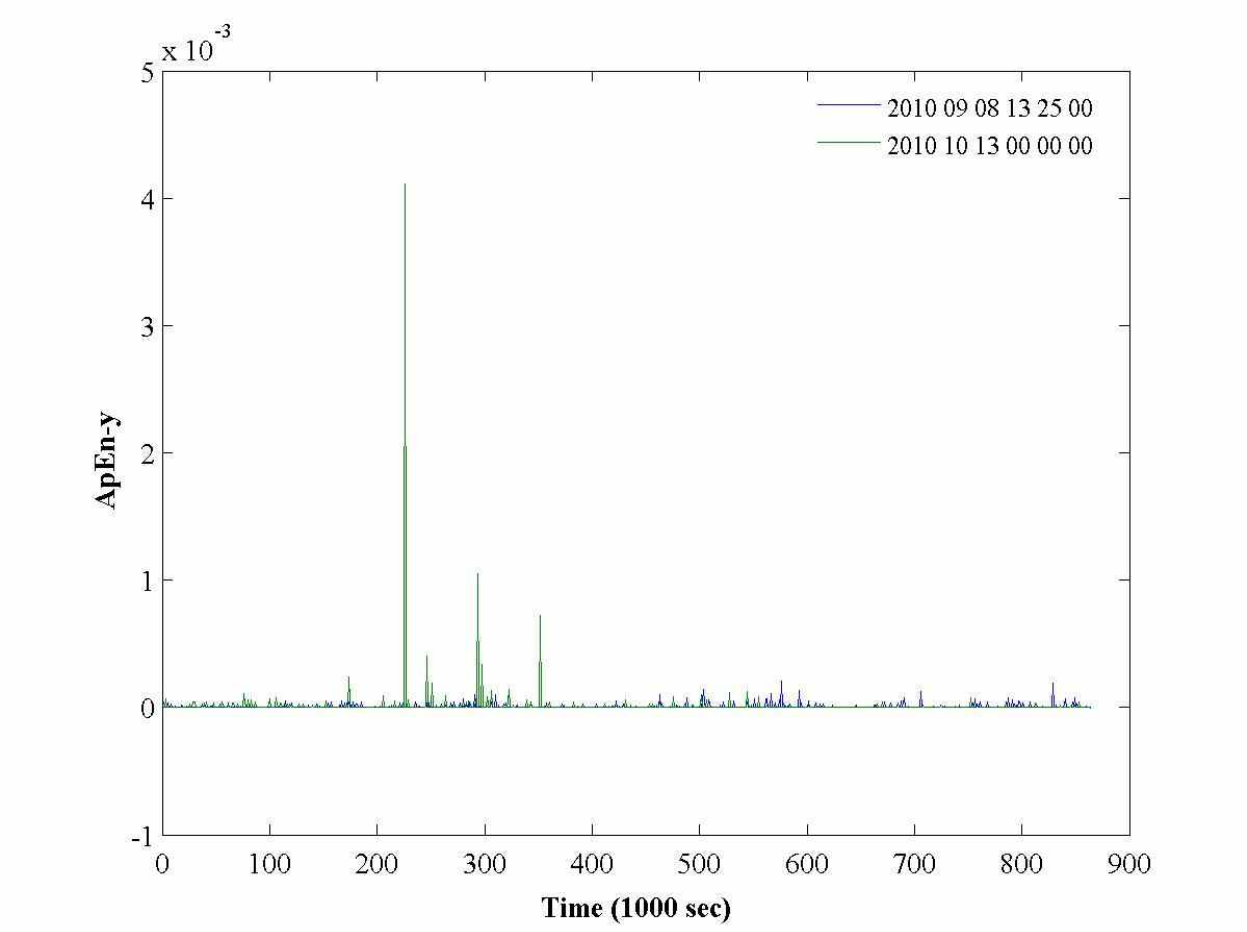

Figure 4.13 – Rotary Joint A ApEn in X with Low Pass Filter 5 Hz

It shows value above 400 µg for October 13, and then decreases rapidly. It also starts to increase gradually between times 25 to 121 of 1000 sec., which approaches a RMS value of 438.40 µg at time 20 of 100 sec. There is another significant RMS value that increase at time 185 of 1000 sec. with a 319.2 µg magnitude. The plot has a high reduction after time 550 of 1000 sec. September 8 data doesn't have values as high as October 13 but they are significant too. The more notorious are at time 129 and 192 of 1000 sec. with magnitudes of 272.3 and 287 µg respectively. The data starts to become more stable afterwards but more intense than October 13.

Kurtosis was also plotted, similar to the RMS, for the Rotary Joint A triaxial accelerometer assembly. The datasets that showed a significant kurtosis value, in the y direction,

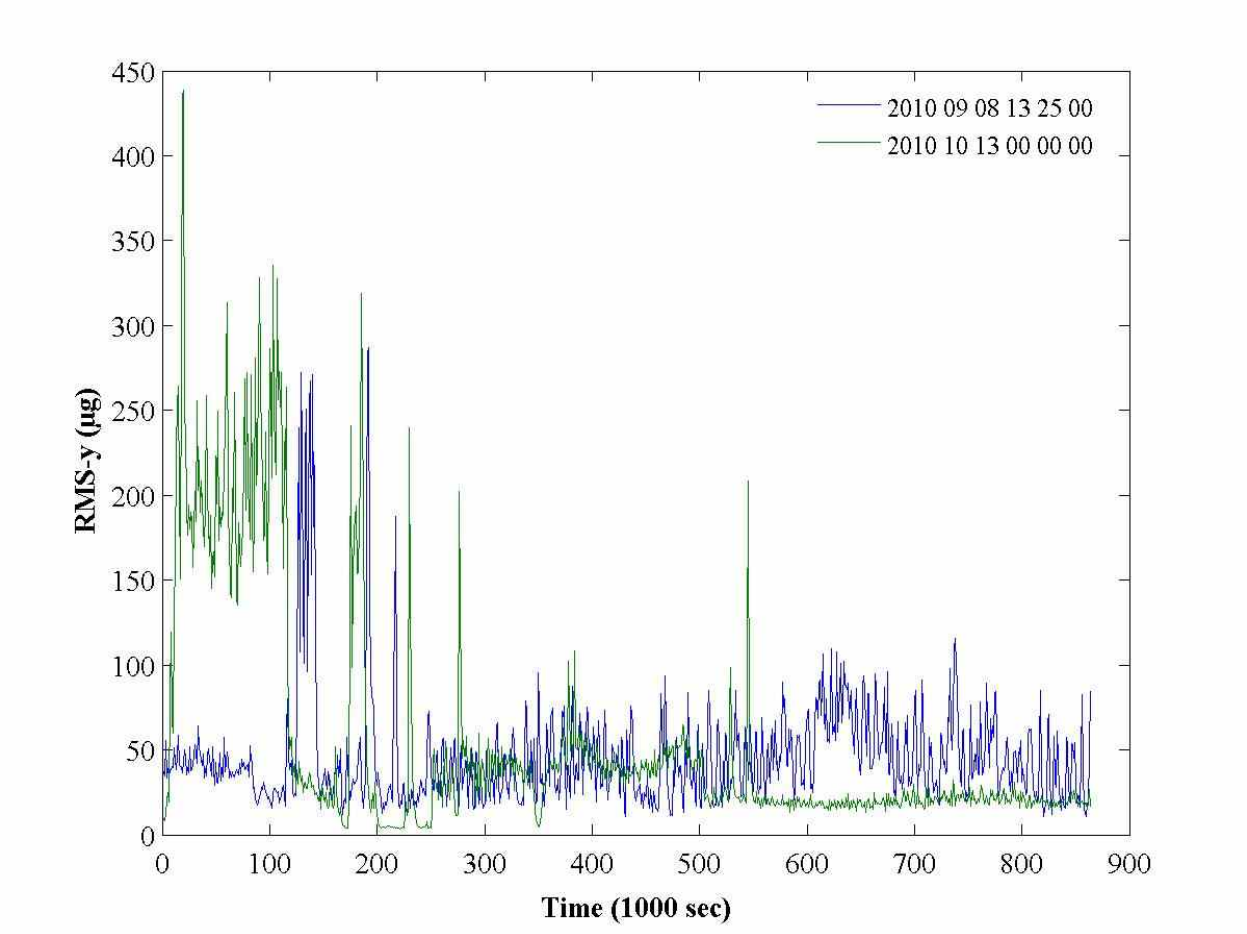

Figure 4.14 - Rotary Joint A RMS in Y with Low Pass Filter 5 Hz

were the same dates as the previous technique. A plot was created with a low-pass filter of 5 Hz where Figure 4.15 illustrates it. October 13, the more significant kurtosis value is located at time 226 of 1000 sec., which it is 25.09. On the other hand, September 8 dataset does not show kurtosis values higher than 10. There is not a lot of similarity between the PSD and kurtosis plots at the time the peaks occurred.

The final technique used, in the y direction, was the Approximate Entropy (ApEn) where a plot was created to determine a rotary joint possible problem. The pattern length and tolerance constant chosen are the same as the x direction data. Figure 4.16 shows the Approximate Entropy with 5 Hz low-pass filter. The highest value is located at time 226 of 1000 sec with a value of

0.0041 for October 13 data. Other notorious peaks, for the same dataset, are on time 300 and 360 of 1000 sec. September data do not seem to have high peaks as the PSD plot had at the initial time.

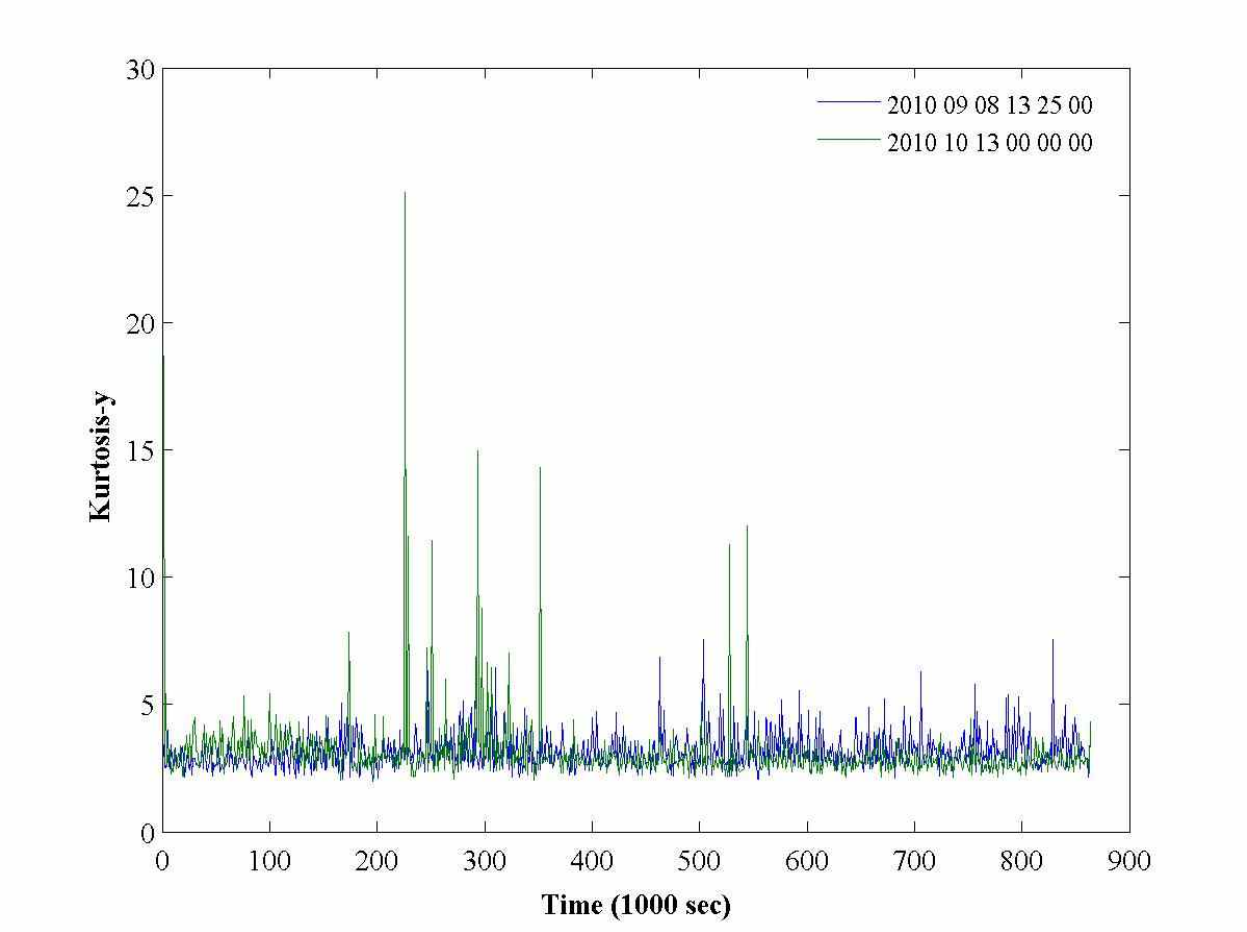

Figure 4.15 - Rotary Joint A Kurtosis in Y with Low Pass Filter 5 Hz

4.5 Rotary Joint B Results in the X Direction

The same techniques mentioned above were used to identify Rotary Joint B problems. There were more dates that had considerable vibrations than the Rotary Joint A data for the RMS. The dates selected are May 26, July 21, August 22, August 25, September 8, and October 13, which were shown on Section 4.3. However, the kurtosis results only showed high mean

values on September 8 and October 13. In order to obtain the results for the three methods, the datasets were divided into 1000 elements subsets too.

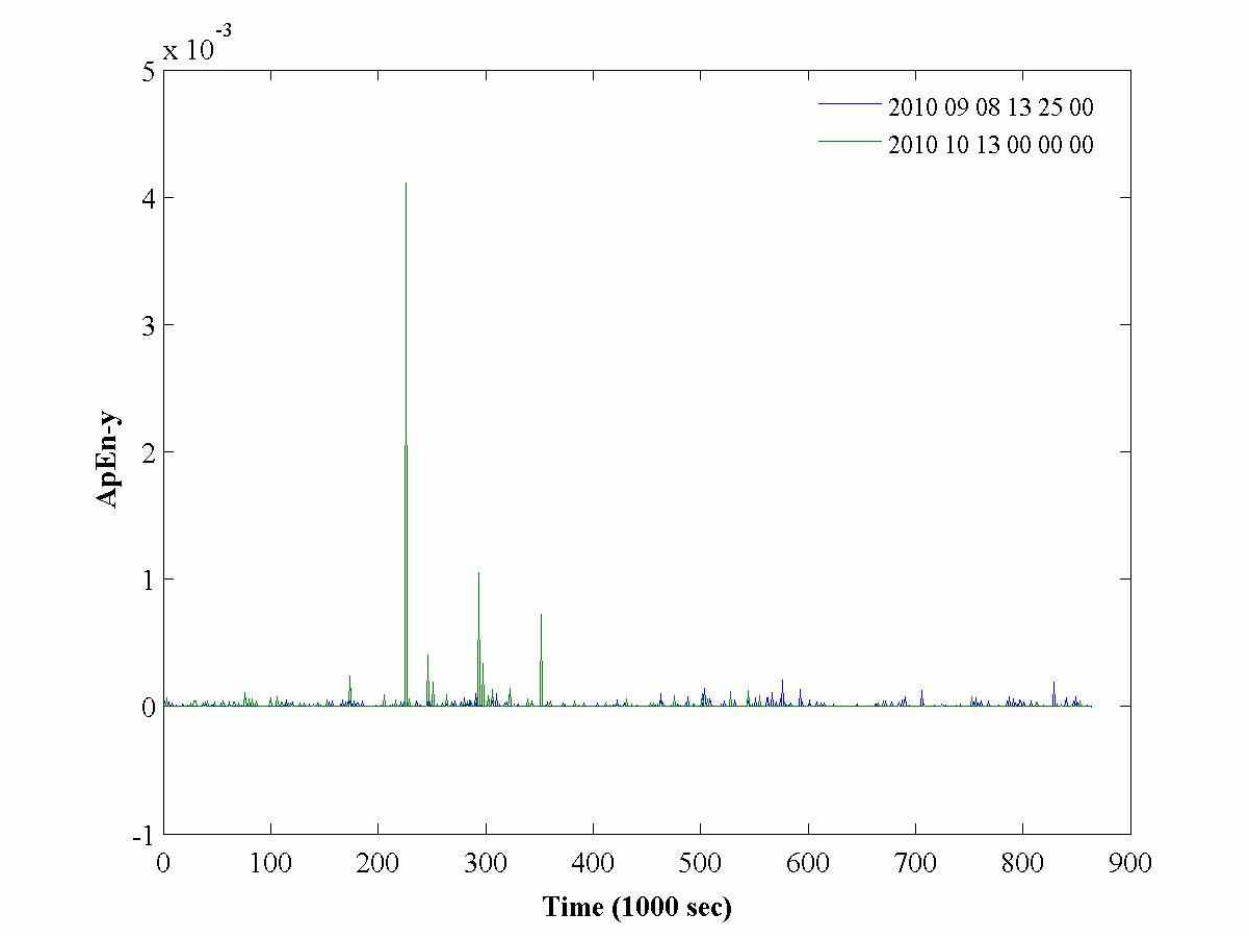

Figure 4.16 - Rotary Joint A ApEn in Y with Low Pass Filter 5 Hz

The RMS in the x direction for the Rotary Joint B data had much higher values for October 13 and September 8 than the other datasets. A plot was created to show the results for these two dates. Figure 4.17 illustrates the RMS plot with 5 Hz low-pass filter, which shows a high initial RMS value, above 500 μg for October 13, then decreases rapidly. There is another significant RMS increase at time 185 of 1000 sec. with a 424.9 μg magnitude. The plot has a high vibration between time 350 and 510 of 1000 sec. September 8 data doesn't have values as high as October 13 but they are significant too. The more notorious is at time 134 of 1000 sec.

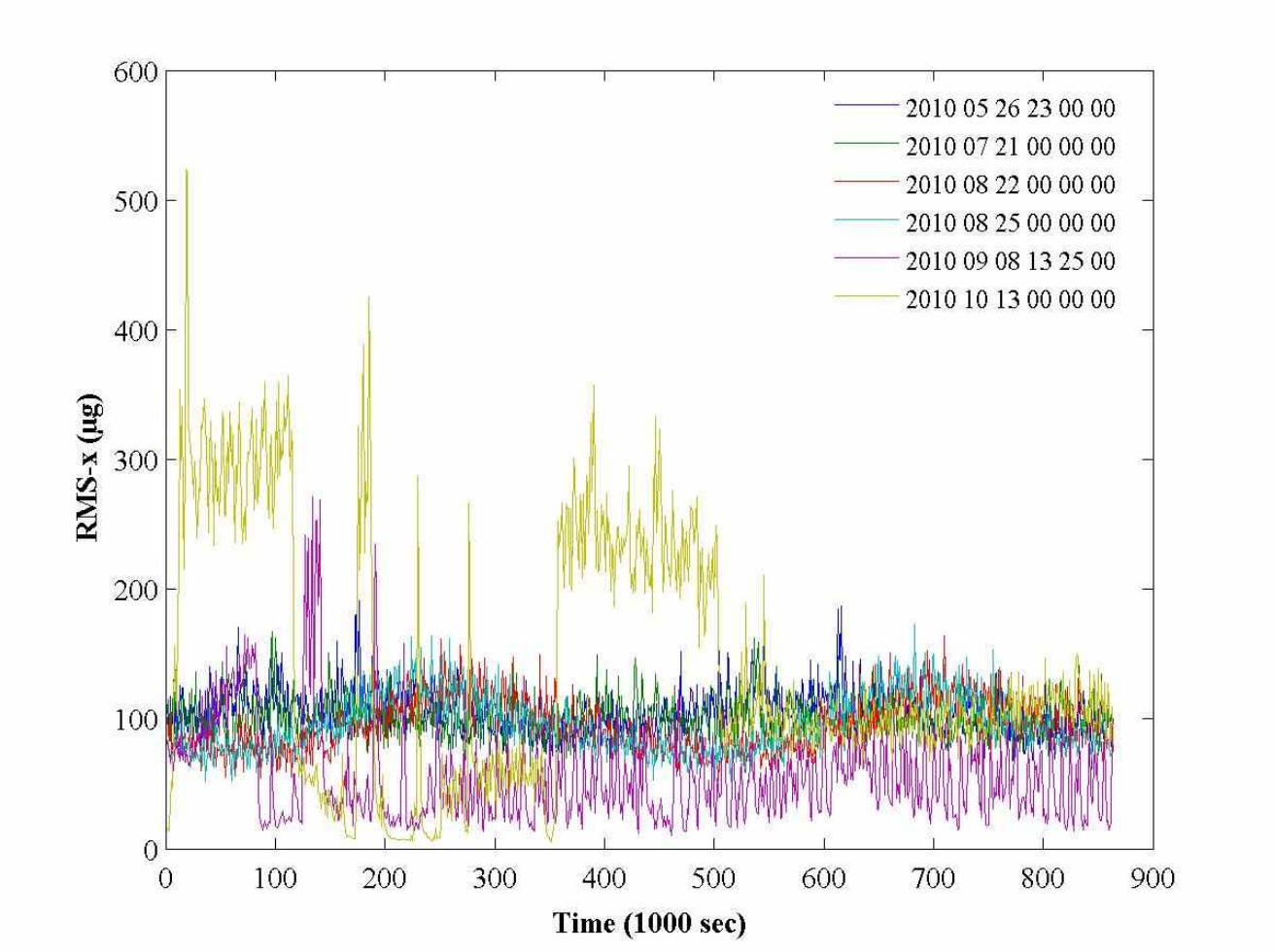

Figure 4.17 – Rotary Joint B RMS in X with Low Pass Filter 5 Hz

with a value of 271.2 µg. The data starts to become more stable at a later time. The dates from May to August do not show a particular peak as the other two datasets; however they show high RMS values through out the whole time where the mean seems to be close to 100 µg. These results show similarity with the PSD plot amplitudes.

Kurtosis, for the Rotary Joint B data, was also plotted. The datasets that showed a significant kurtosis value, in the x direction, were September 8 and October 13 but the other datasets from May to August do not show high kurtosis values. Figure 4.18 illustrates kurtosis

versus time plot. For September 8, the more significant kurtosis values are located after time 290 of 1000 sec where some values go as high as 11. For October 13 data, the high values are

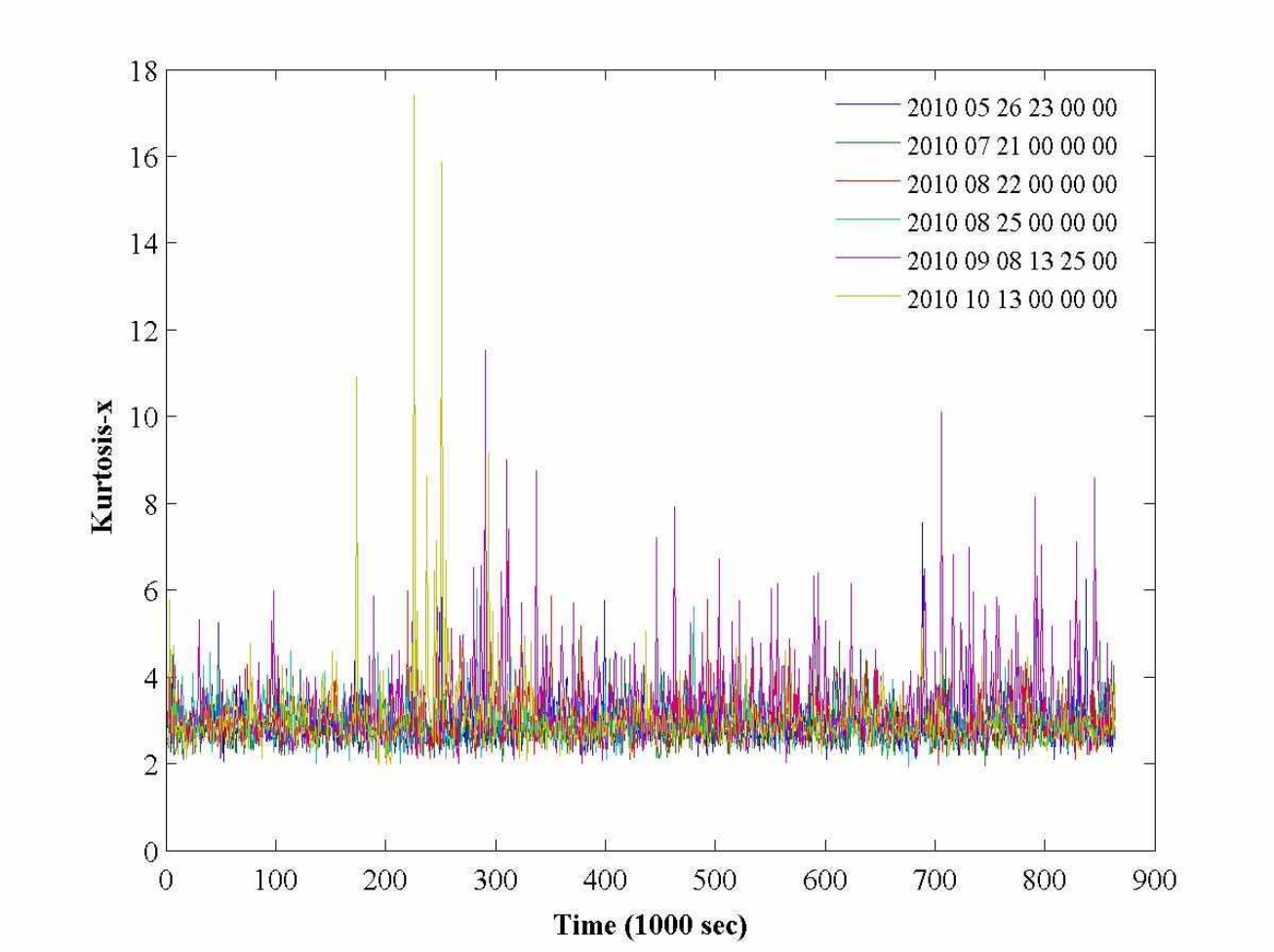

Figure 4.18 – Rotary Joint B Kurtosis in X with Low Pass Filter 5 Hz

between time 170 and 294 where the highest is 17.41 at time 226 of 1000 sec. The other dataset do not show a particular peak, the results have values close to three through the whole time. These do not show very similar results with the PSD plot since it is not able to detect the high vibrations from May to August.

The final technique used was the Approximate Entropy (ApEn). The pattern length chosen was two and tolerance constant chosen was six, which are the same used in Rotary Joint

A. Figure 4.19 shows the Approximate Entropy with 5 Hz low-pass filter. The highest value is located at time 226 of 1000 sec with a value of 0.00391 for October 13 data. The September data does not show peaks as high as October but they tend to increase at the final time. This might be a spurious peak since there are no high amplitudes in the PSD plot final time. The other months of May through August do not show particular peaks. Similarly to kurtosis, it is not able to detect all the high vibrations as the PSD plot.

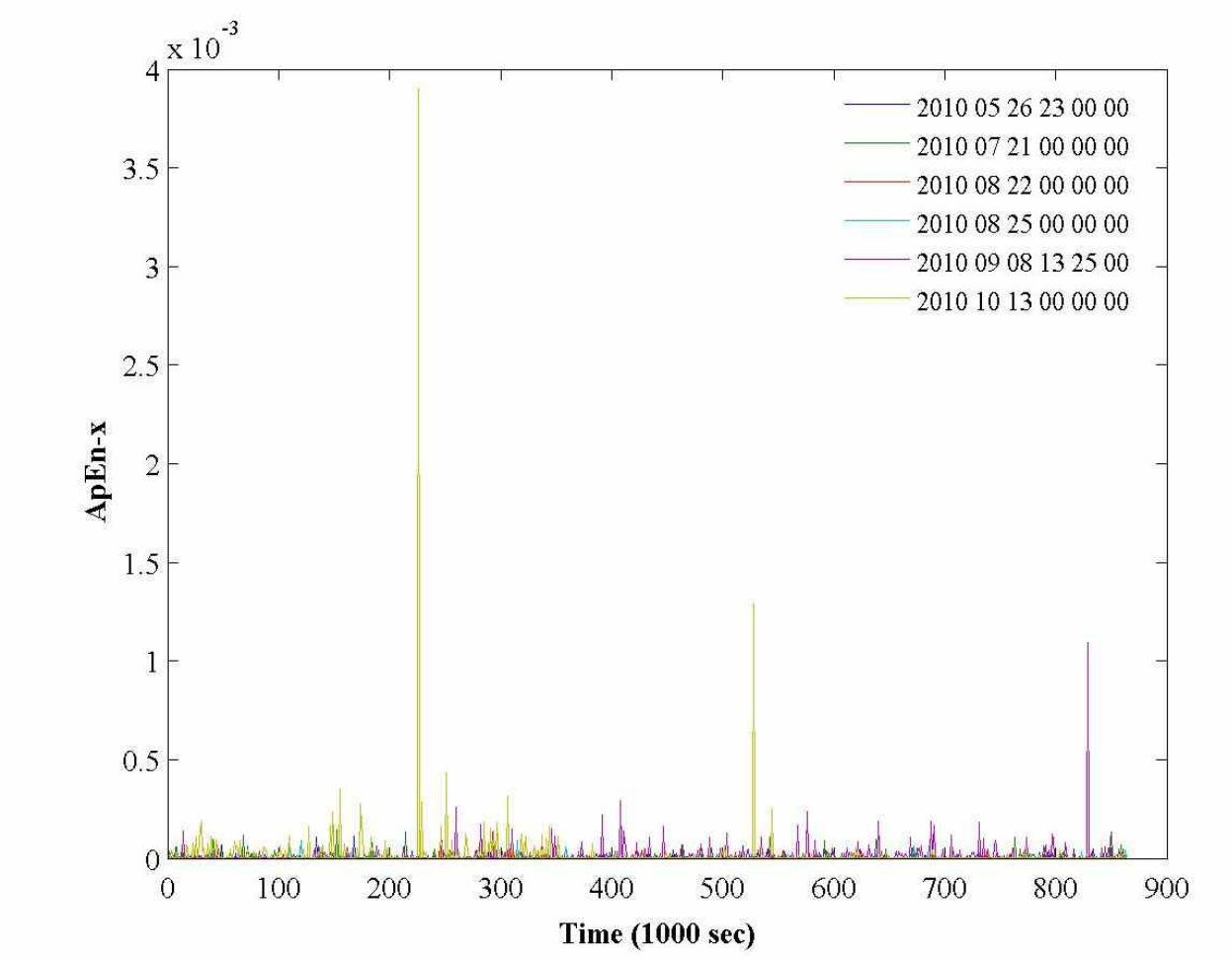

Figure 4.19 – Rotary Joint B ApEn in X with Low Pass Filter 5 Hz

4.6 Rotary Joint B Results in the Y Direction

There were two dates that had considerable vibrations for Rotary Joint B in the y direction data. The datasets were September 8 and October 13, which is different than the other direction since this had less datasets with considerable values.

The RMS in the y direction for the Rotary Joint B data had much higher values for October 13 followed by September 8 than the other dates. A plot was created to show the results for these two dates, the plot has a low-pass filter of 5 Hz. Figure 4.20 illustrates the RMS plot, which shows a high initial RMS value, above 250 µg for October 13, then decreases rapidly.

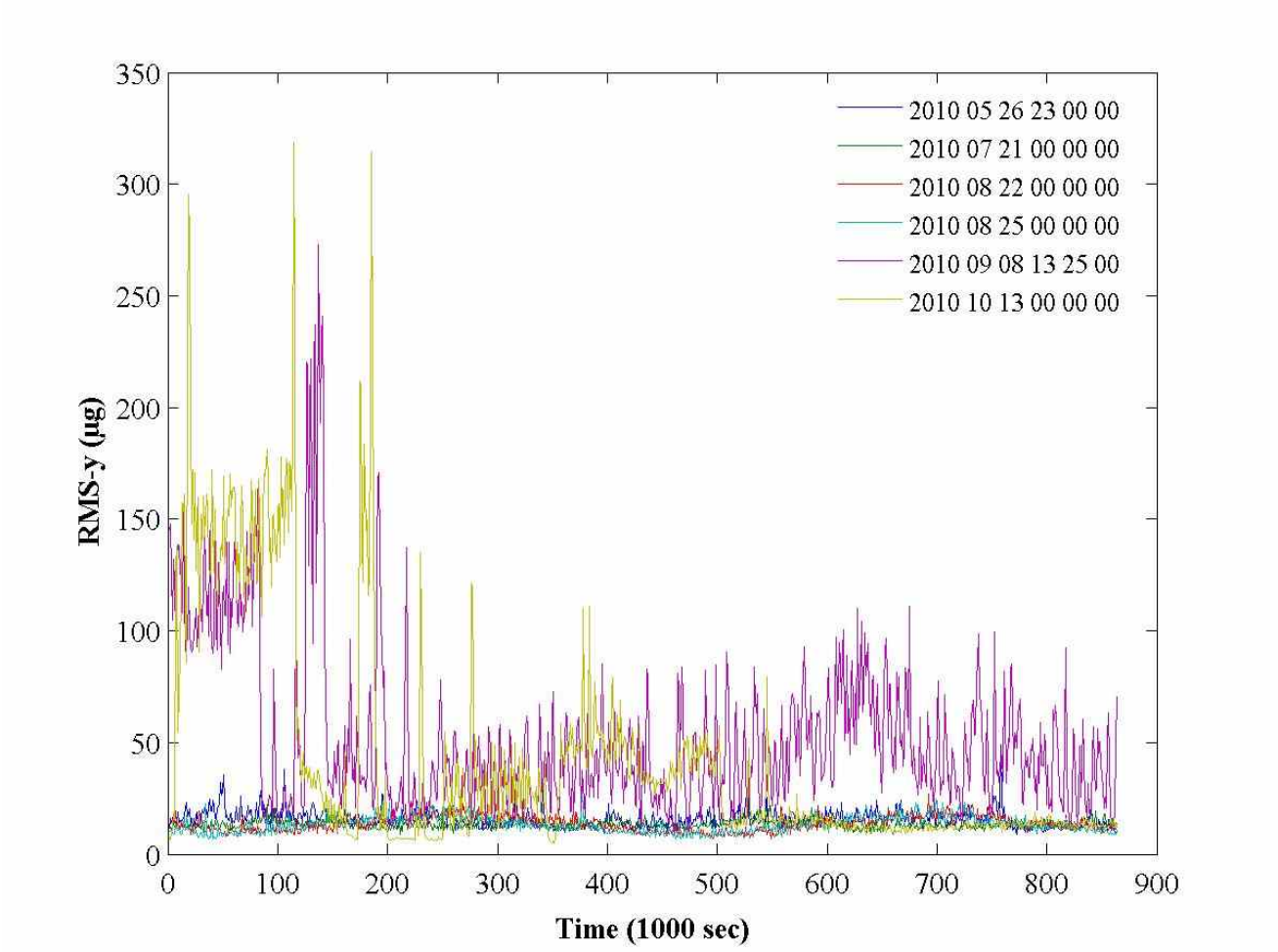

Figure 4.20 – Rotary Joint B RMS in Y with Low Pass Filter 5 Hz

Then it starts to increase gradually between times 22 to 113 of 1000 sec., which approaches a RMS value of 318.5 µg. There is another significant RMS increase at time 185 of 1000 sec. with

a 312.2 µg magnitude. The September 8 most notorious value is at time 134 of 1000 sec. with a value of 273 µg. The data starts to become more stable at a later time. The datasets from May to August don't show a particular peak as the other two; they do not show high RMS values through almost the whole time, which differs from the x direction. It also is able to detect the same excessive vibrations as the PSD plot since they do not detect problems with the first four datasets, May through August, analyzed.

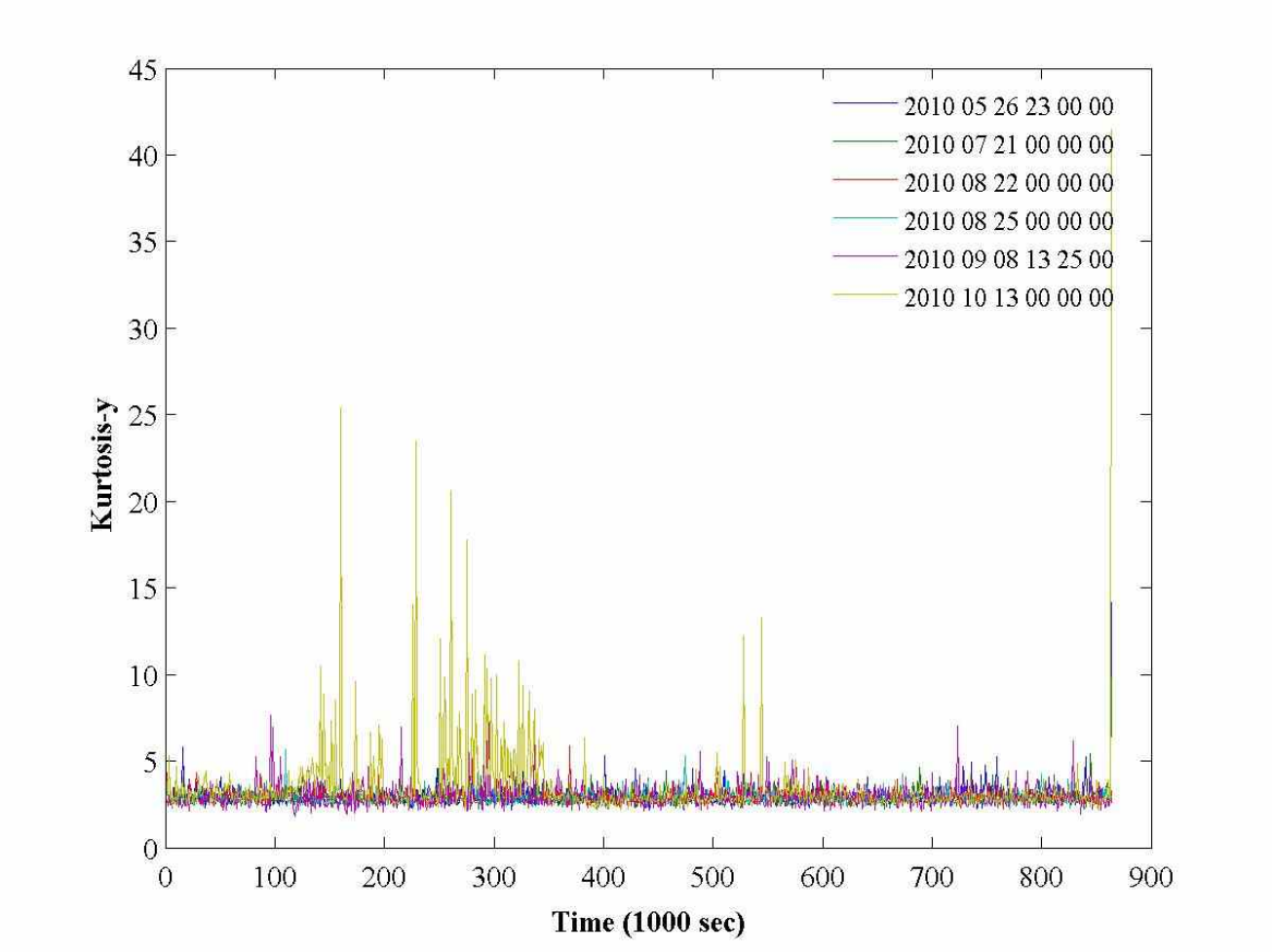

Figure 4.21 – Rotary Joint B Kurtosis in Y with Low Pass Filter 5 Hz

The datasets that showed a significant kurtosis value, in the y direction, were September 8 and October 13 but from May to August do not show high kurtosis values. Figure 4.21 illustrates kurtosis versus time plot with a 5 Hz low-pass filter. For September 8, the more

significant kurtosis values are located after time 215 of 1000 sec. where some values go as high as 7. For October 13 data, the high values are between time 142 and 345 of 1000 sec. where the highest is 25.38 at time 160 of 1000 sec. Also, there is another kurtosis with a value of 41.49 at time 864 of 1000 sec., which is much higher than the other values detected. The other four datasets do not show a particular peak. It is only able to detect some datasets excessive vibrations as the PSD plot.

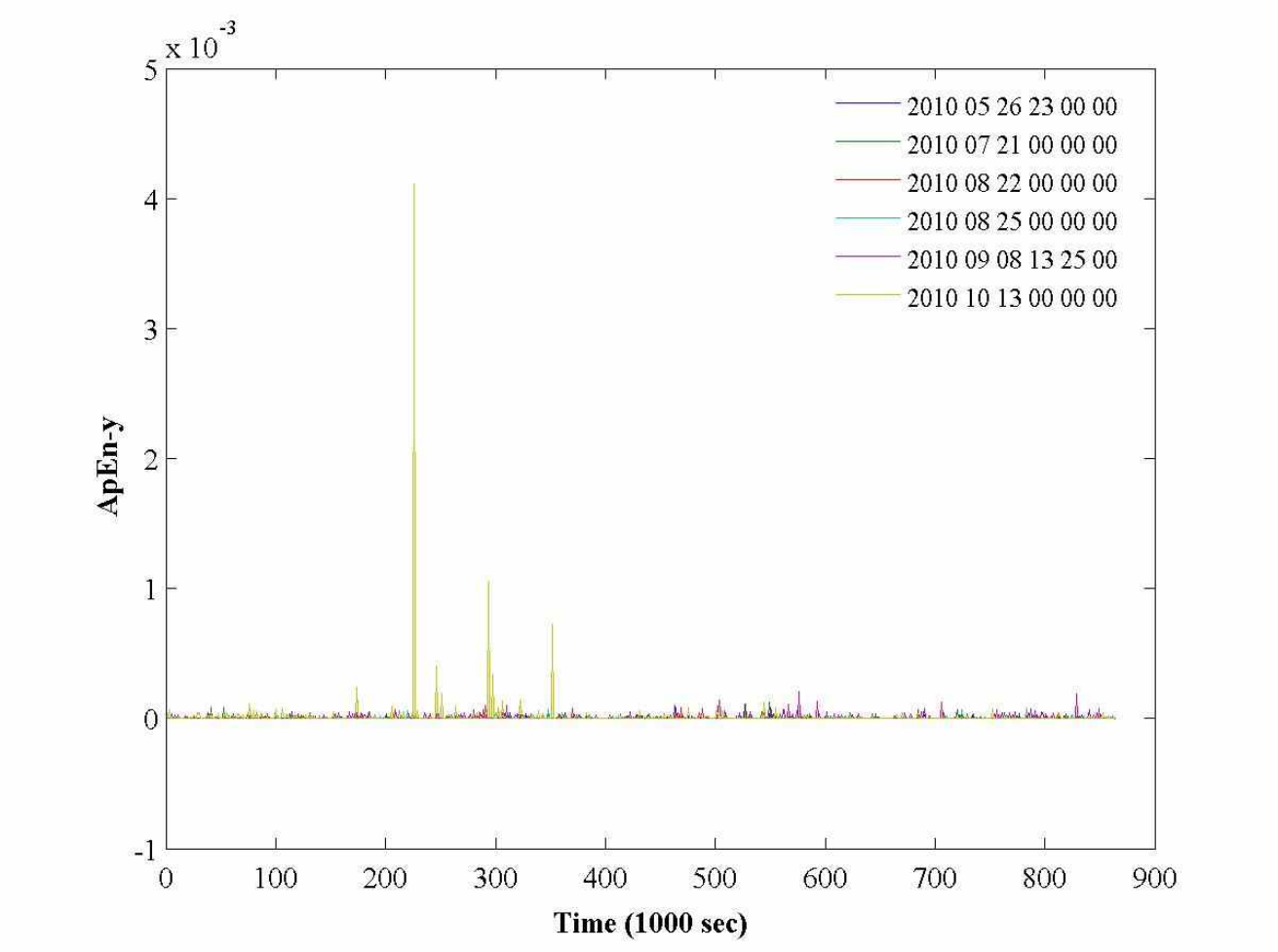

Figure 4.22 – Rotary Joint B ApEn in Y with Low Pass Filter 5 Hz

The final technique used was the Approximate Entropy (ApEn) with the same pattern length and tolerance used before. Figure 4.22 shows the Approximate Entropy with 5 Hz low-pass filter. The highest value is located at time 226 of 1000 sec. with a value of 0.00411 for

October 13 data. The September data does not show high peaks as the October 13 dataset. The other datasets of May through August do not show particular peaks. It is only able to detect an excessive vibration similar to the PSD plot.

Chapter 5

SUMMARY AND CONCLUSIONS

5.1 Summary

The rotary joints anomaly was described in detail and the studies leading to the identification of the cause were discussed. After Rotary Joint A anomaly occurred in September 2007, the investigations determined that this was produced by the lubrication lost and excessive friction between the race ring and bearing rollers. The bearing assemblies replacement and a new lubricant were necessary to improve the anomaly. However the collection of accelerometers data continues in order to investigate the station vibration. Several monitoring techniques were found to be useful in detecting bearing defects where three were selected due to their effectiveness in identifying defects. The monitoring techniques were the Root-Man-Square (RMS), kurtosis, and Approximate Entropy (ApEn). Theses methods were used to identify changes in the response of the rotary joints that might indicate a possible progression of damage. The analyses consisted in determining the datasets with high vibrations by using the three signal processing methods. Then, Power Spectral Density (PSD) plots for the Rotary Joints A and B in the two directions (x and y) were developed to better understand and make comparisons of datasets showing excessive vibration. The result indicated that the RMS technique has more similarity to the created spectrograms (PSD) followed by kurtosis, and then ApEn.

5.2 Conclusion and Recommendations

The results obtained indicate that the Rotary Joint B had more datasets with excessive vibration than the Rotary Joint A, which was the one with problems before the re-lubrication and replacement of the damaged bearing assemblies. The RMS plots results were able to detect most

datasets with excessive vibration. Kurtosis was able to detect the two datasets with the most excessive vibrations but it was not able to detect the other four considerable vibrations in Rotary Joint B. ApEn was only able to identify the dataset with the most excessive vibration but not the other considerable ones. Although the results show a level of success in identifying datasets with excessive vibrations, the methods used were not able to indicate the exact location of the excessive vibrations. This thesis results can conclude that the three techniques were able to detect the same dataset with the most excessive vibration. Based on the results, the RMS is the technique that should be used to monitor the most considerable vibrations.

In order to improve the results a new division of the individual datasets into subsets must be considered, specially in the results of the approximate entropy. Also, the optimization of approximate entropy computation must be taken into account to reduce MATLAB code execution time. Finally, the development of a Graphical Unit Interface (GUI) to automate the identification of the datasets with excessive vibration is recommended.

REFERENCES

[1] Allmon, C. Wilkinson, W. & Loewenthal, S. *Test Validation of the Repair to the Space Station Solar Alpha Rotary Joint (SARJ).* Lockheed Missiles and Space Systems Company. May 7-9, 2010.

[2] Basta, E. A., et al. *Solar Alpha Rotary Joint Anomaly: The Materials & Processes Perspective.* Boeing and NASA. 5 May 2009.

[3] Cao, M. & Xiao, J. *A Comprehensive Dynamic Model of Double-row Spherical Bearing – Model Development and Case Studies on Surface Defects, Preloads, and Radial Clearance.* General Motors R&D, 30500 Mound Road, Warren, MI 48071, USA. 12 July 2007.

[4] Ericsson, S., et al. *Towards Automatic Detection of Local Bearing Defects in Rotating Machines.* Department of Mathematics, Lulea University of Technology, SE-971 87 Lulea, Sweden and Naiden Teknik AB, Aurorum 30, SE-977 75 Lulea, Sweden and Department of Mathematics/NADA, Royal Institute of Technology, SE-100 44 Stockholm, Sweden. 17 December 2003.

[5] Fitzpatrick, K., Grygier, M. & Bartkowicz, T. *ISS Stage 12A Post-Flight Modal Analysis, Model Validation and Correlation.* The Boeing Company, 3700 Bay Area Blvd. Houston, Texas and NASA, Johnson Space Center, Houston, Texas. February 9-12, 2009.

[6] Harik, E. P., et al. *The International Space Station Solar Alpha Rotary Joint Anomaly Investigation.* The Boeing Company, Houston, TX and Johnson Space Center, Houston, TX. May 7-9, 2010.

[7] Harik, E., et al. *NASA Project Management Challenge 2011: The International Space Station Solar Alpha Rotary Joint Anomaly Investigation.* Boeing Company and NASA,

2011.

[8] Harvey, T.J., Wood, R.J.K., Powrie, H.E.G. *Electrostatic Wear Monitoring of Rolling Element Bearing.* School of Engineering Sciences, University of Southampton, Southampton, Hampshire SO17 1BJ, UK and Smiths Aerospace Information Systems, School Lane, East Leigh, Hampshire SO53 4YG, UK. 21 December 2006.

[9] Heng, R.B.W. & Nor, M. J. M. *Statistical Analysis of Sound and Vibration Signals for Monitoring Rolling Element Bearing Condition.* School of Engineering, Sheffield Hallam University, Pond Street, Sheffield Sl IWB, UK. 6 March 1997.

[10] Jamaludin, N. & Mba, D. *Monitoring Extremely Slow Rolling Element Bearing: Part I.* Department of Mechanical and Material Engineering, Faculty of Engineering, UKM, 43600 Bangi, Selangor, Malaysia and School of Mechanical Engineering, Cranfield University, Building 52; Cranfield MK43 0AL, United Kingdom. 19 December 2001.

[11] Jamaludin, N. & Mba, D. *Monitoring Extremely Slow Rolling Element Bearing: Part II.* Department of Mechanical and Material Engineering, Faculty of Engineering, UKM, 43600 Bangi, Selangor, Malaysia and School of Mechanical Engineering, Cranfield University, Building 52; Cranfield MK43 0AL, United Kingdom. 19 December 2001.

[12] James Li, C. & Li, S. Y. *Acoustic Emission Analysis for Bearing Condition Monitoring.* Department of Mechanical Engineering, Aeronautical and Mechanics RPI Troy, NY 12180, USA and Department of Precision Machinery and Instruments, Changsha Institute of Technology, Changsha, Human, China. 12 January 1995.

[13] Karacay, T. & Akturk, N. *Experimental Diagnostics of Ball Bearings Using Statistical and Spectral Methods.* Gazi University, Faculty of Engineering and Architecture, The Department of Mechanical Engineering, G.U. Muh.-Mim. Fak., 06570

Maltepe, Ankara, Turkey. 12 November 2008.

[14] Lim, T. X., Cooper, P.A, & Ayers, J. K. *Structural Dynamics Interaction with Solar Tracking Control for Evolutionary Space Station Concepts.* Langley Research Center Hampton, Virginia 23665. May 1992.

[15] Salazar, V.L., et al. *Failure Analysis in Space: International Space Station (ISS) Starboard Solar Alpha Rotary Joint (SARJ) Debris Analysis*. National Aeronautics and Space Administration, Kennedy Space Center, USA. June 2007.

[16] Singh, G. & Al Kazzaz, S.A.S. *Isolation and Identification of Dry Bearing Faults in Induction Machine Using Wavelet Transform.* Department of Electrical Engineering, Indian Institute of Technology, Roorkee 247667, Uttaranchal, India and Department of Electrical Engineering, University of Mosul, Mosul, Iraq. 17 November 2008.

[17] Tandon, N. & Choudhury, A. *A Review of Vibration and Acoustic Measurement Methods for the Detection of Defects in Rolling Element Bearings,* ITMME Centre Indian Institute of technology Hauz Khas, New Delhi 11016, India and Department of mechanical Engineering, Regional Engineering College, Silchar 788010, India. 12 October 1999.

[18] Tandon, N., Yadava, & G.S., Ramakrishna, K.M. *A Comparison of Some Condition Monitoring Techniques for the Detection of Defect in Induction Motor Ball Bearings*. ITMME Centre, India Institute of technology, Hauz Khas, New Delhi 110016, India, 5 August 2005.

[19] Tandon, N., Yadava, & G.S., Ramakrishna, K.M. *Condition Monitoring of Electric Motor ball Bearings for the Detection of Grease Contaminants.* ITMME Centre, Indian Institute of Technology, Hauz Khas, New Delhi 110016, India. 25 January 2006.

[20] Tao, B., et al. *An Alternative Time-domain Index for Condition Monitoring of Rolling*

Element Bearings – A Comparison Study. School of mechanical Science and Engineering, Huazhong University of science & Technology, Wuhan, PR China and School of Mechanical Engineering, Shanghai Jiao Tong University, Shanghai, PR China. 23 March 2006.

[21] Yan, R. & Gao, R. X. *Approximate Entropy as a Diagnostic Tool for Machine Health Monitoring.* Department of mechanical and Industrial Engineering, University of Massachusetts, Amherst, MA 01003, USA 22 February 2006.

[22] Zhen, L., et al. *Bearing Condit in Monitoring Based on Shock Pulse Method and Improved Redundant Lifting Scheme.* School of Mechanical Engineering, Xi'an Jiao tong University, 710049 Xi'an, China and State Key Lab for Manufacturing Systems Engineering, Xi'an Jiao tong University, 710049 Xi'an, China. 28 December 2007.

APPENDIX: ACCELEROMETER DATA ANALYSES

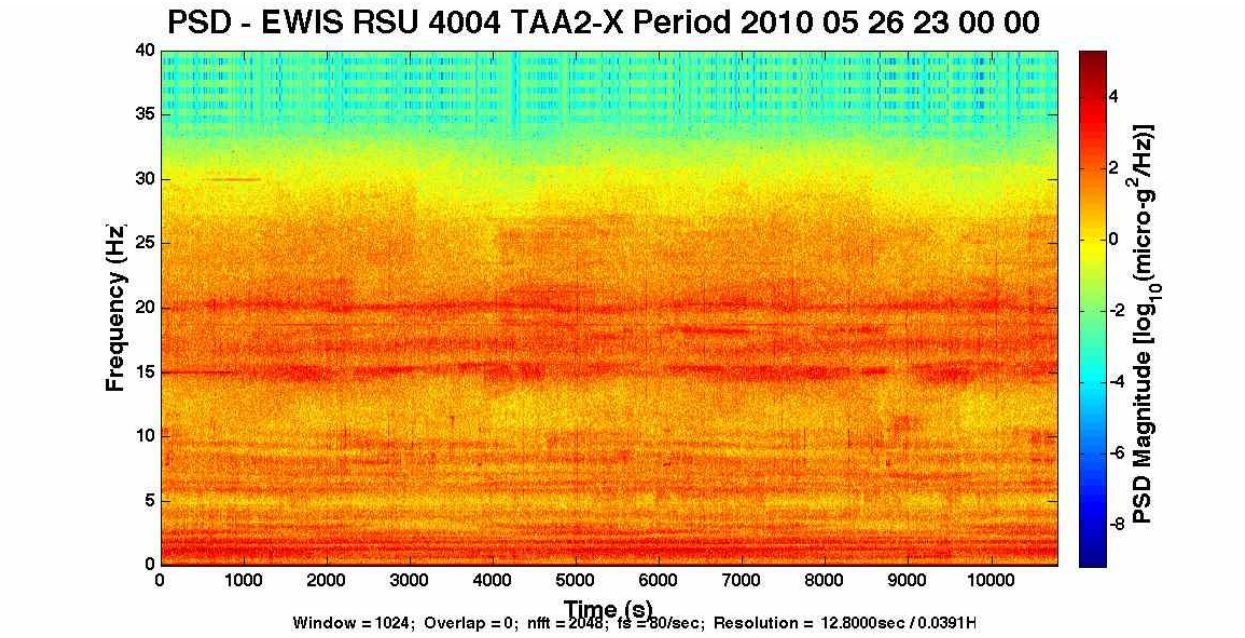

Figure A. 1- Rotary Joint B Spectrogram in x for 05/26/2010 23:00:00

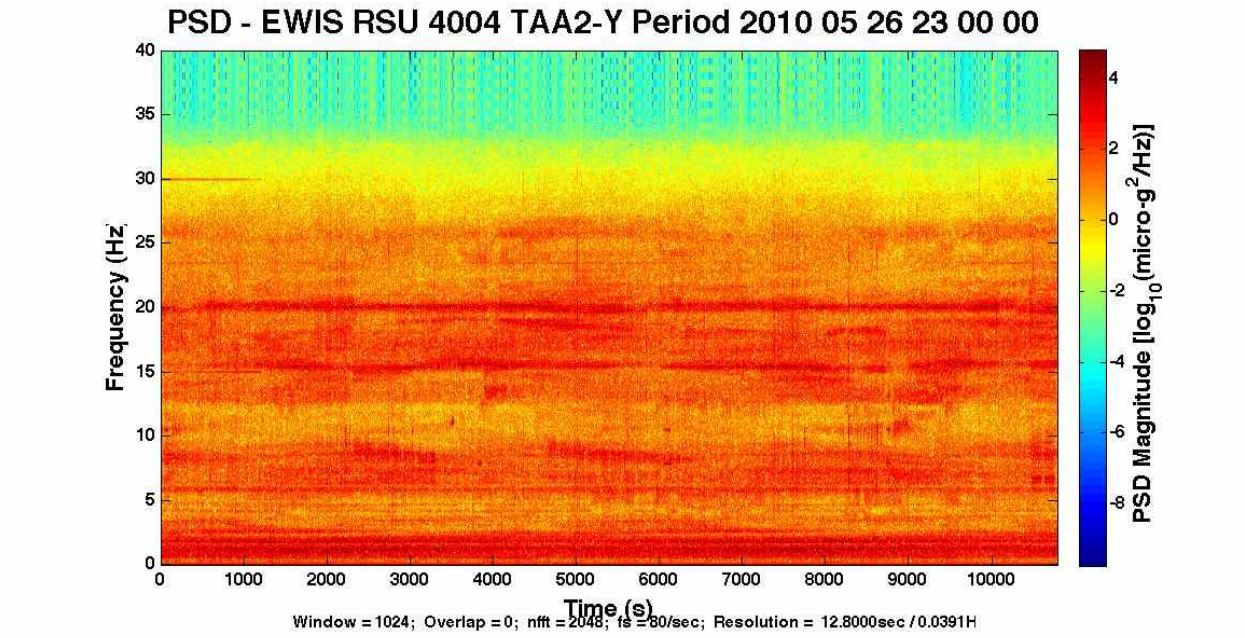

Figure A.1- Rotary Joint B Spectrogram in y for 05/26/2010 23:00:00

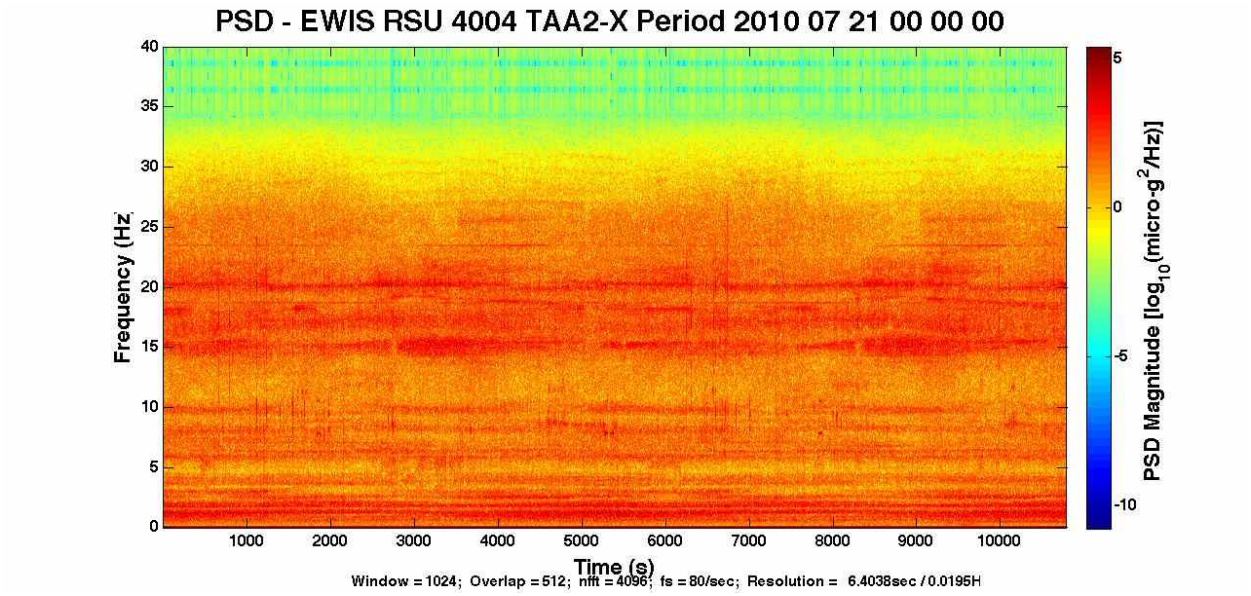

Figure A.3 - Rotary Joint B Spectrogram in x for 07/21/2010 00:00:00

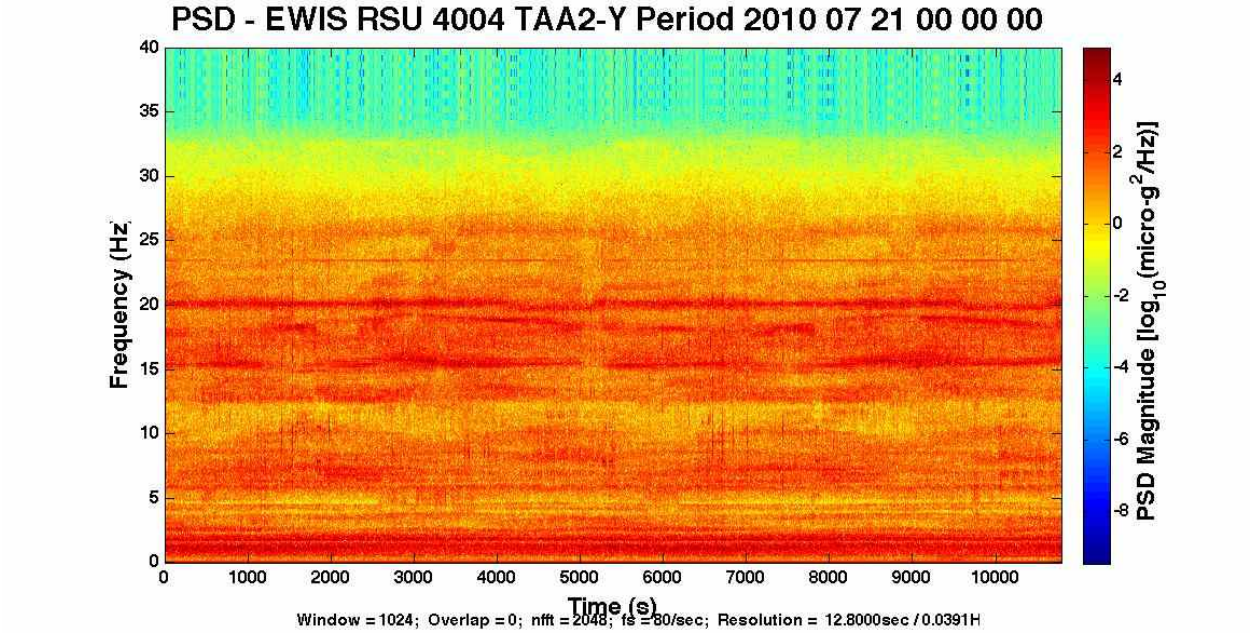

Figure A.4 - Rotary Joint B Spectrogram in y for 07/21/2010 00:00:00

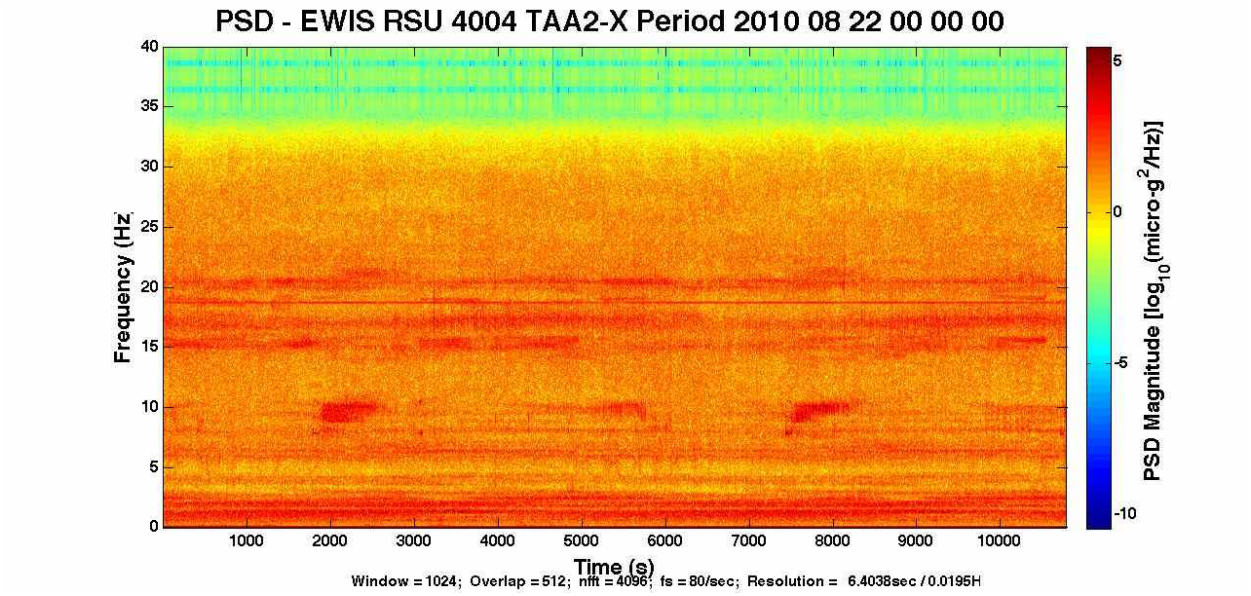

Figure A.5 - Rotary Joint B Spectrogram in x for 08/22/2010 00:00:00

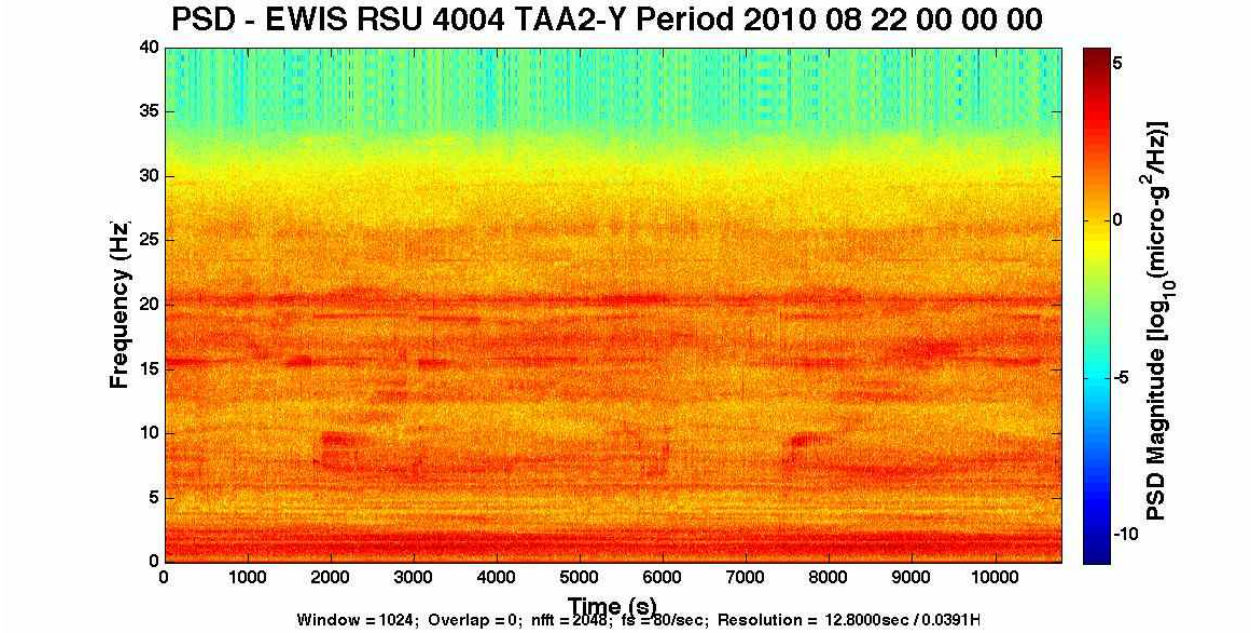

Figure A.6 - Rotary Joint B Spectrogram in y for 08/22/2010 00:00:00

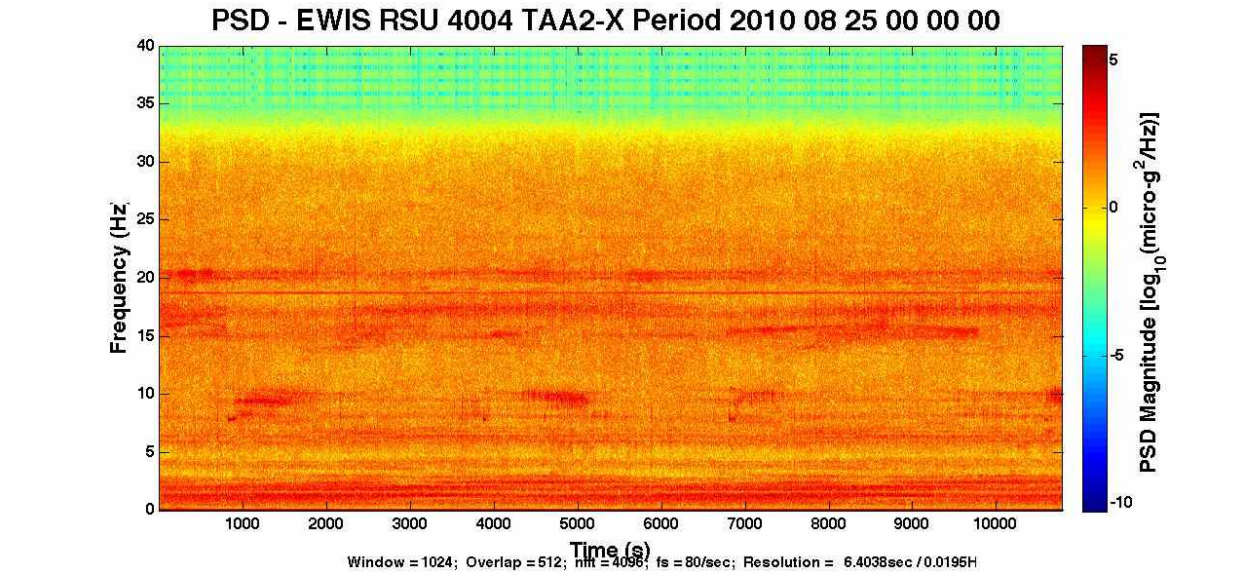

Figure A.7 - Rotary Joint B Spectrogram in x for 08/25/2010 00:00:00

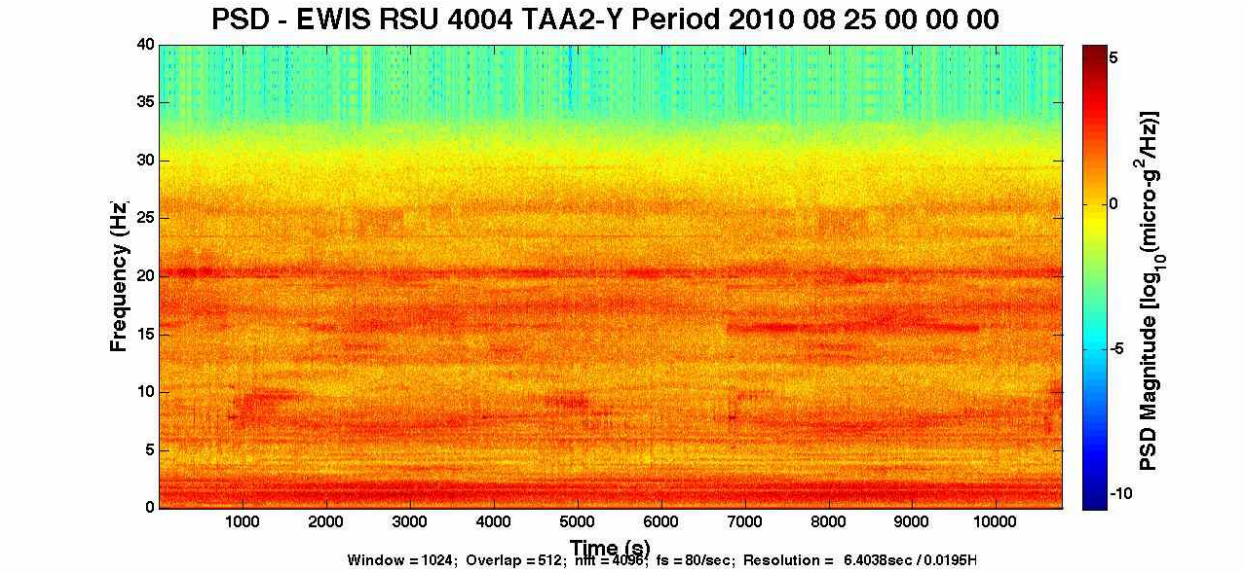

Figure A.8 - Rotary Joint B Spectrogram in y for 08/25/2010 00:00:00

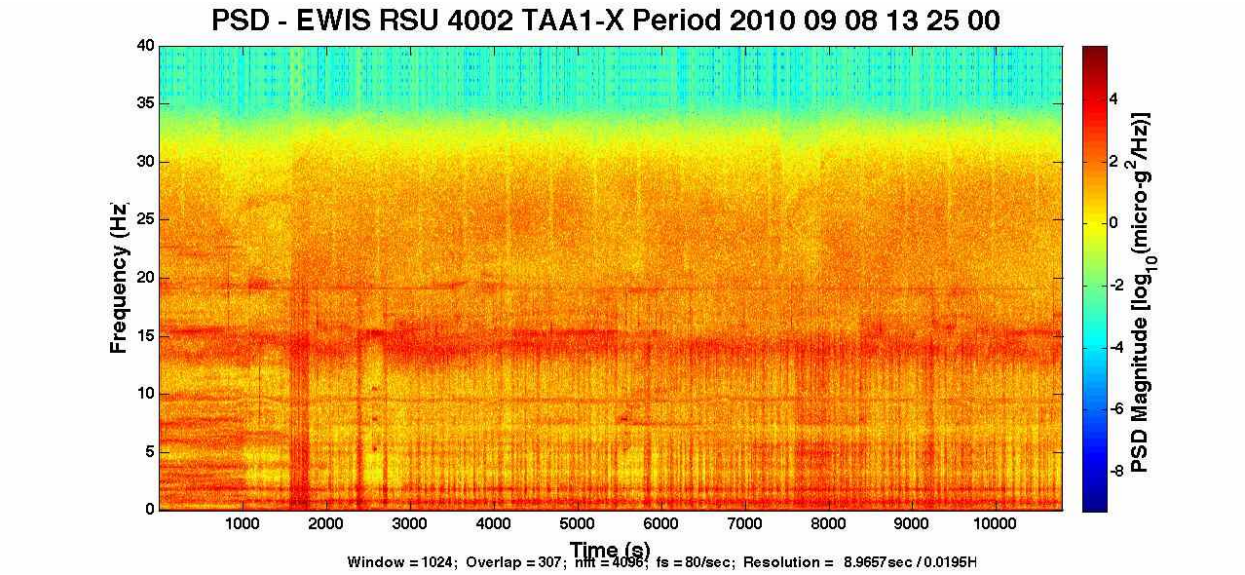

Figure A.9 - Rotary Joint A Spectrogram in x for 09/08/2010 13:25:00

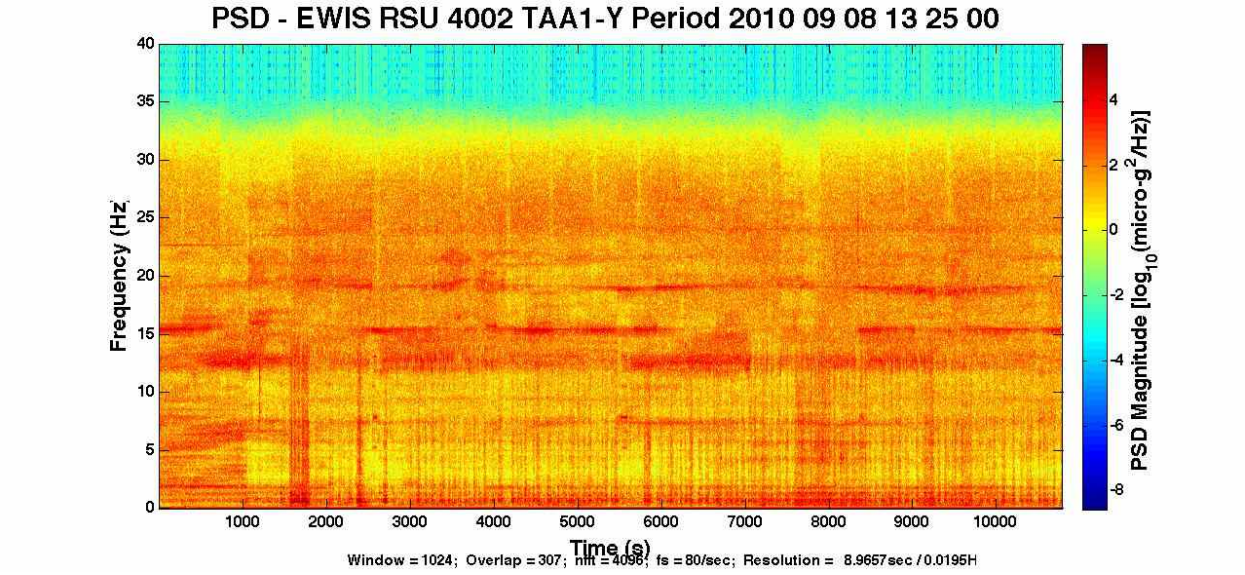

Figure A.10 - Rotary Joint A Spectrogram in y for 09/08/2010 13:25:00

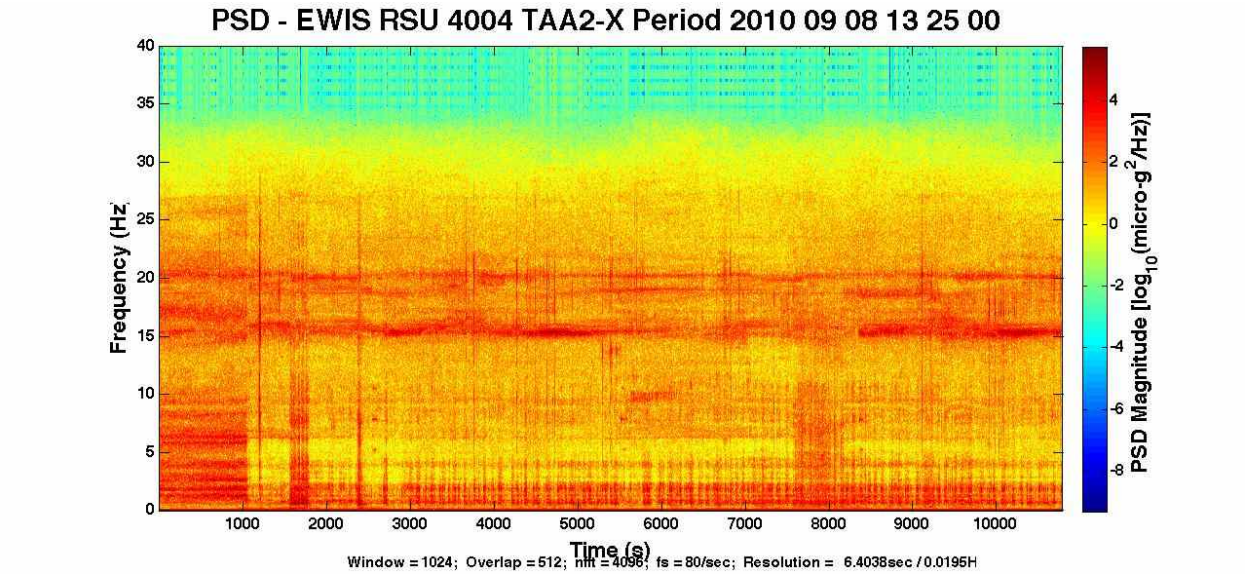

Figure A.11 - Rotary Joint B Spectrogram in x for 09/08/2010 13:25:00

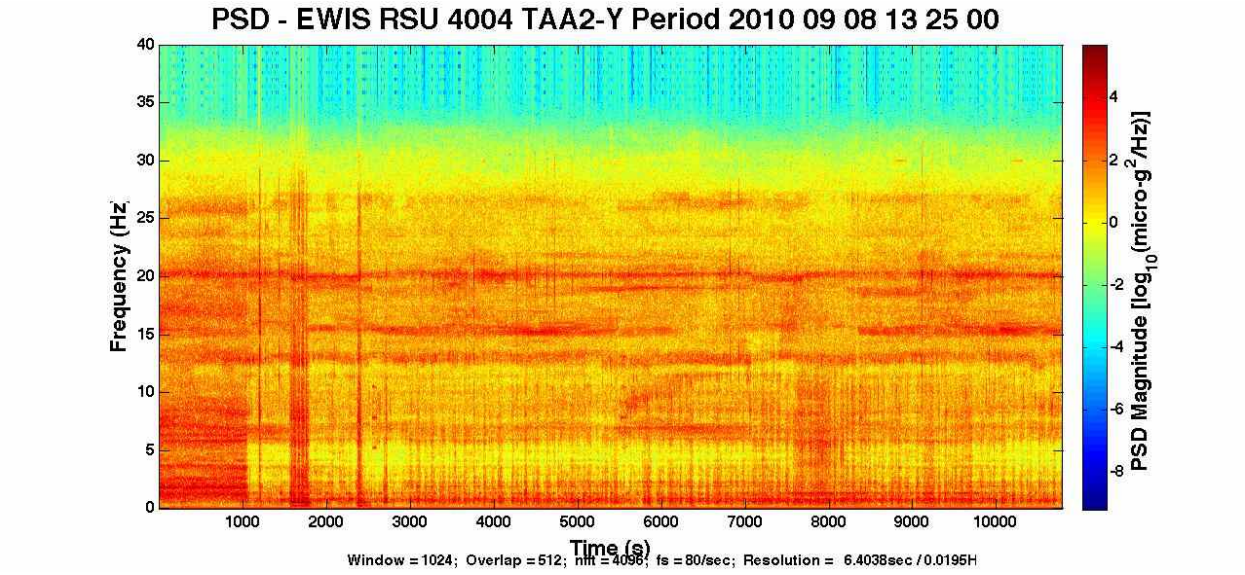

Figure A.12 - Rotary Joint B Spectrogram in y for 09/08/2010 13:25:00

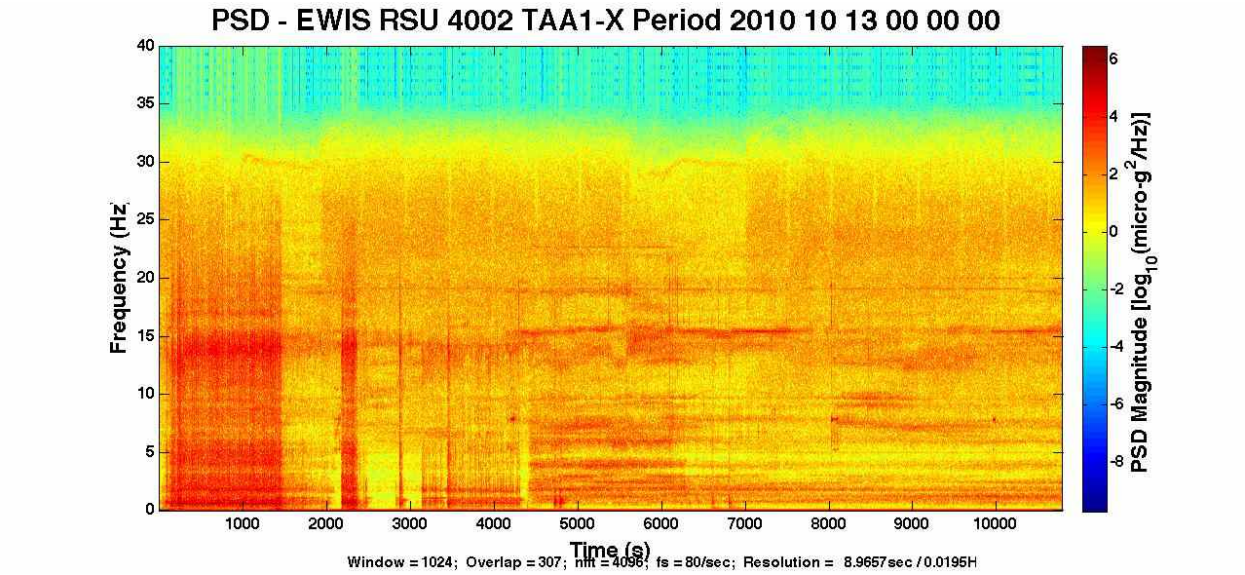

Figure A.13 - Rotary Joint A Spectrogram in x for 10/13/2010 00:00:00

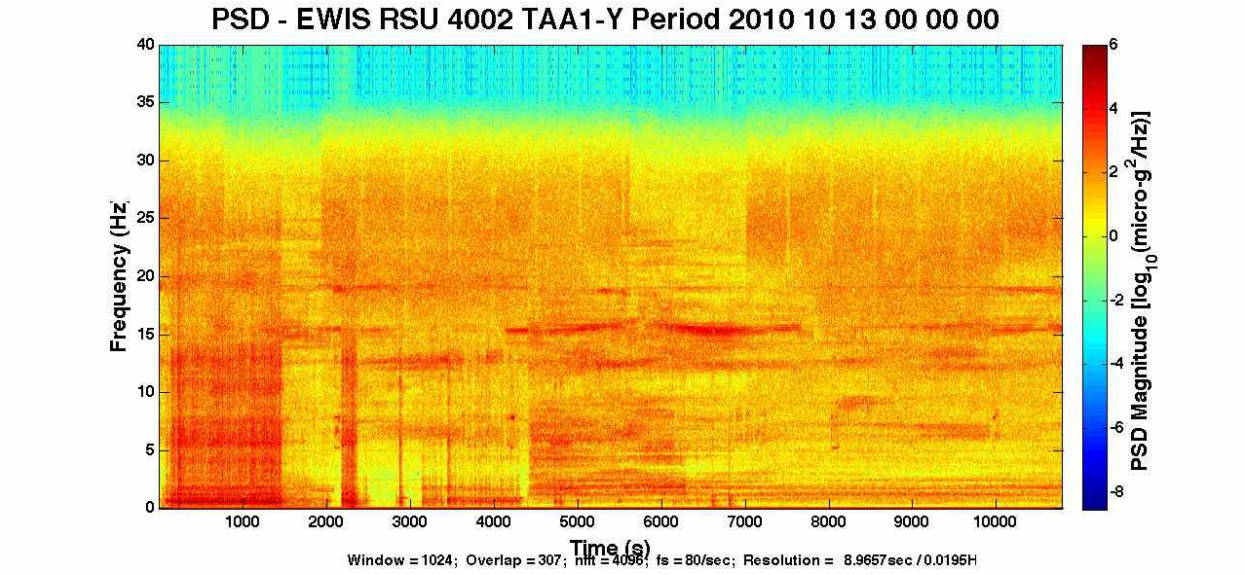

Figure A.14 - Rotary Joint A Spectrogram in y for 10/13/2010 00:00:00

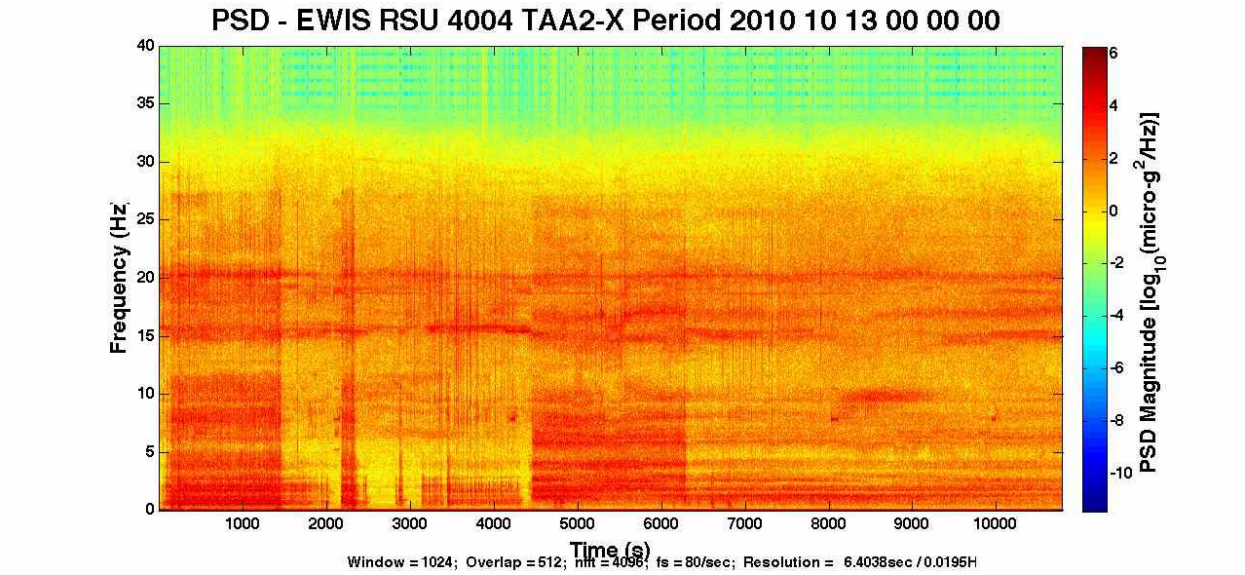

Figure A.15 - Rotary Joint B Spectrogram in x for 10/13/2010 00:00:00

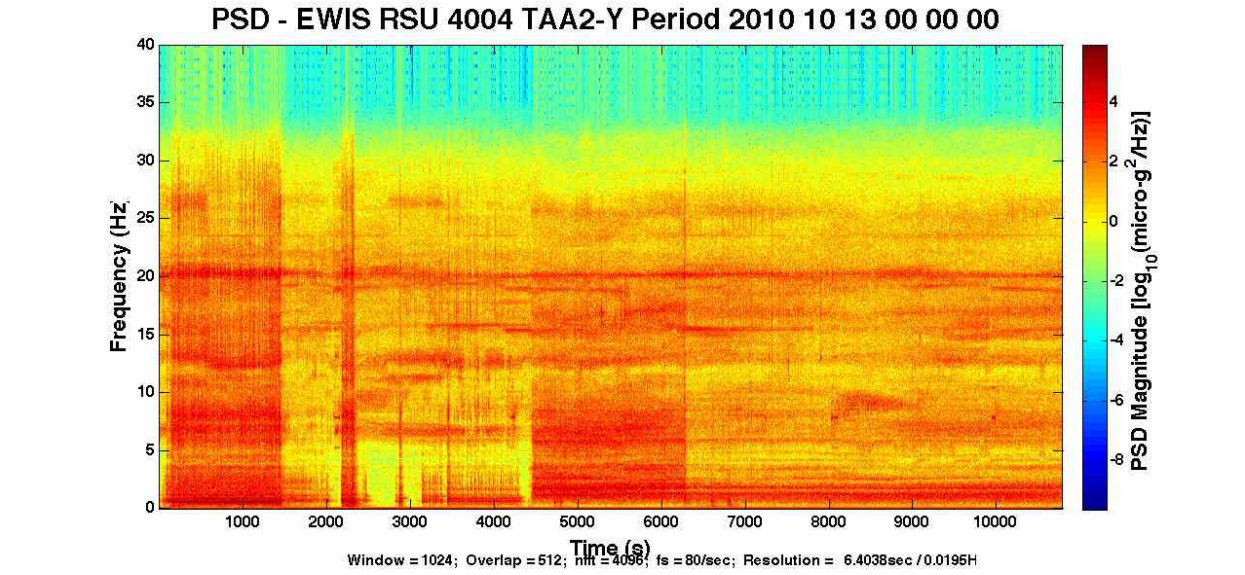

Figure A.16 - Rotary Joint B Spectrogram in y for 10/13/2010 00:00:00

This information includes the Root-Mean-Square, kurtosis, Approximate Entropy, for the data subsets, with 5 and 15 Hz low-pass filters and without filters. The spectrograms for Rotary Joint A and Rotary Joint B are also included for the x and y directions.

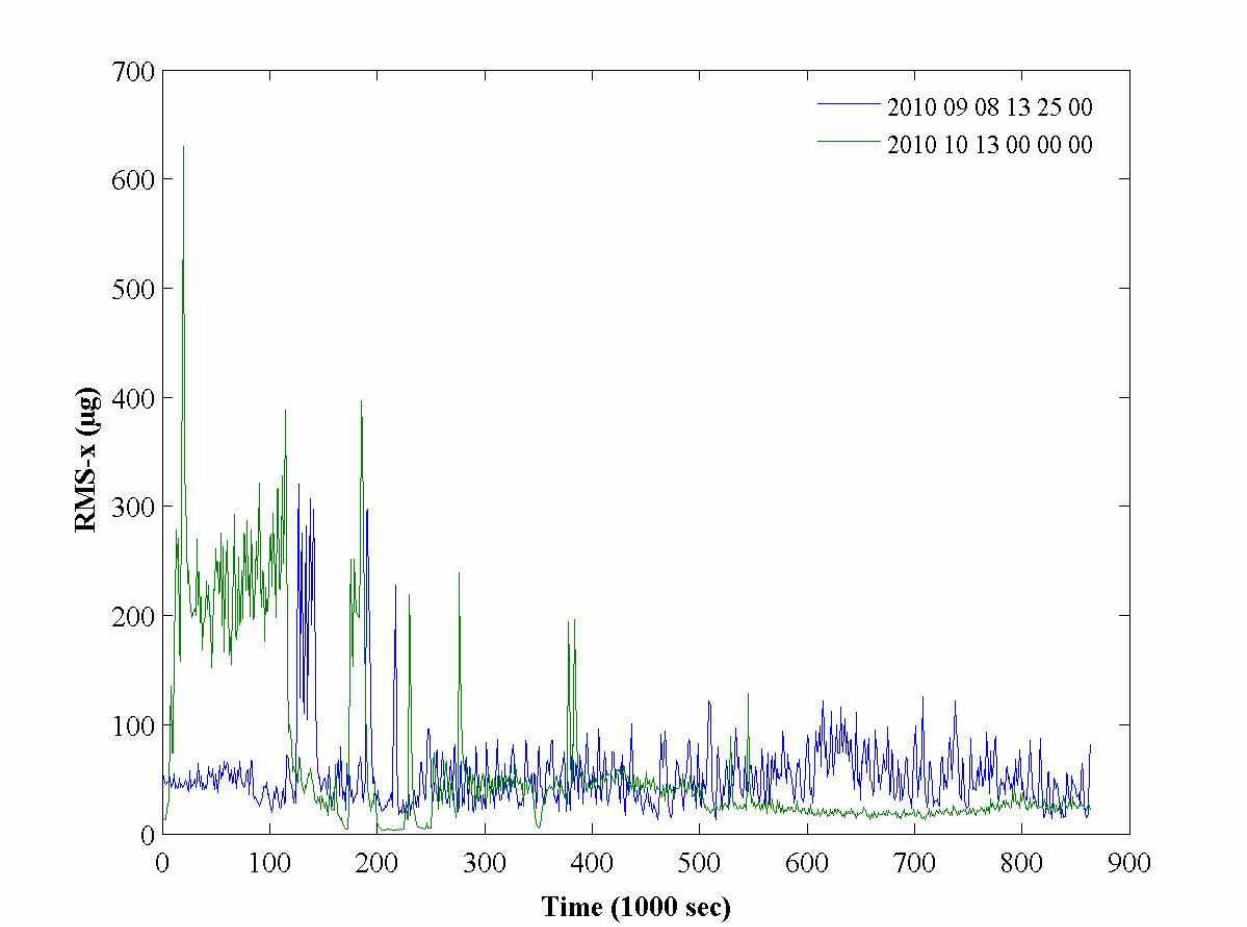

Figure A.17 - Rotary Joint A RMS in x with 5 Hz low-pass filter

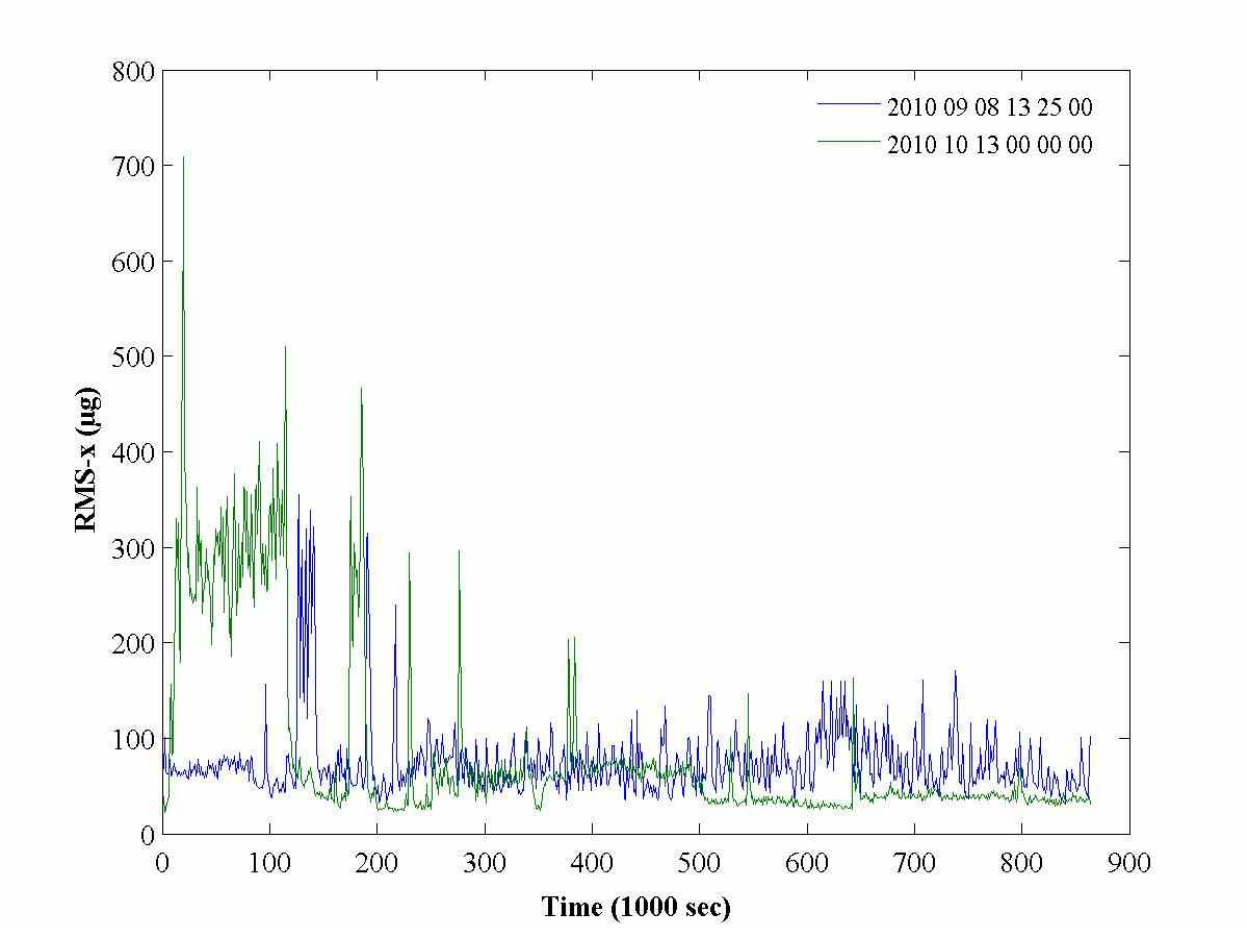

Figure A.18 - Rotary Joint A RMS in x with 15 Hz low-pass filter

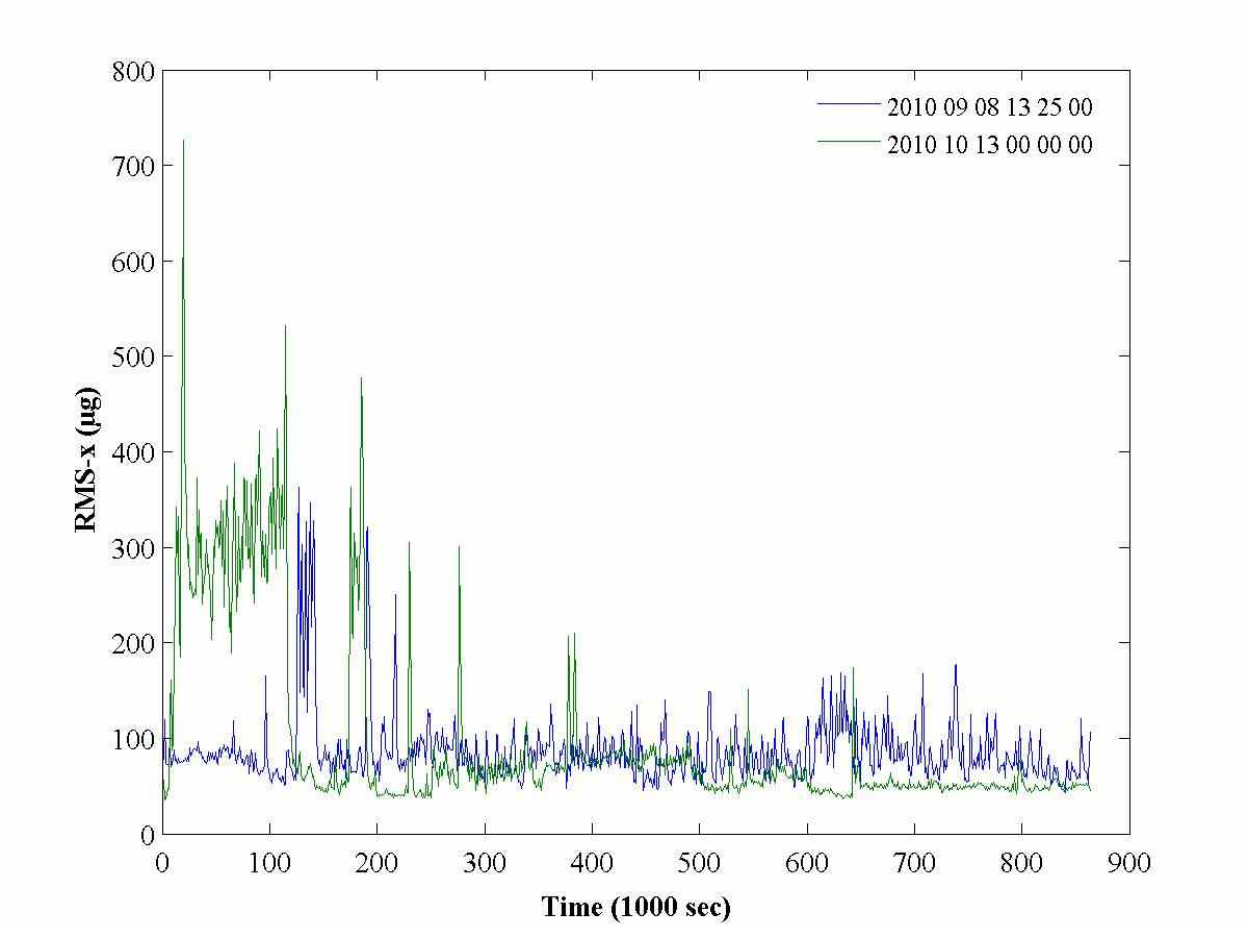

Figure A.19 - Rotary Joint A RMS in x

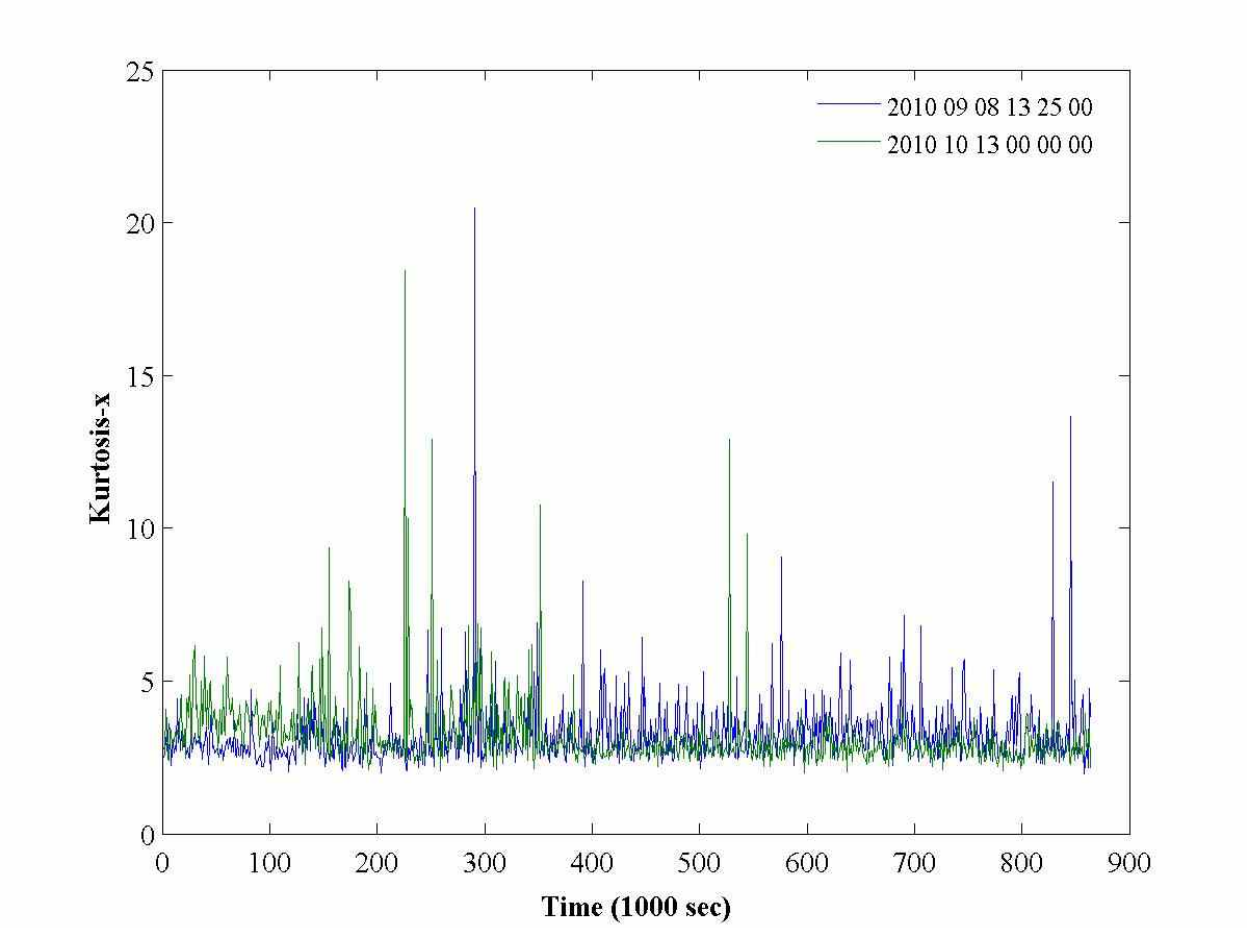

Figure A.20 - Rotary Joint A Kurtosis in x with 5 Hz low-pass filter

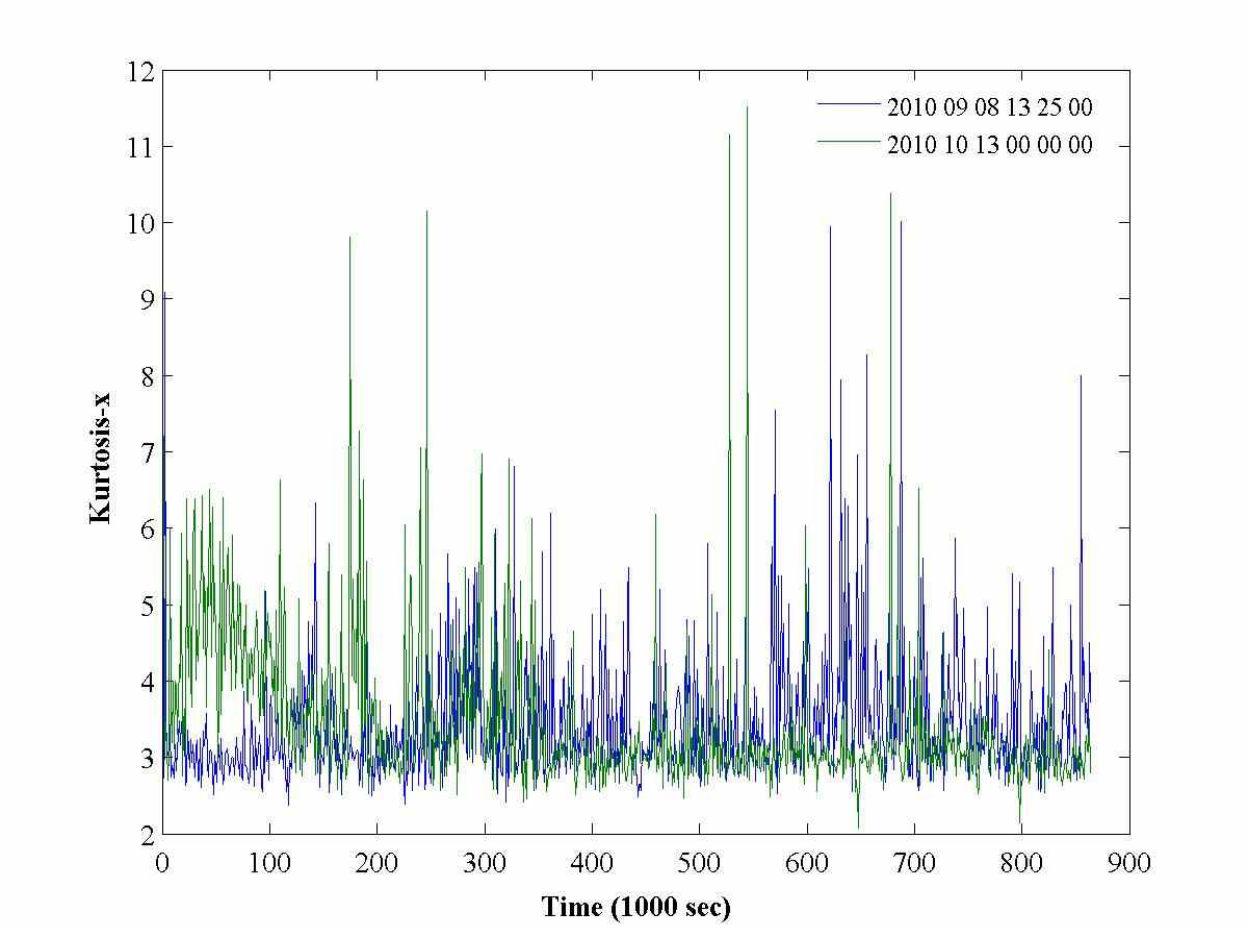

Figure A.21 - Rotary Joint A Kurtosis in x with 15 Hz low-pass filter

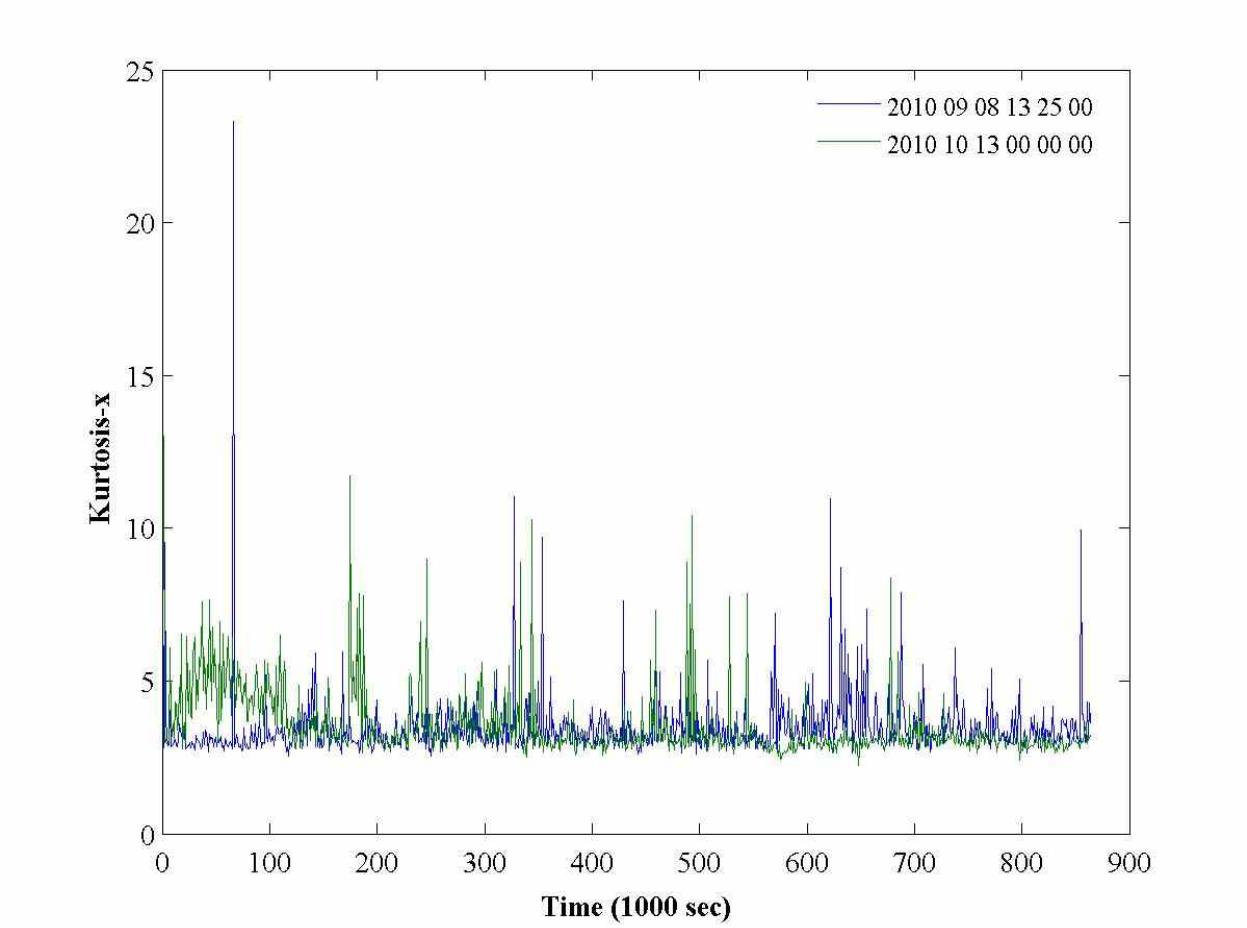

Figure A.22 - Rotary Joint A Kurtosis in x

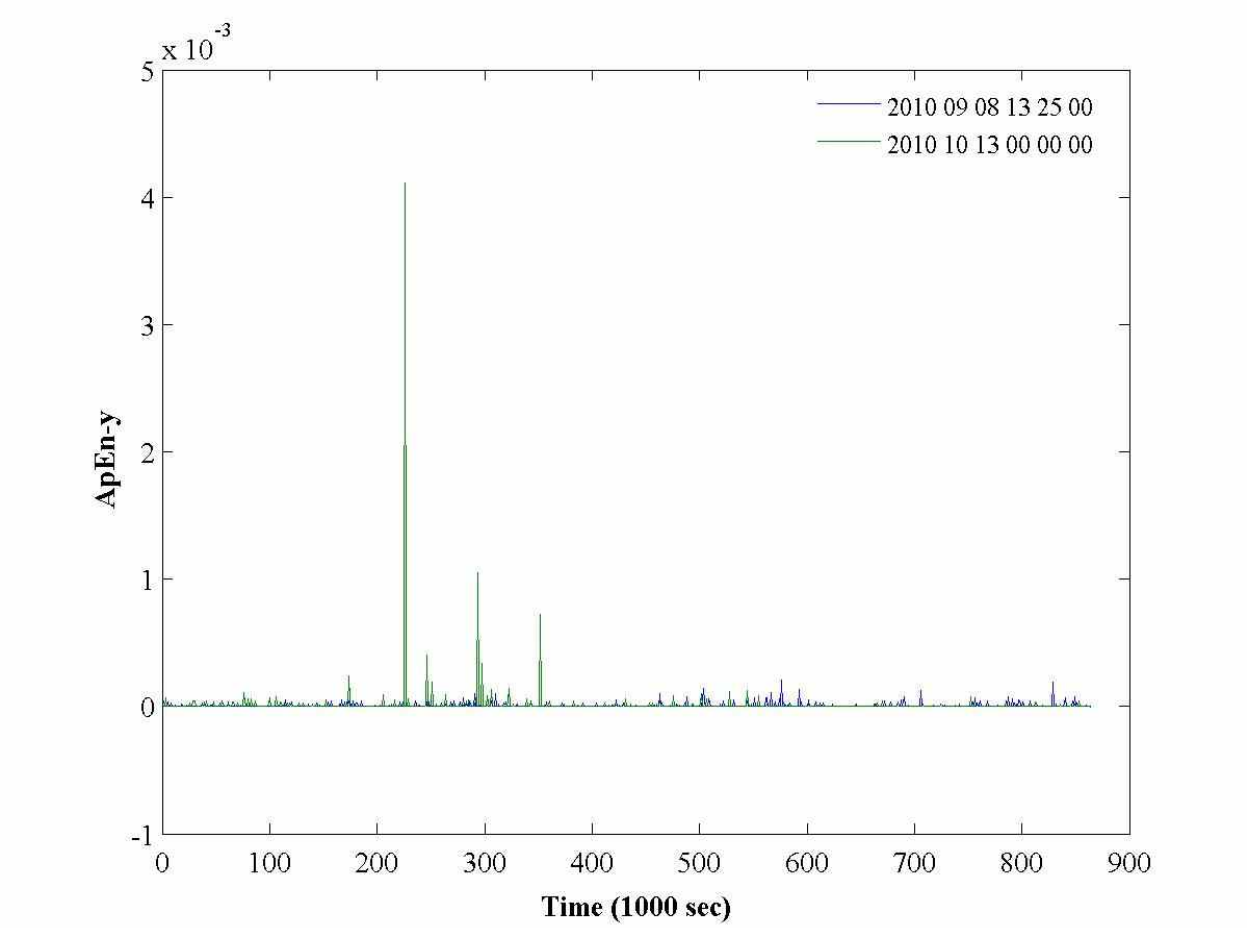

Figure A.23 - Rotary Joint A ApEn in x with 5 Hz low-pass filter

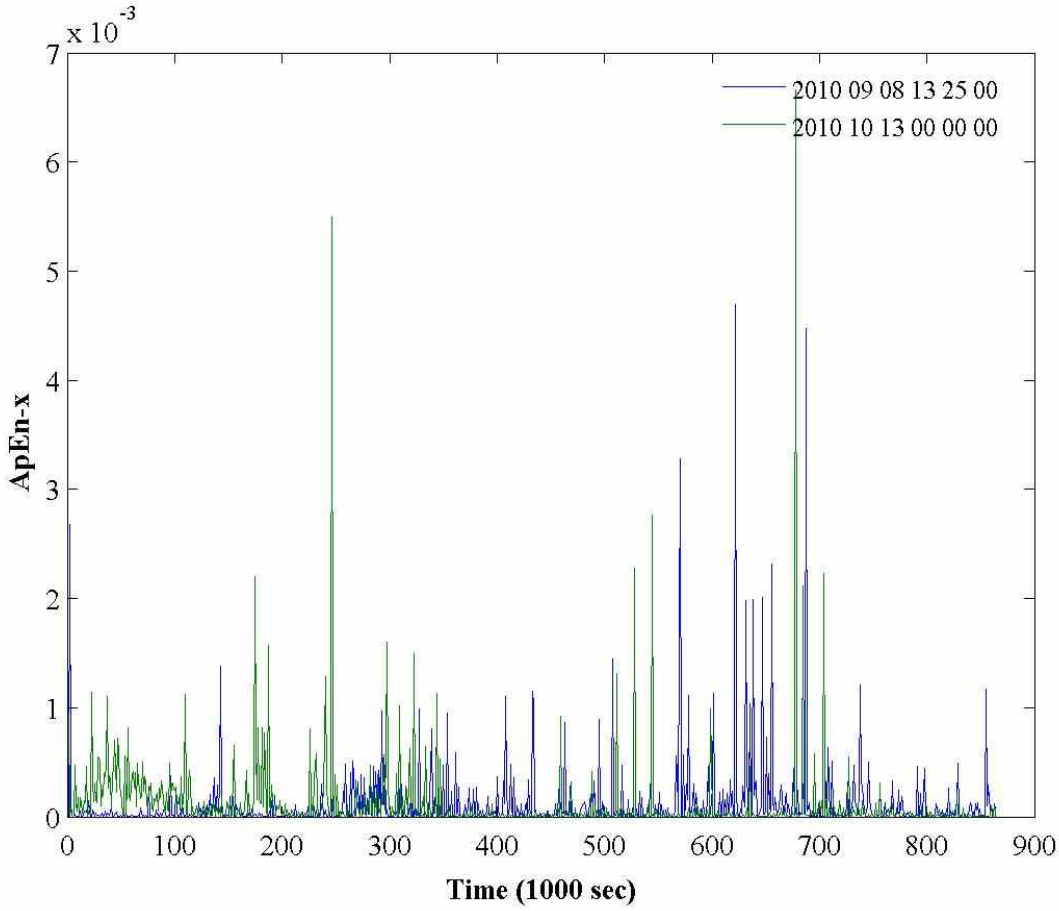

Figure A.24 - Rotary Joint A ApEn in x with 15 Hz low-pass filter

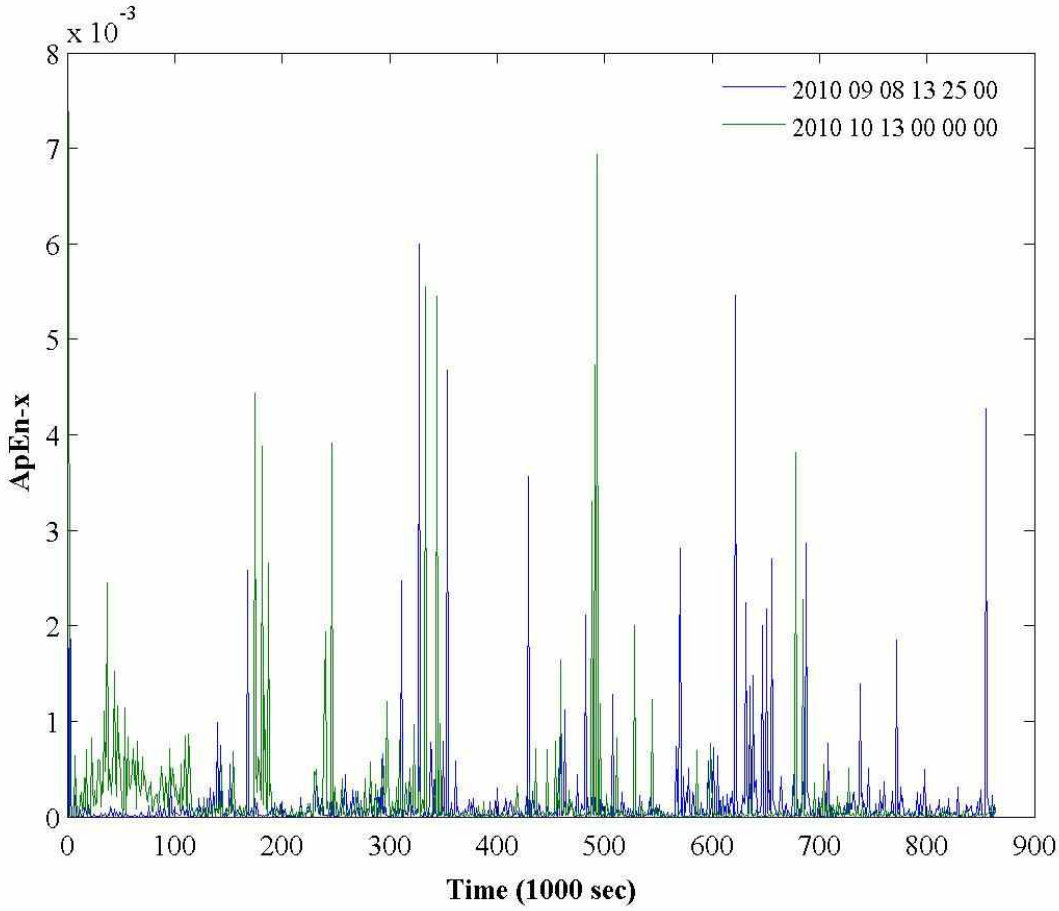

Figure A.25 - Rotary Joint A ApEn in x

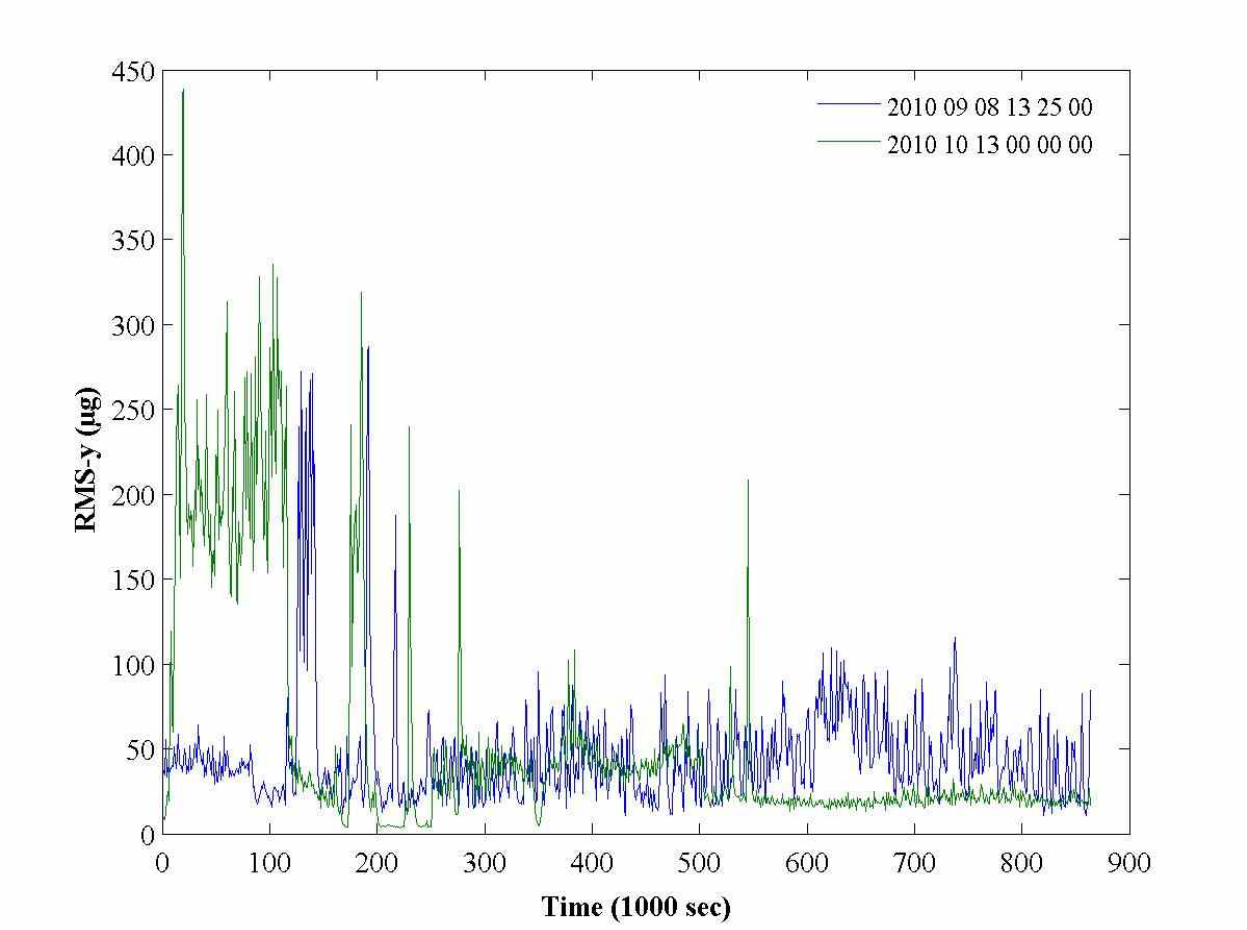

Figure A.26 - Rotary Joint A RMS in y with 5 Hz low-pass filter

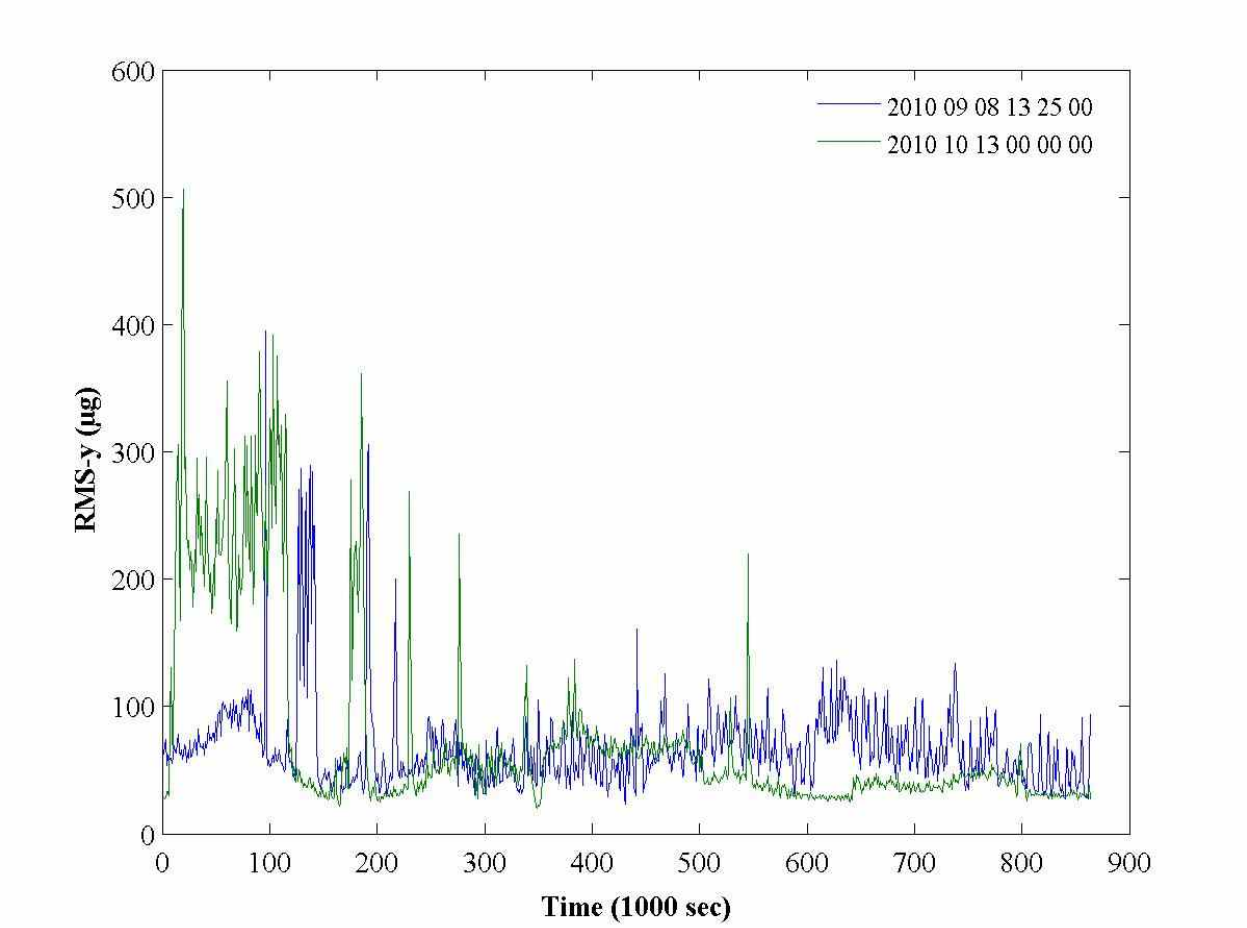

Figure A.27 - Rotary Joint A RMS in y with 15 Hz low-pass filter

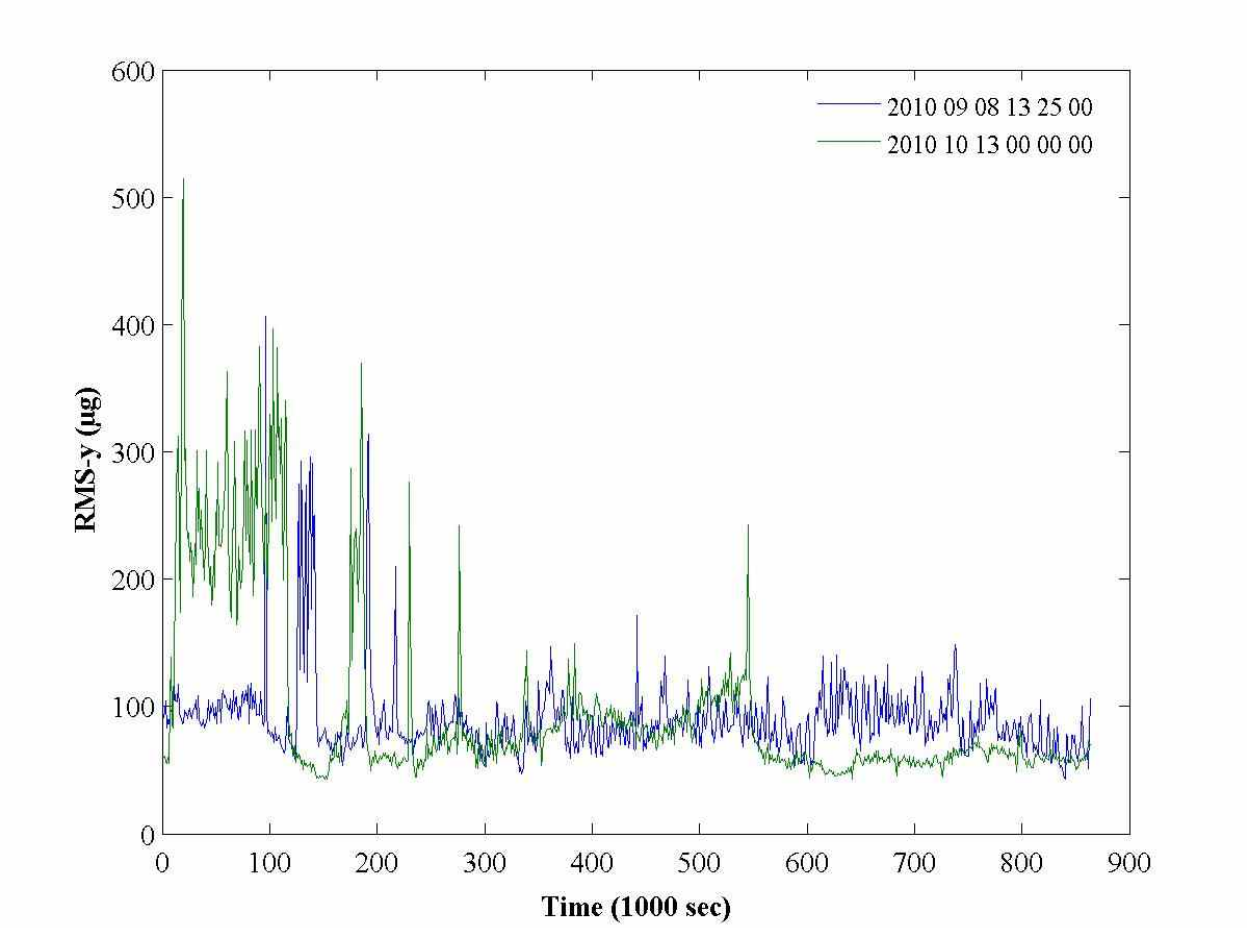

Figure A.28 - Rotary Joint A RMS in y

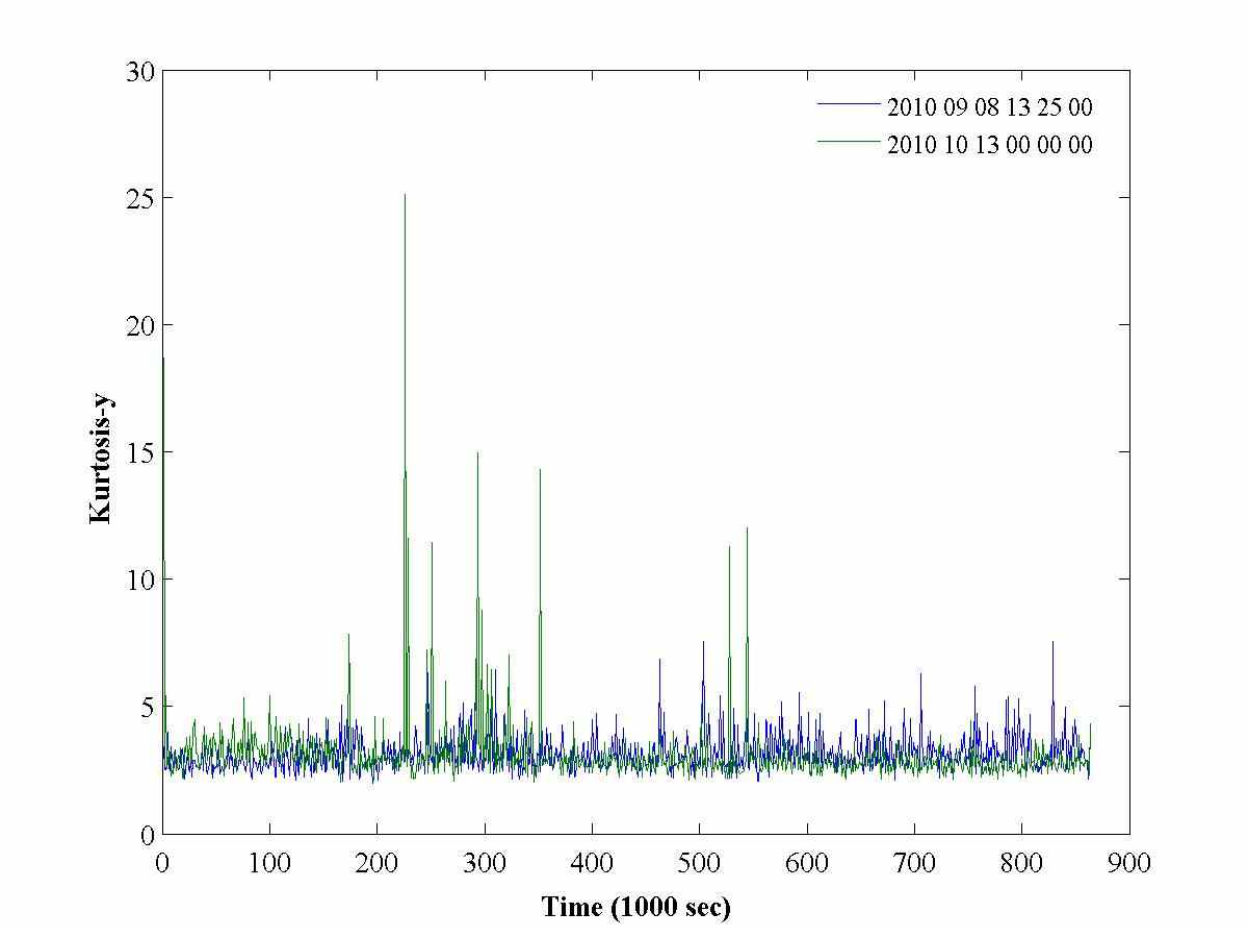

Figure A.29 - Rotary Joint A Kurtosis in y with 5 Hz low-pass filter

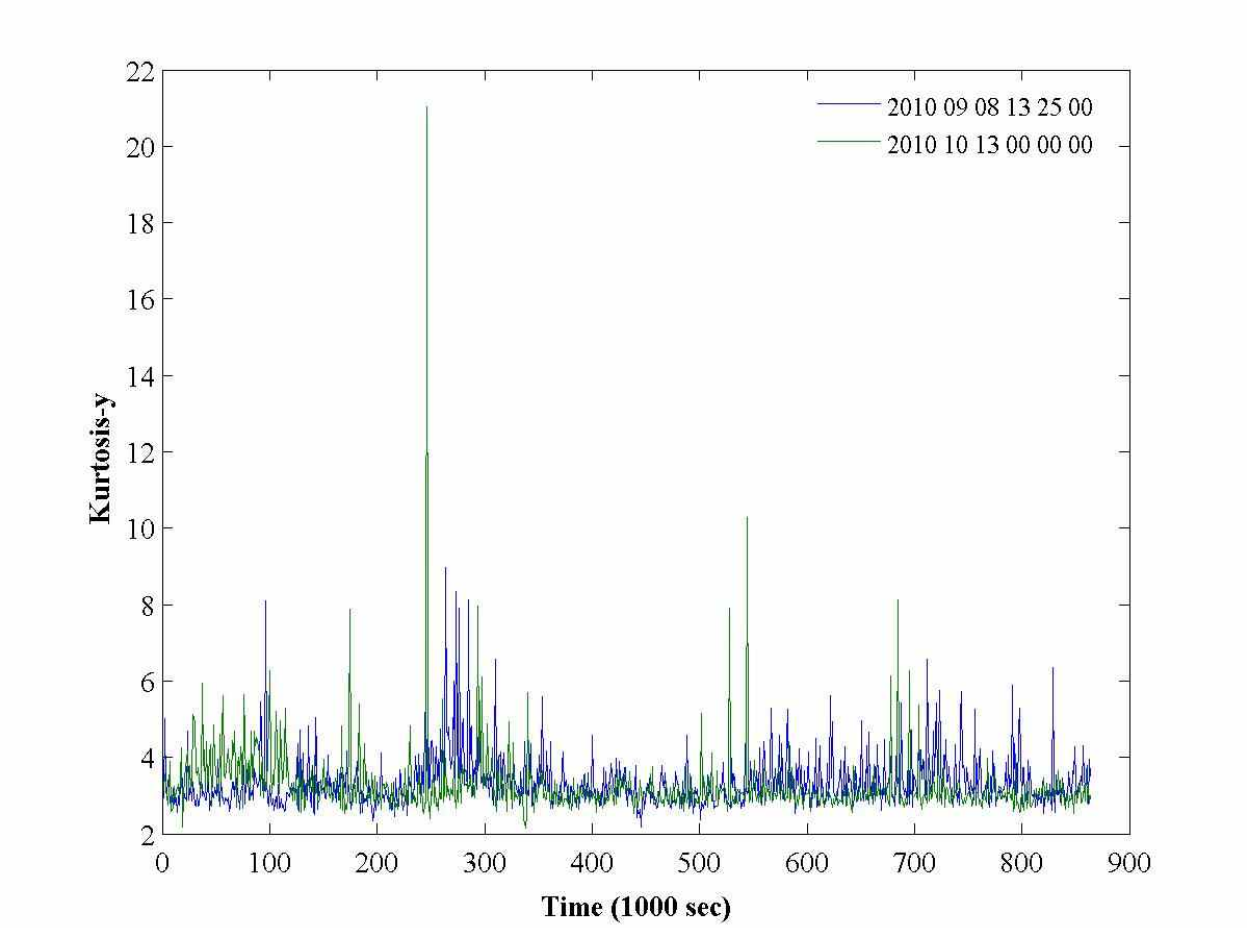

Figure A.30 - Rotary Joint A Kurtosis in y with 15 Hz low-pass filter

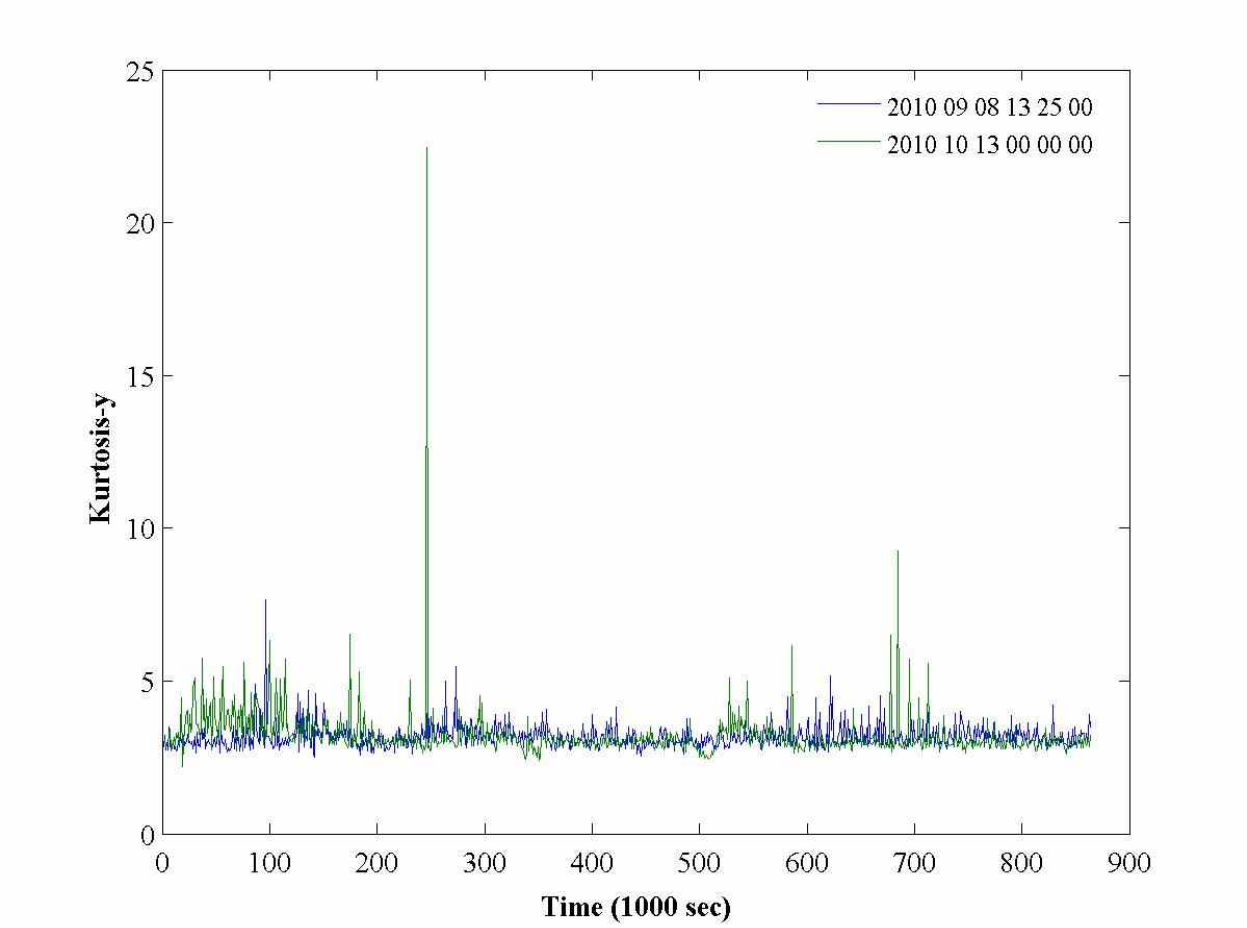

Figure A.31 - Rotary Joint A Kurtosis in y

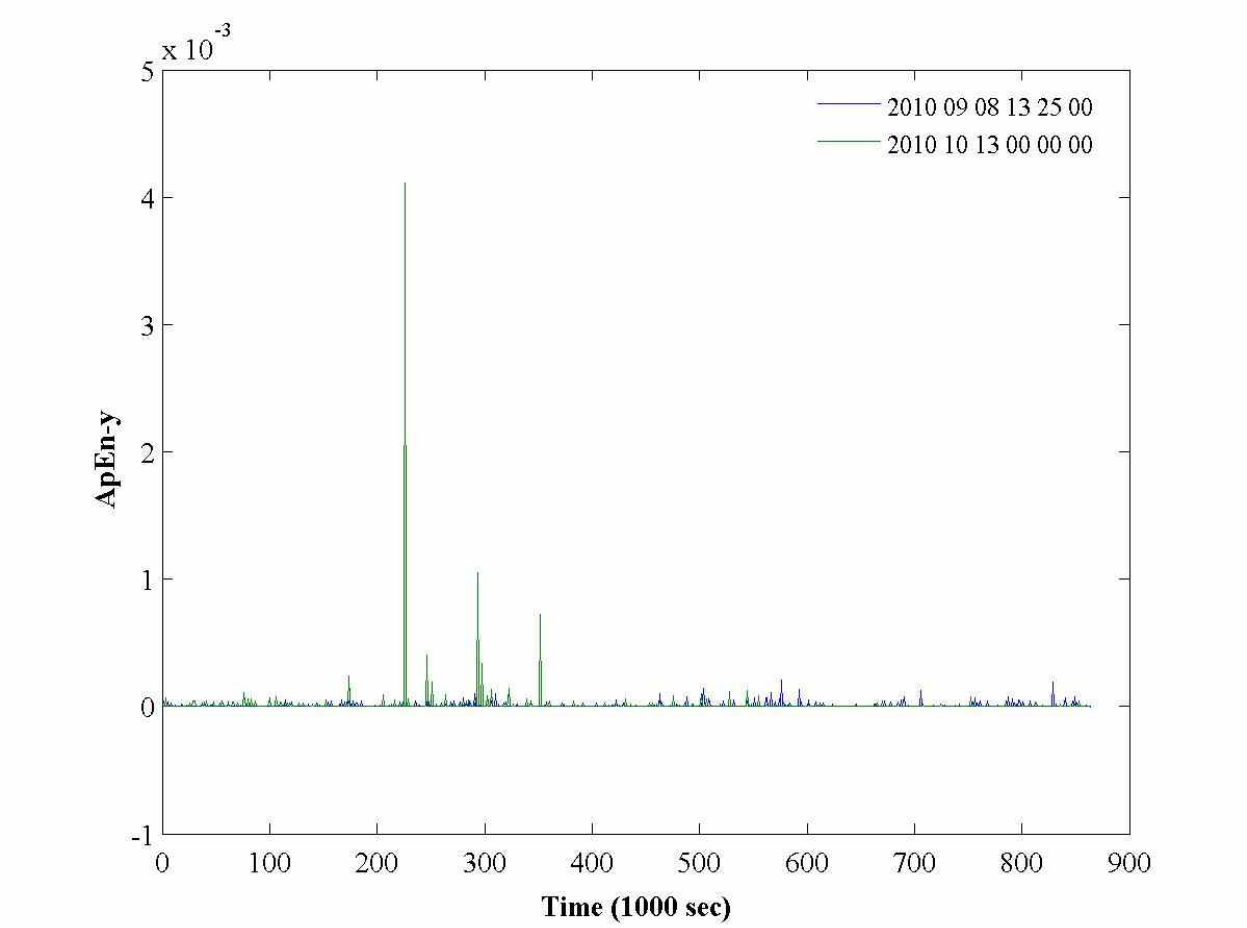

Figure A.32 - Rotary Joint A ApEn in y with 5 Hz low-pass filter

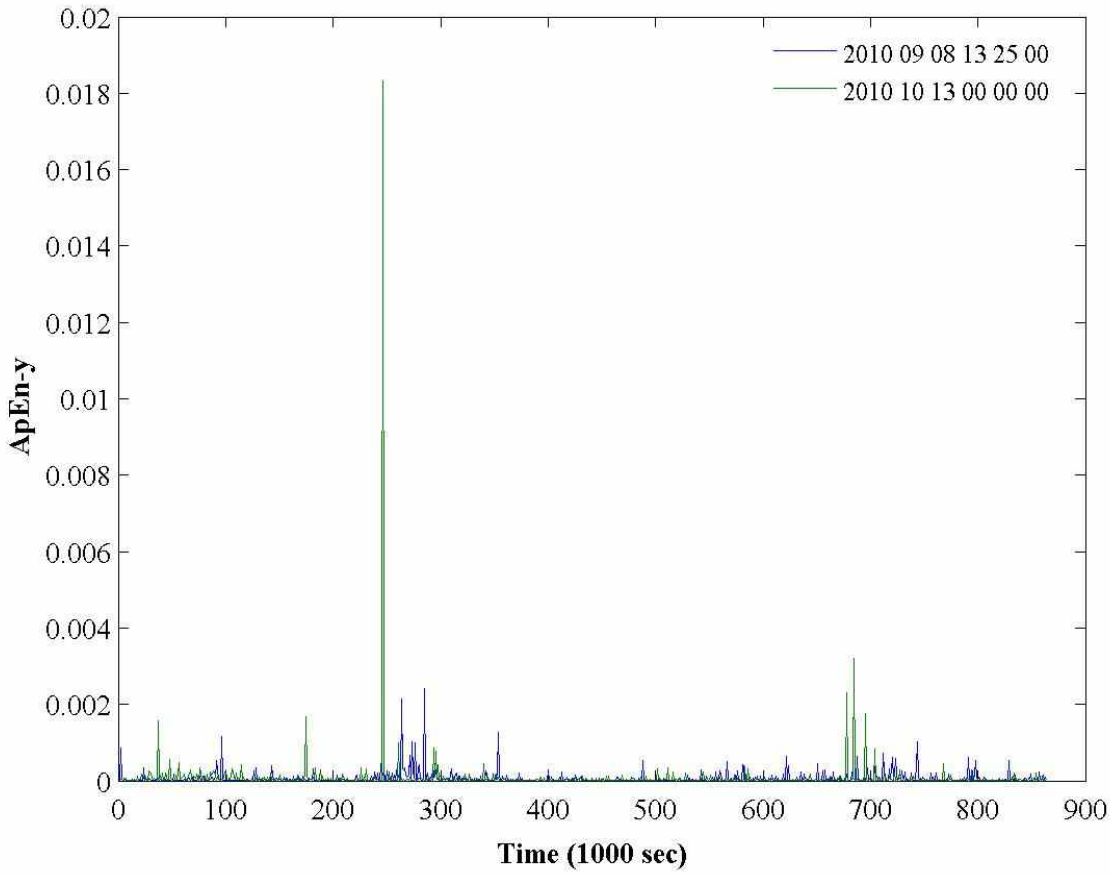

Figure A.33 - Rotary Joint A ApEn in y with 15 Hz low-pass filter

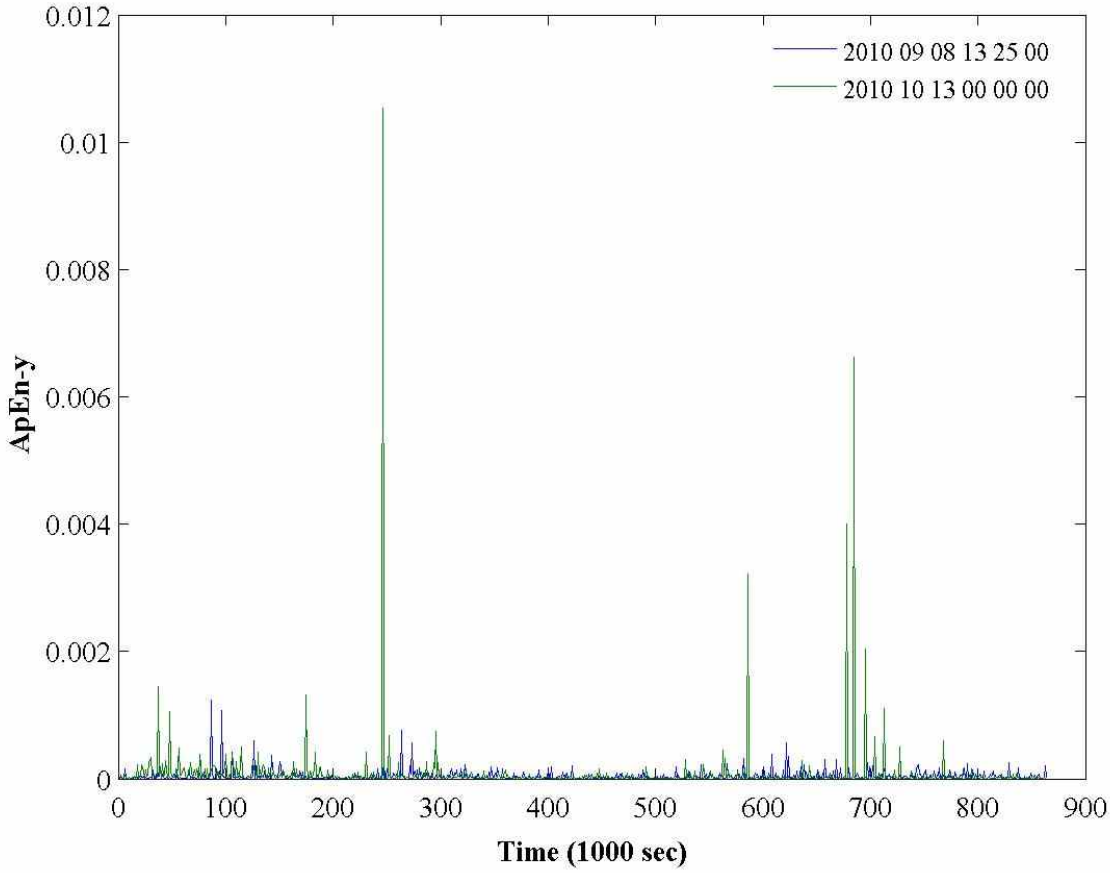

Figure A.34 - Rotary Joint A ApEn in y

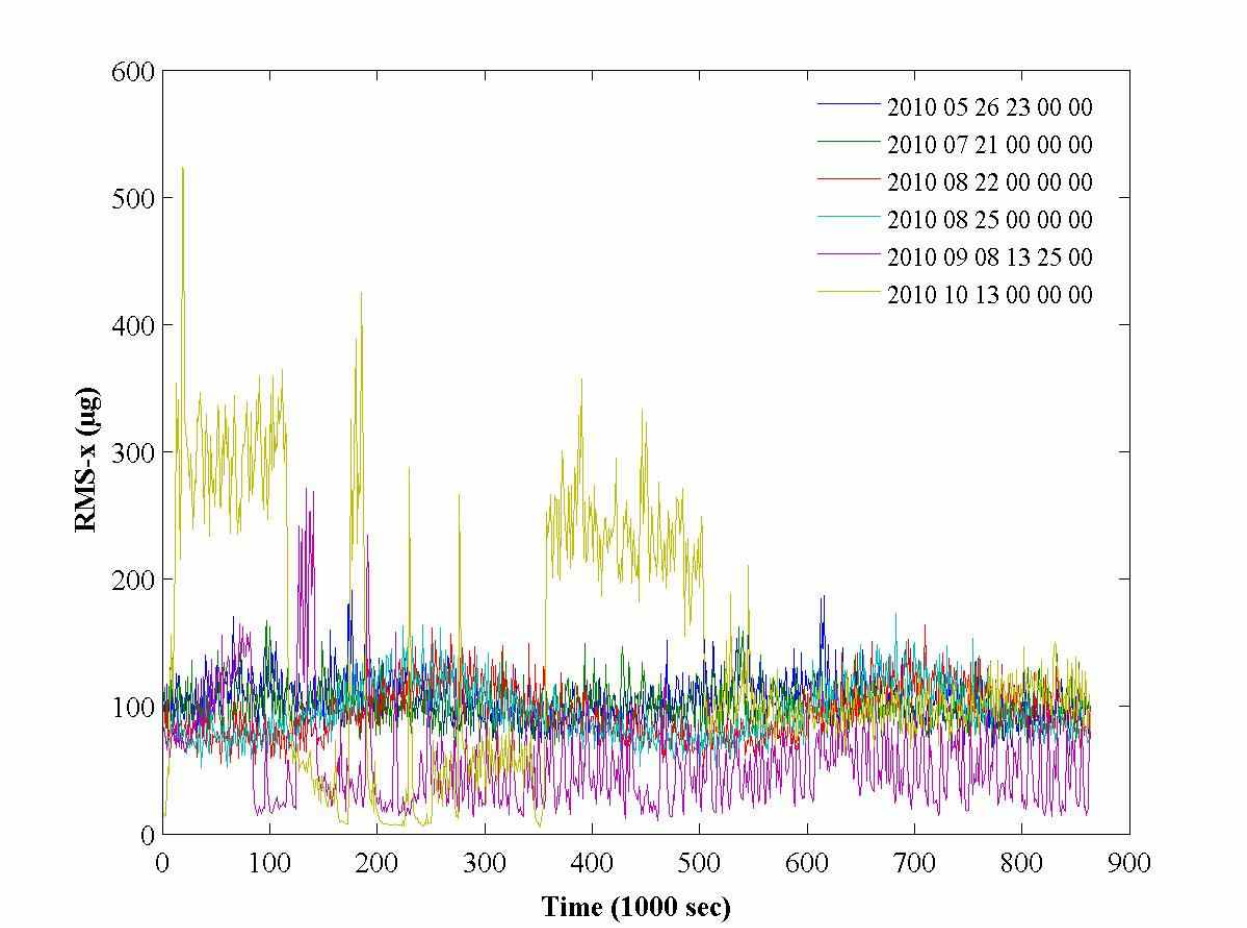

Figure A.35 - Rotary Joint B RMS in x with 5 Hz low-pass filter

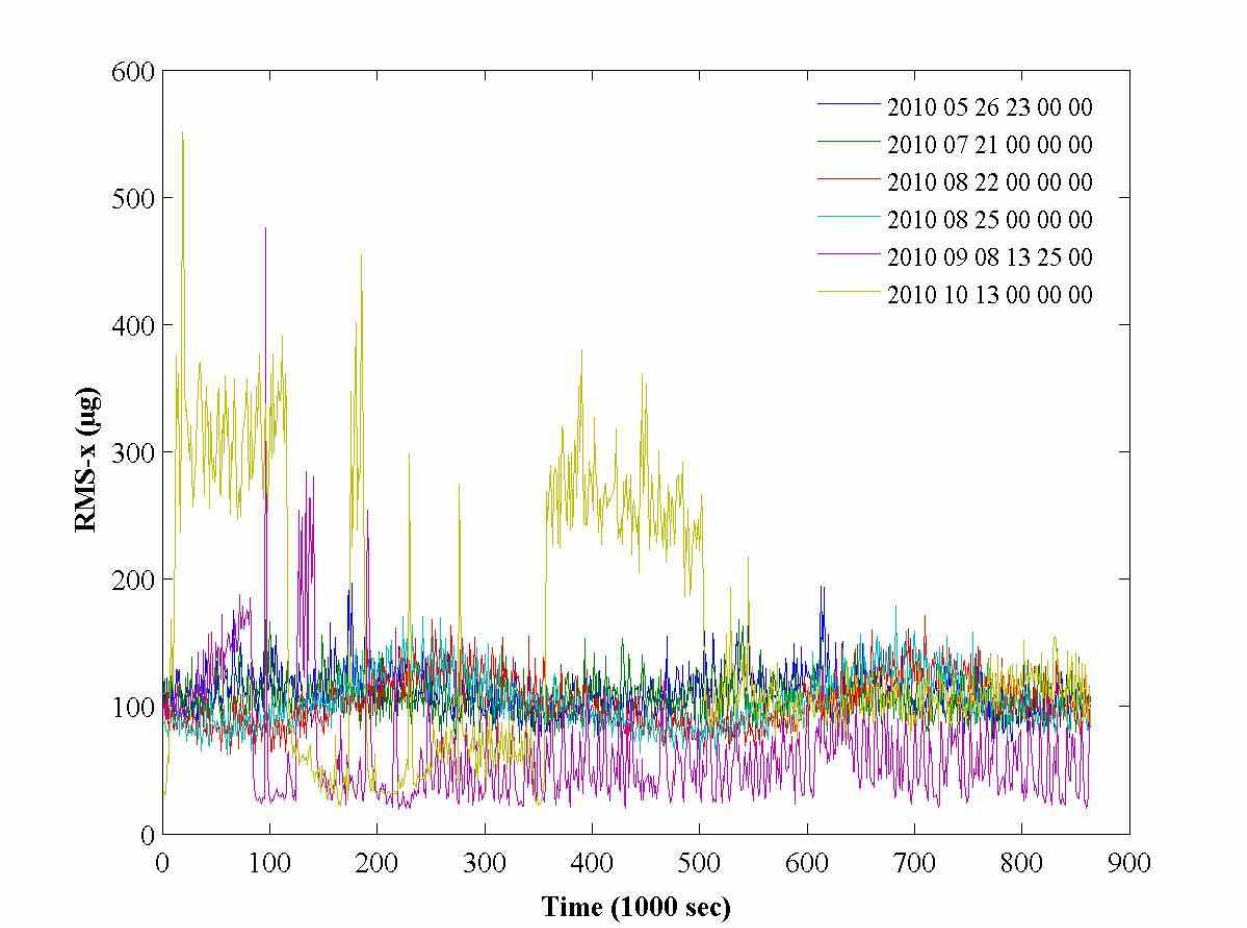

Figure A. 36 - Rotary Joint B RMS in x with 15 Hz low-pass filter

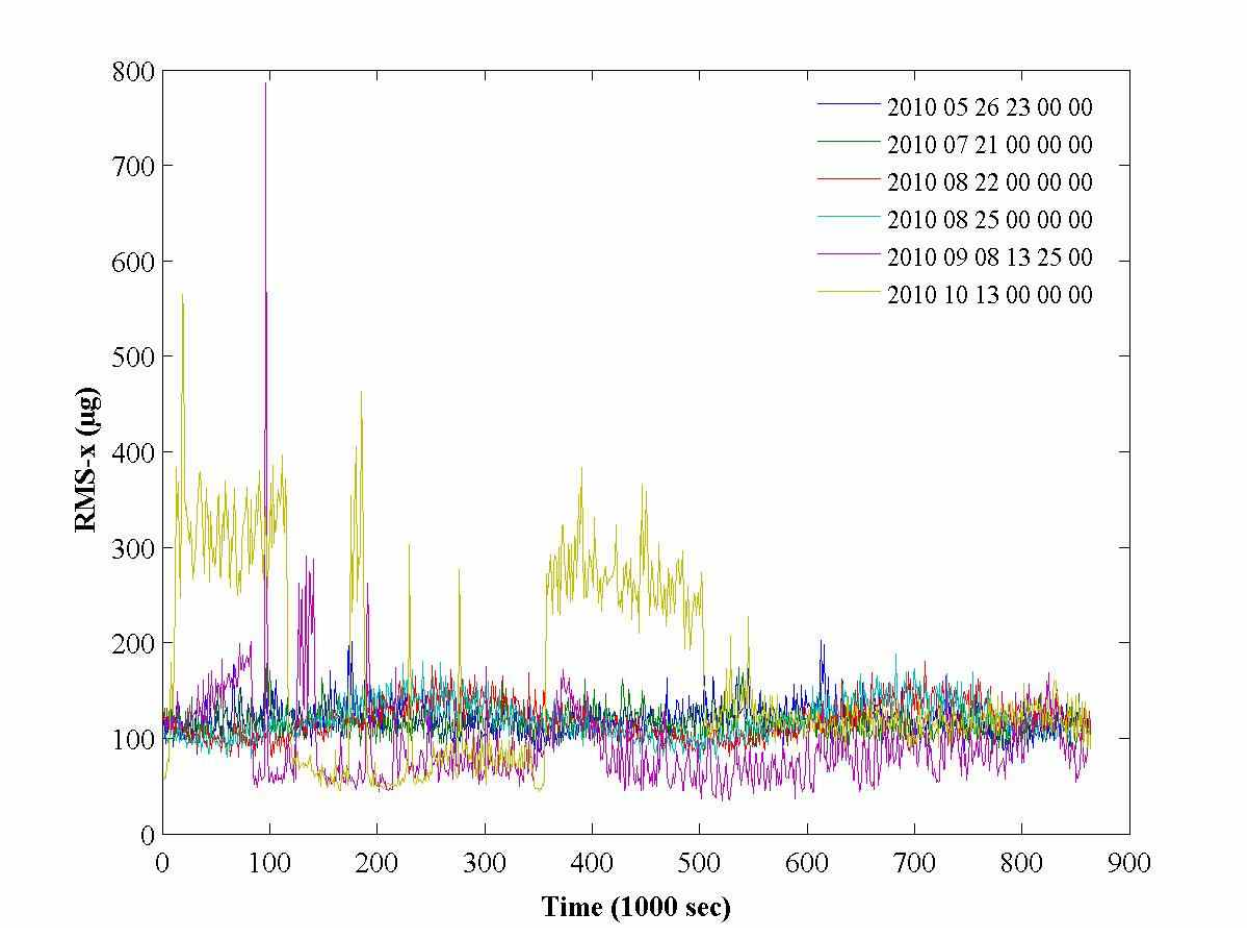

Figure A.37 - Rotary Joint B RMS in x

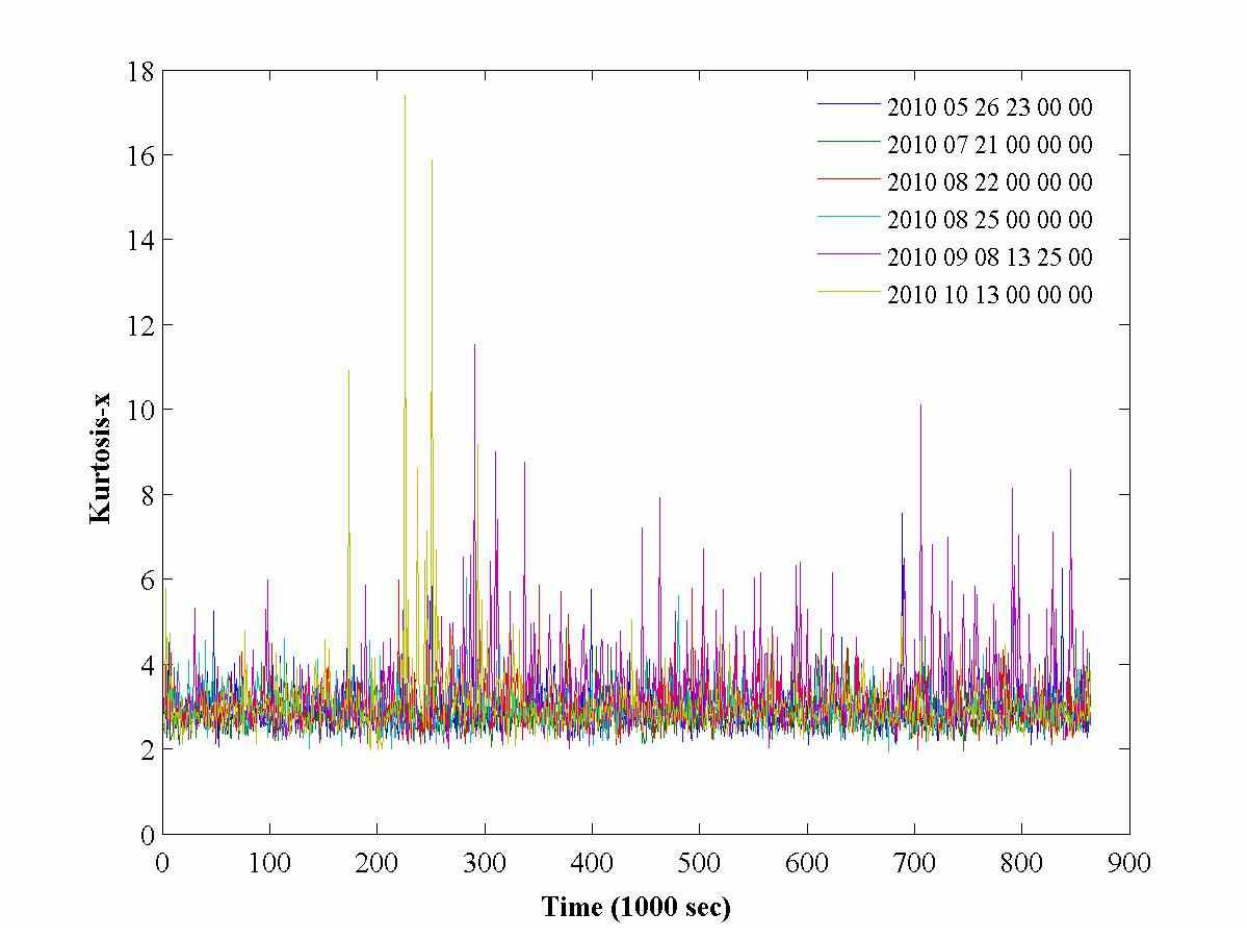

Figure A.38 - Rotary Joint B Kurtosis in x with 5 Hz low-pass filter

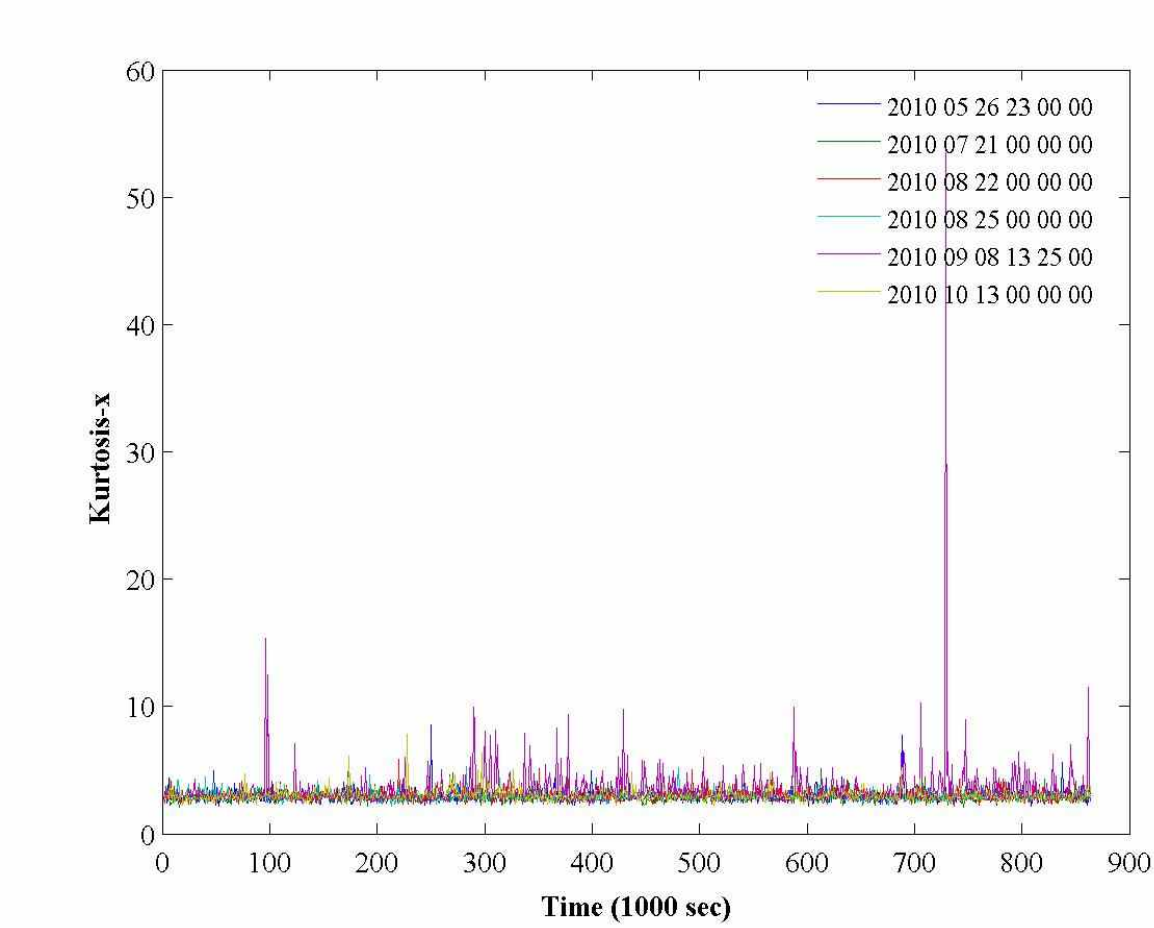

Figure A.39 - Rotary Joint B Kurtosis in x with 15 Hz low-pass filter

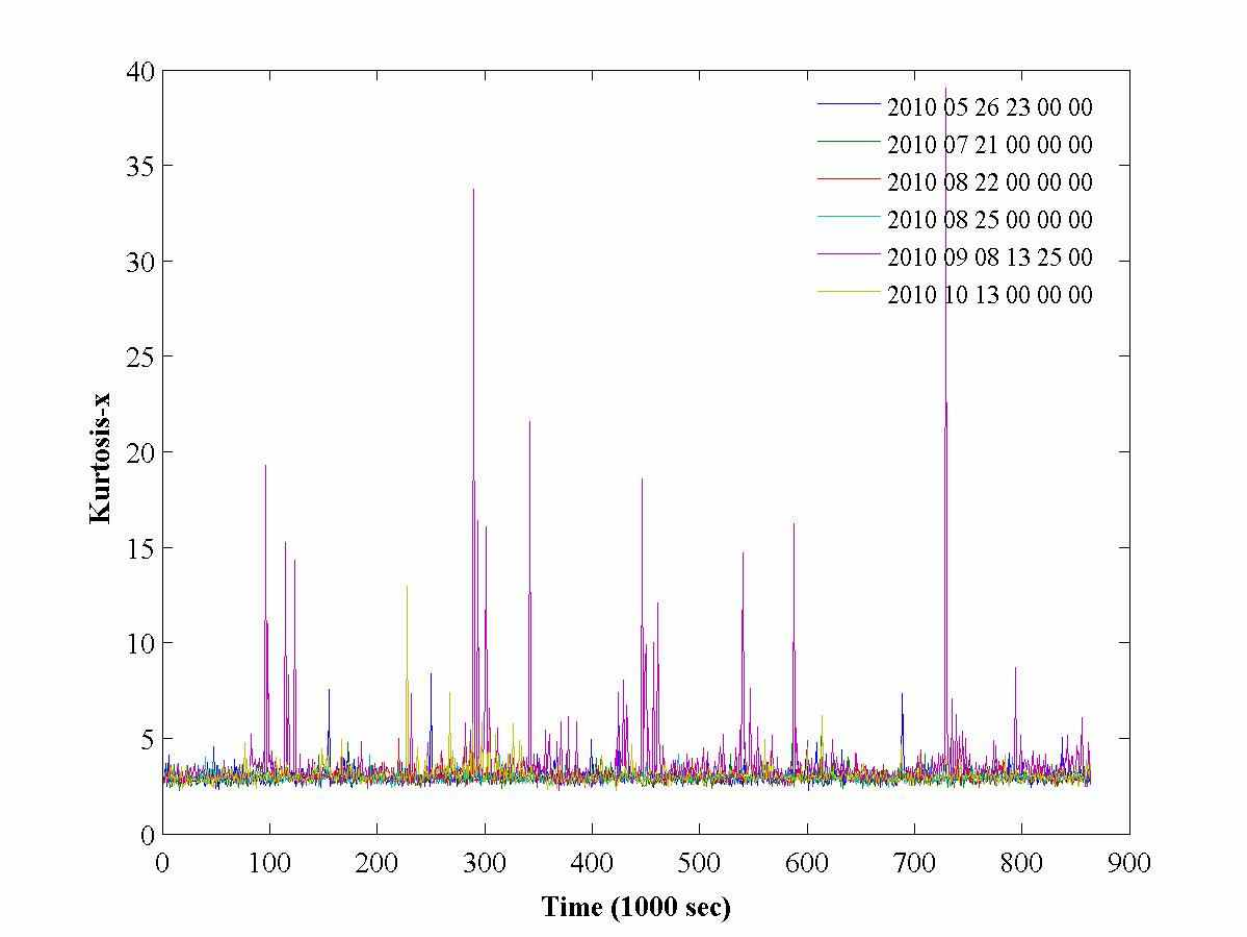

Figure A.40 - Rotary Joint B Kurtosis in x

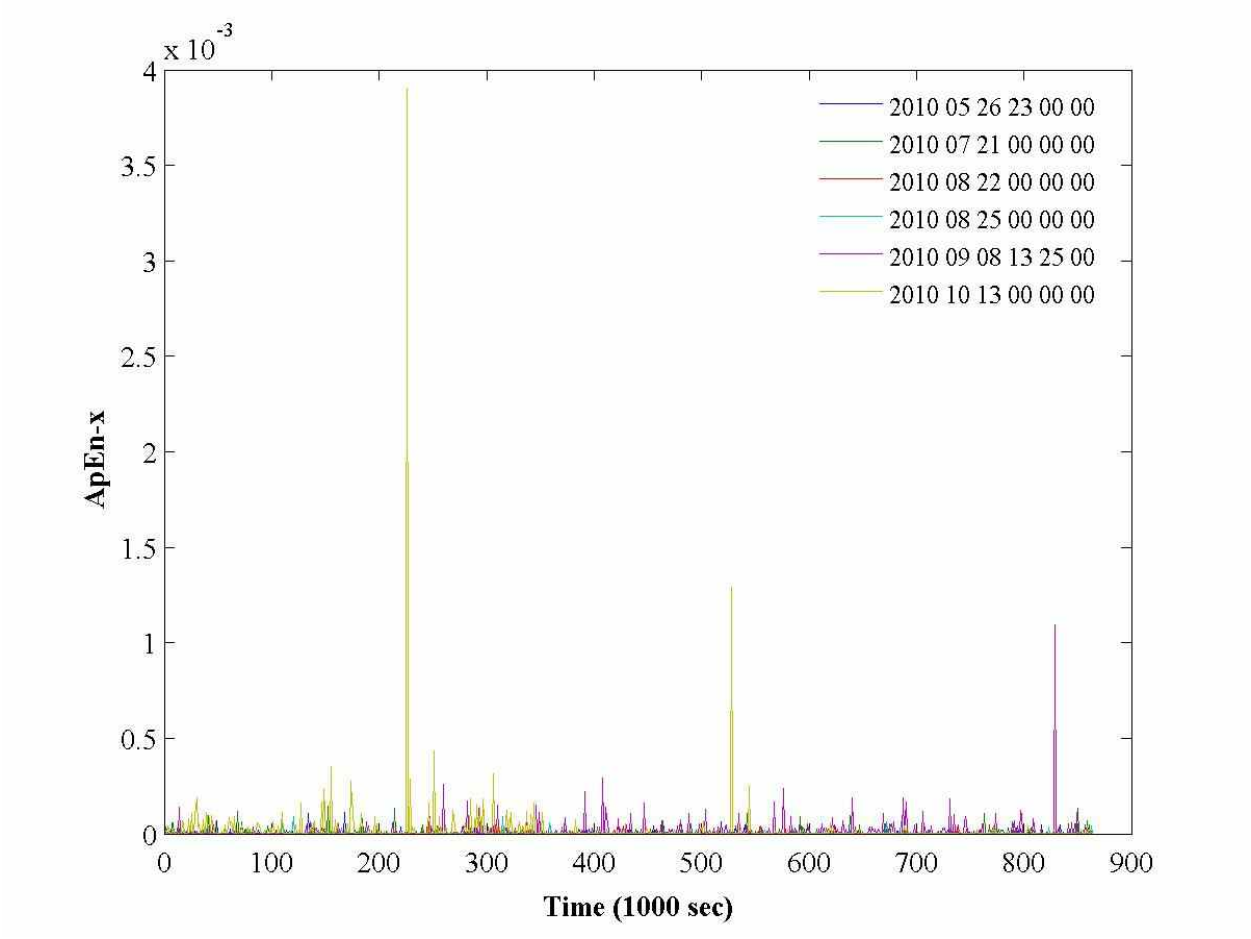

Figure A.41 - Rotary Joint B ApEn in x with 5 Hz low-pass filter

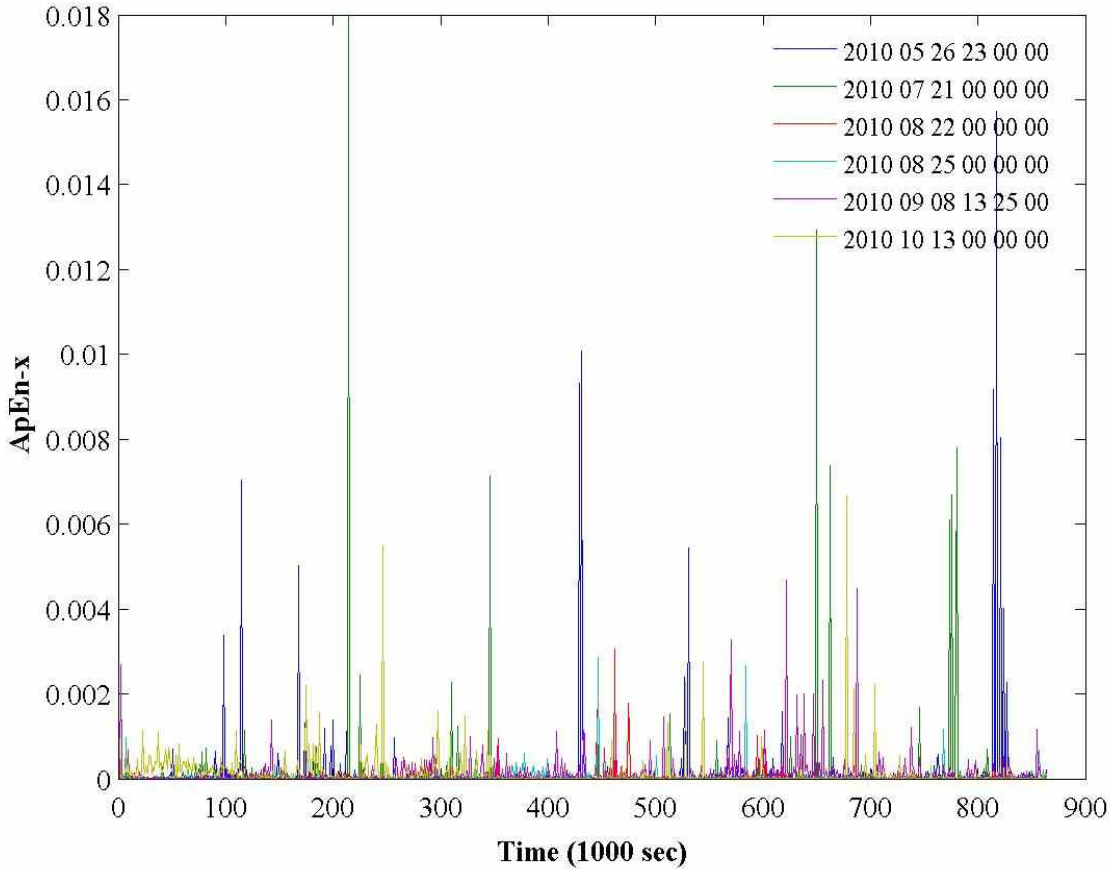

Figure A.42 - Rotary Joint B ApEn in x with 15 Hz low-pass filter

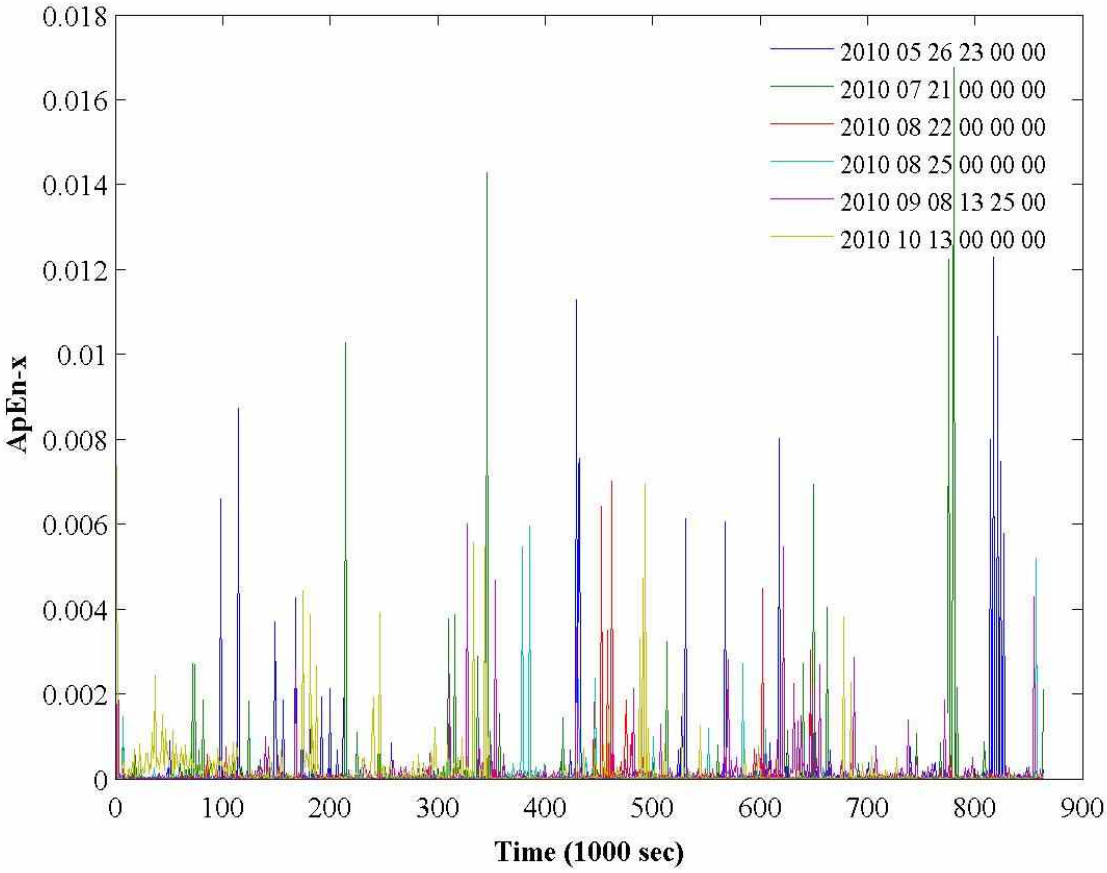

Figure A.43 - Rotary Joint B ApEn in x

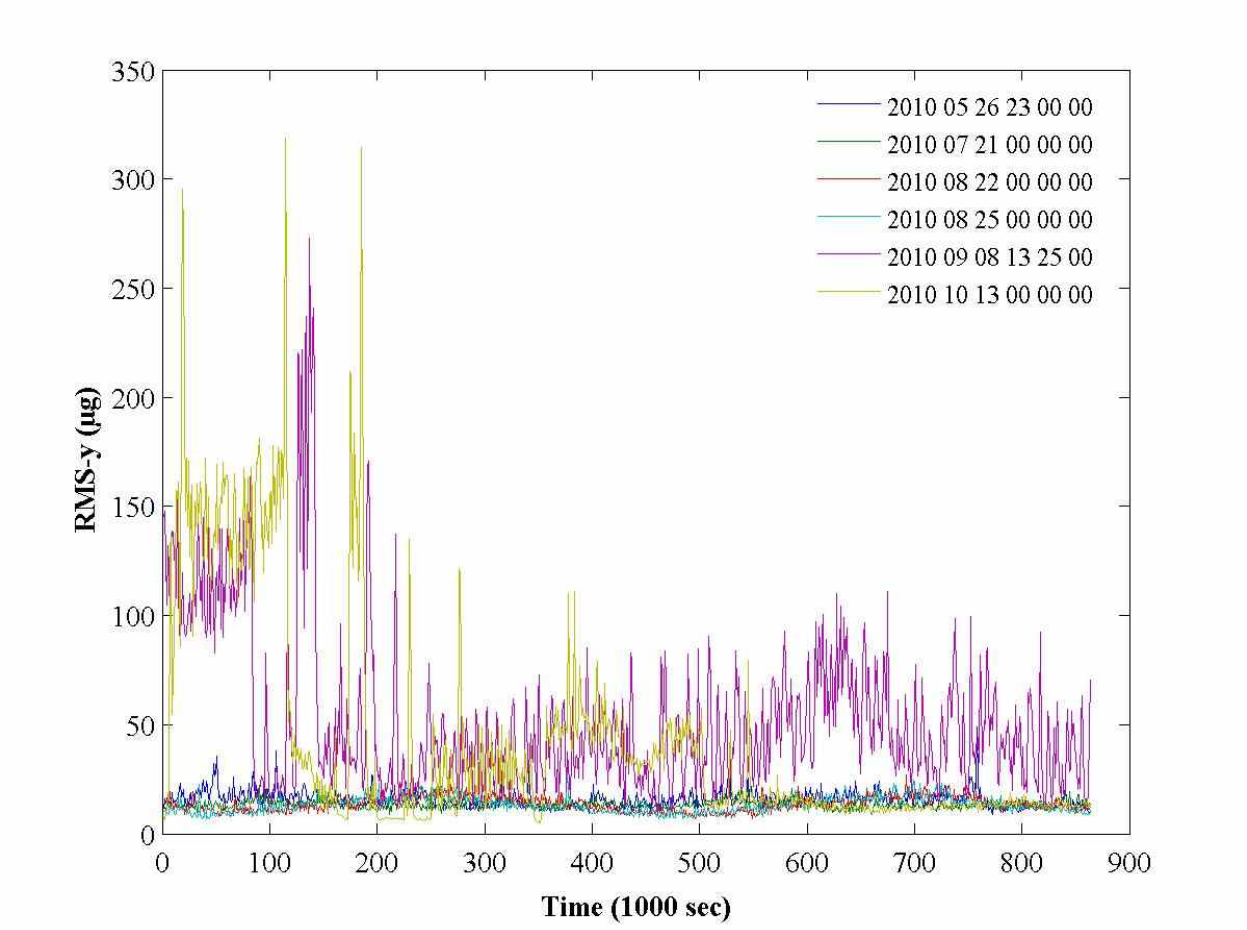

Figure A.44 - Rotary Joint B RMS in y with 5 Hz low-pass filter

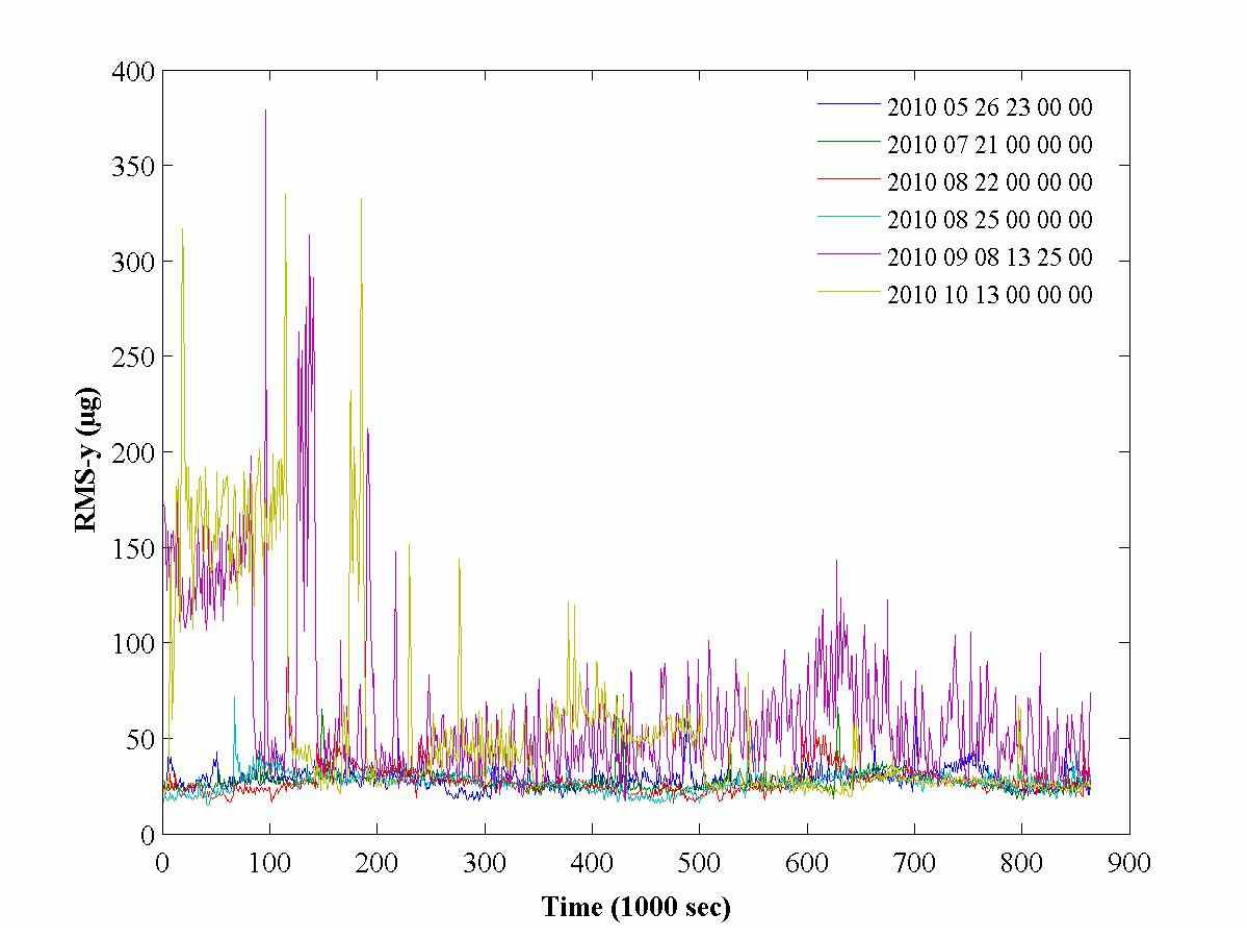

Figure A.45 - Rotary Joint B RMS in y with 15 Hz low-pass filter

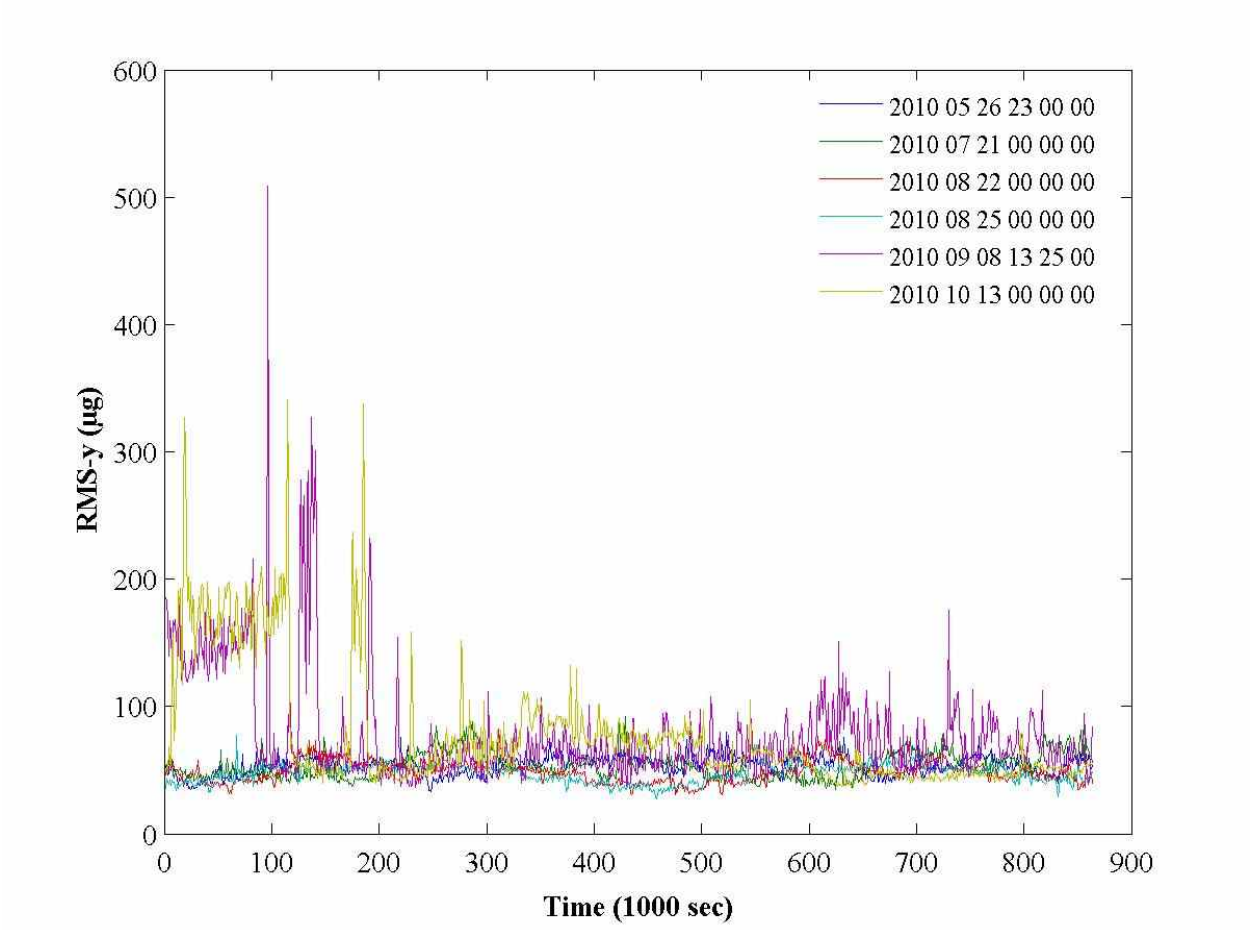

Figure A.46 - Rotary Joint B RMS in y

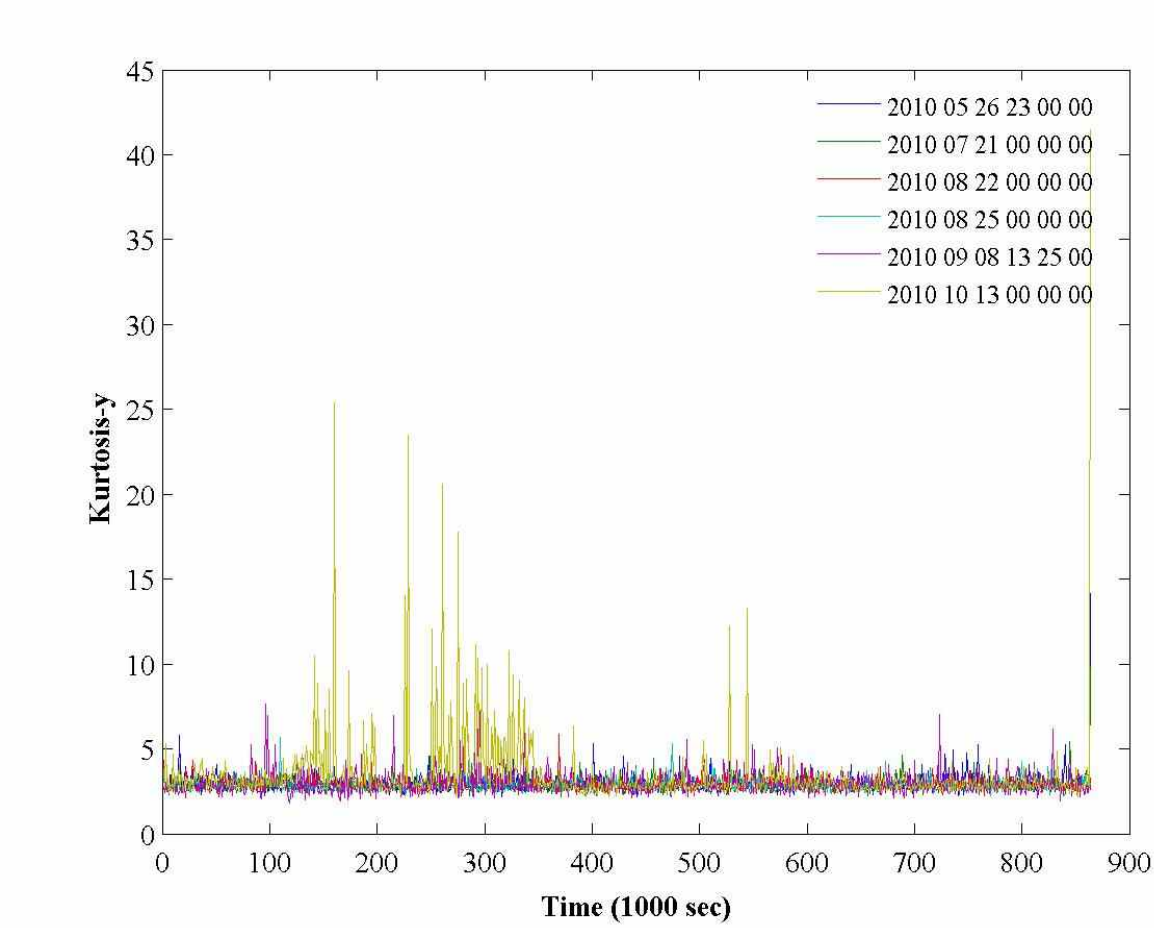

Figure A.47 - Rotary Joint B Kurtosis in y with 5 Hz low-pass filter

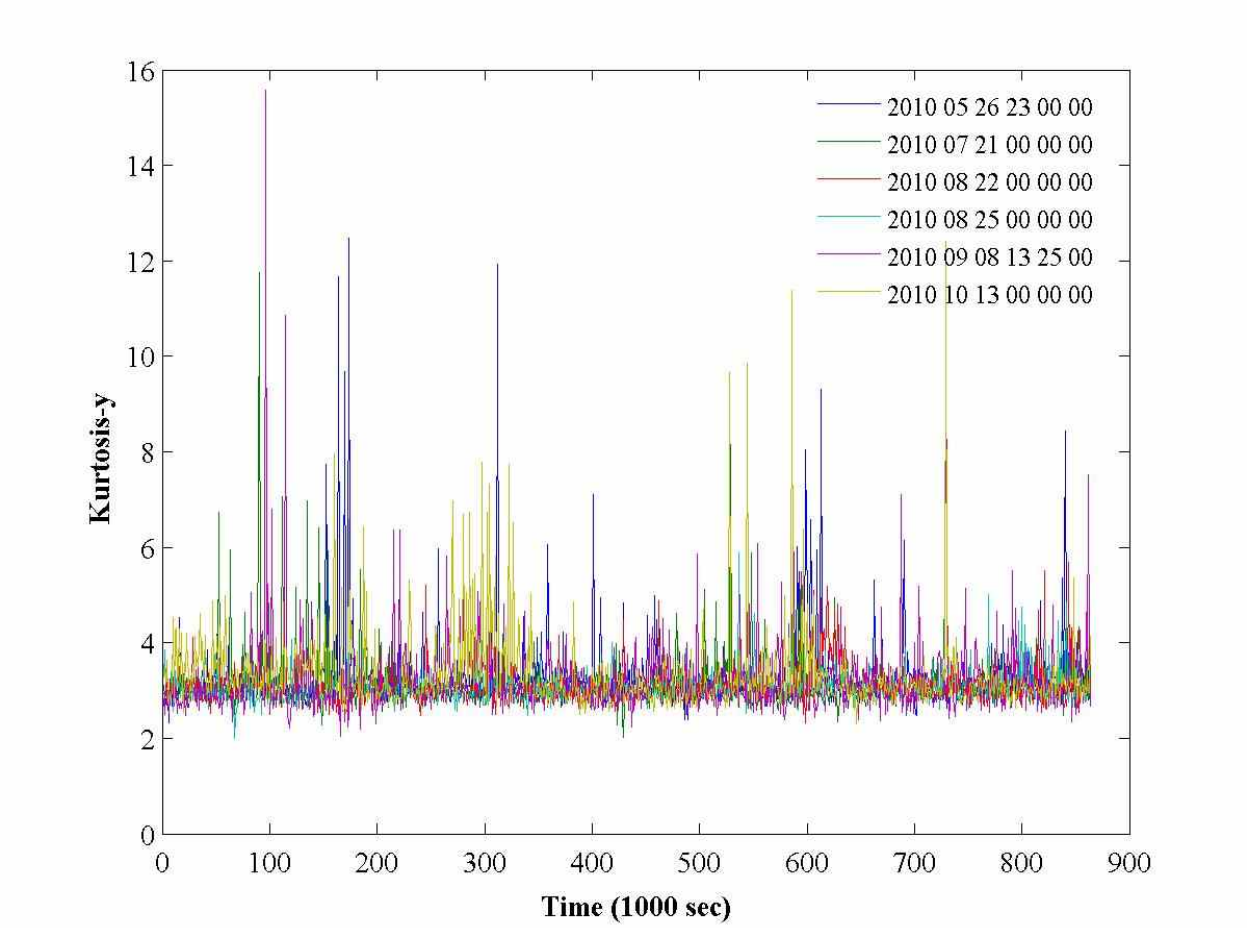

Figure A.48 - Rotary Joint B Kurtosis in y with 15 Hz low-pass filter

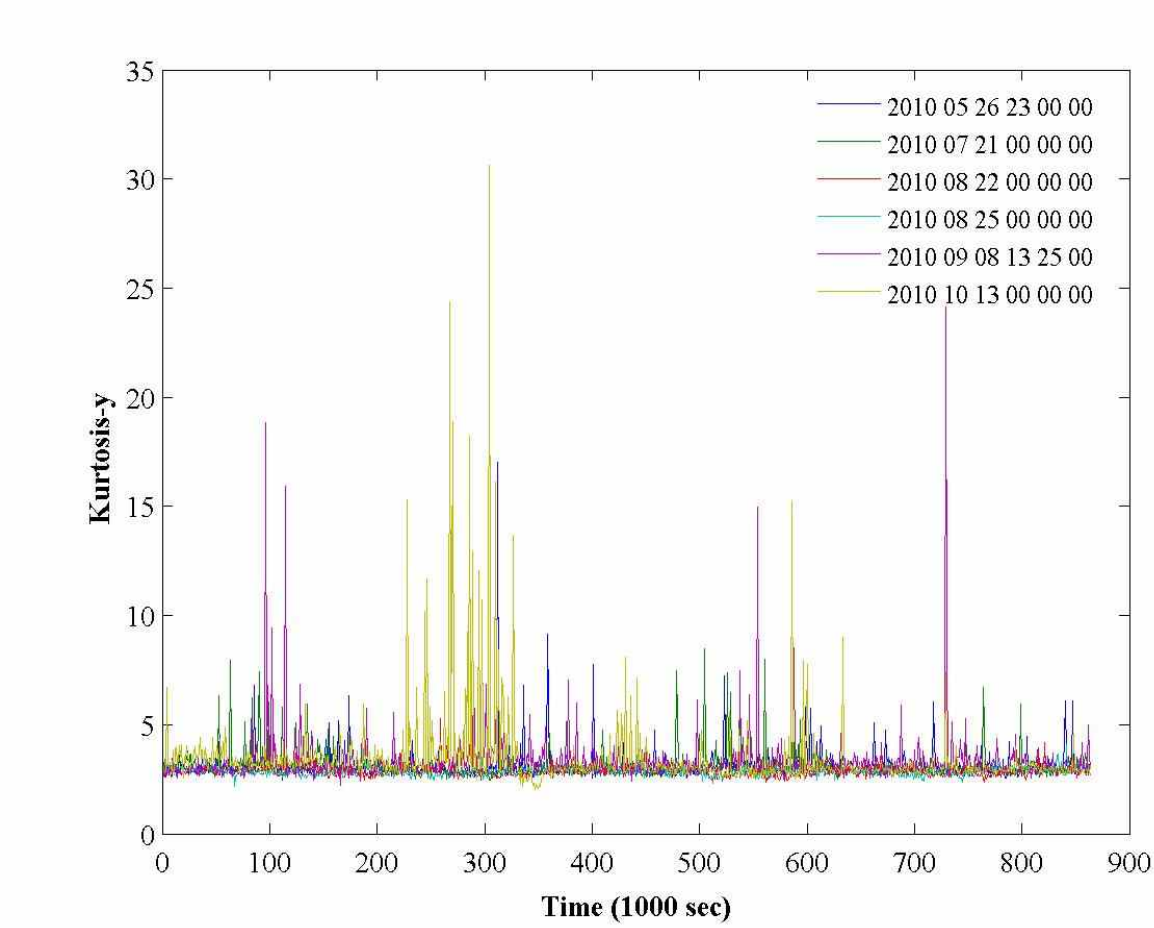

Figure A.49 - Rotary Joint B Kurtosis in y

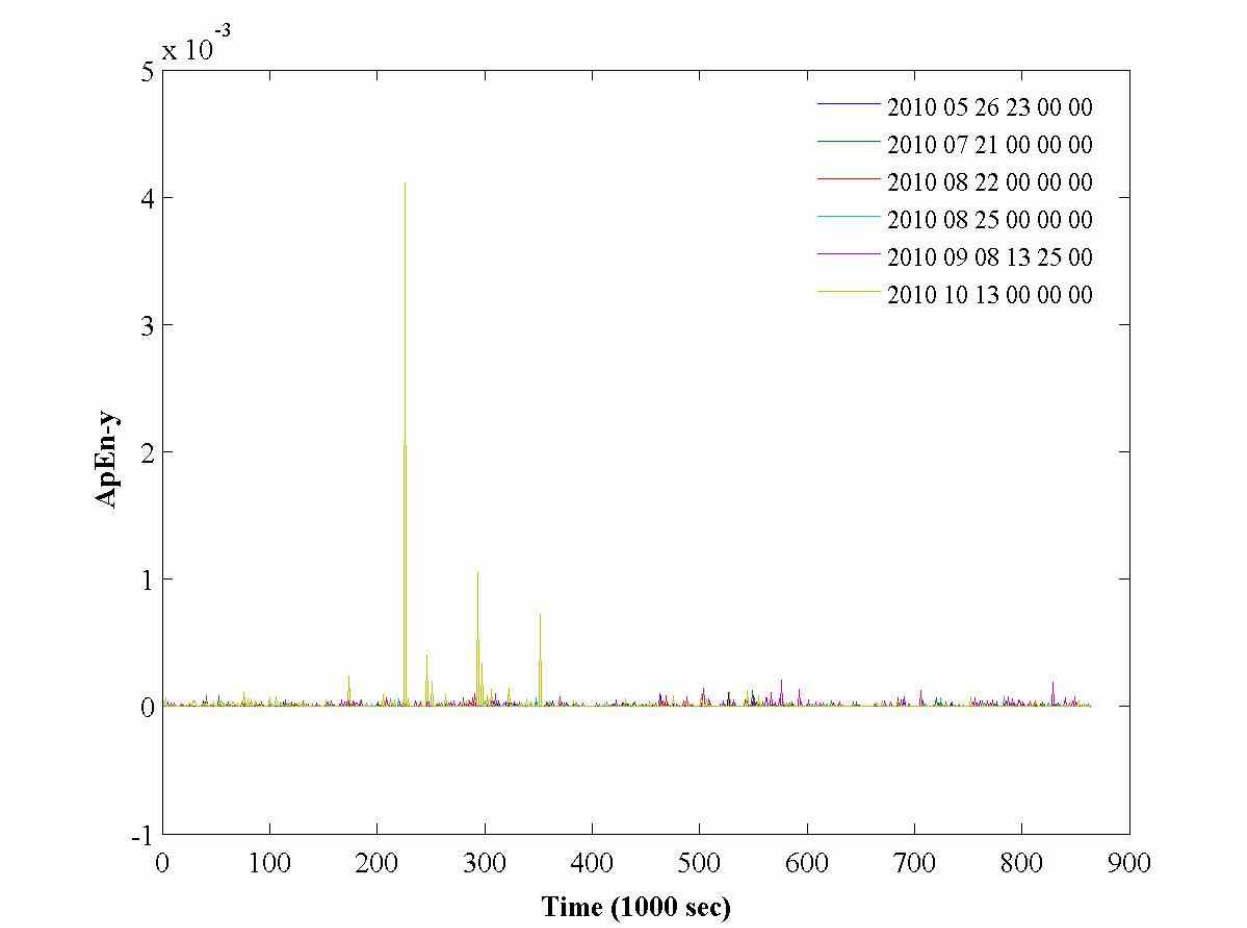

Figure A.50 - Rotary Joint B ApEn in y with 5 Hz low-pass filter

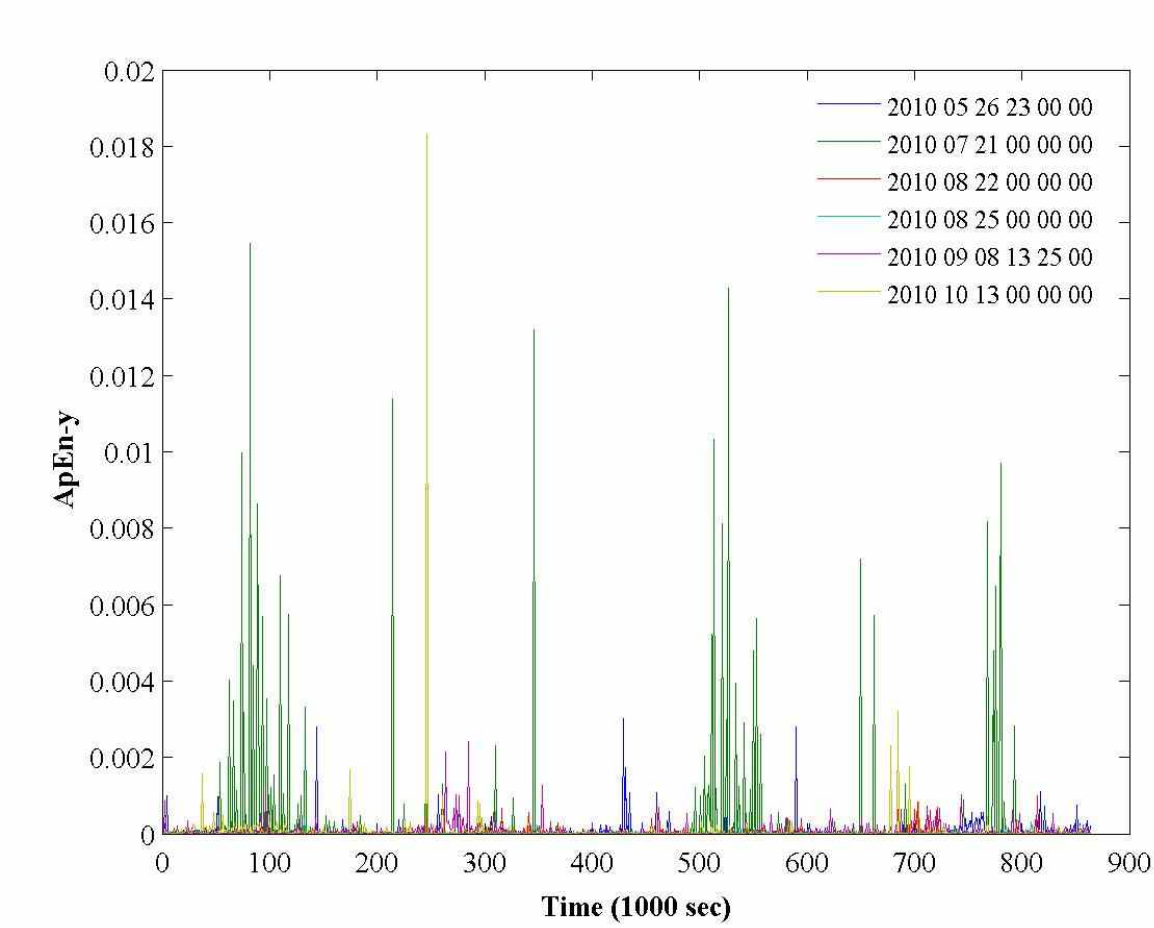

Figure A.51 - Rotary Joint B ApEn in y with 15 Hz low-pass filter

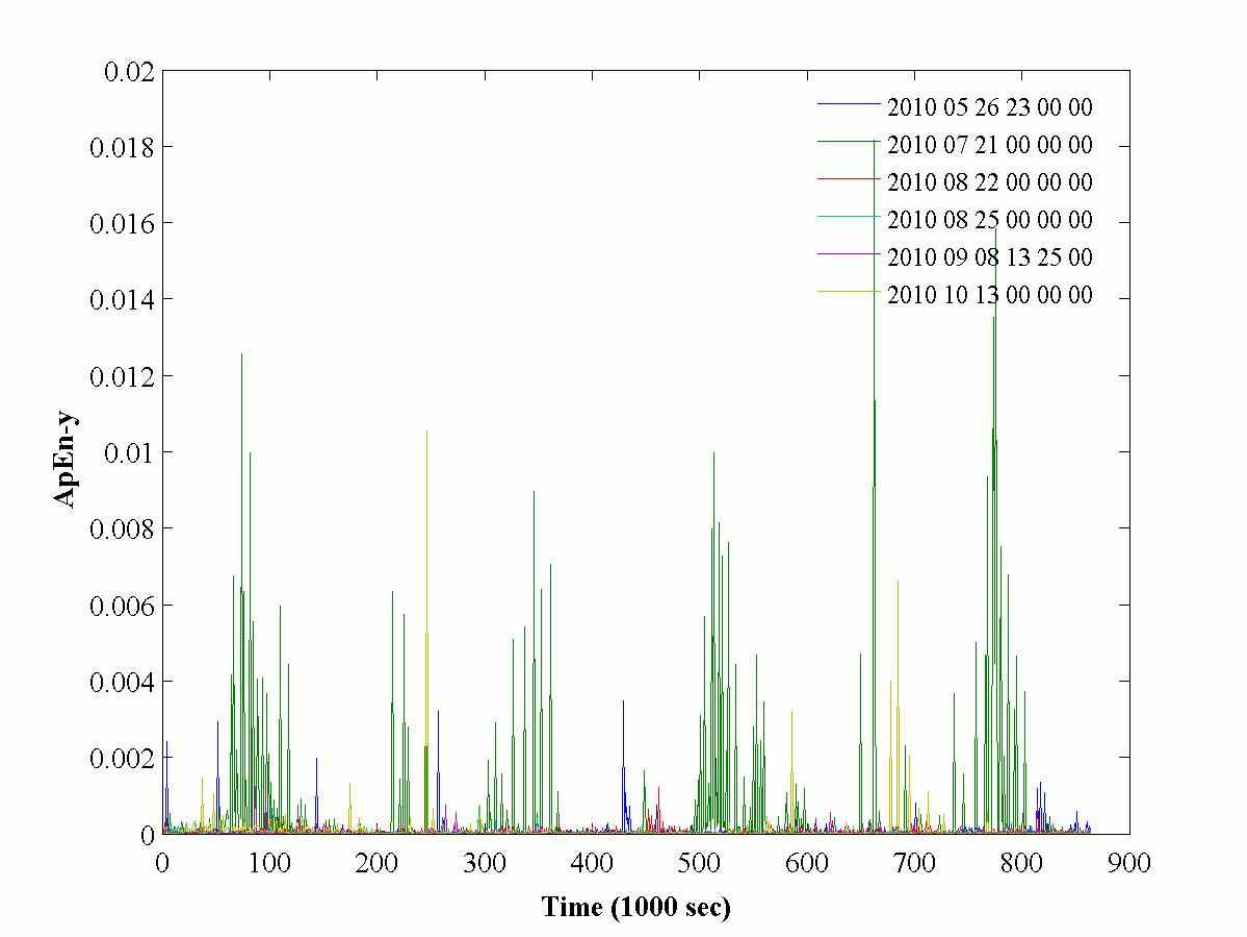

Figure A.52 - Rotary Joint B ApEn in y

CURRICULUM VITAE

Sergio A Navarro was born on March 4, 1988. The second son of Ruben Navarro and Araceli Navarro, he graduated from Lydia Patterson Institute High School, El Paso, Texas, in the spring of 2005. He entered El Paso Community College in the fall of 2005, and in the spring of 2008, he transferred, as a full time student, to the University of Texas at El Paso. While pursuing a bachelor's degree in Civil Engineering, he worked as an undergraduate research assistant for the Center of Space Exploration and Technology Research, during the end of the fall 2009 to the beginning of the spring 2011 semesters. He received his bachelor's degree in Civil Engineering in the fall of 2010.

In the spring of 2011, he entered the Graduate School of the University of Texas at El Paso. While pursuing a master's degree in Civil Engineering, he worked as a graduate research assistant at the Future Aerospace Science and Technology Center. He was a member of the American Society of Civil Engineers and Structural Engineers Association of Texas.

Permanent address: 3681 La Cuesta

El Paso, Texas 79936-0745